

UNCLASSIFIED

AD NUMBER

ADB002628

LIMITATION CHANGES

TO:

Approved for public release; distribution is unlimited.

FROM:

Distribution authorized to U.S. Gov't. agencies only; Test and Evaluation; FEB 1975. Other requests shall be referred to Army Ballistic Research Laboratory, Attn: AMXBR-SS, Aberdeen Proving Ground, MD 21005.

AUTHORITY

usaardc ltr, 8 mar 1978

THIS PAGE IS UNCLASSIFIED

THIS REPORT HAS BEEN DELIMITED
AND CLEARED FOR PUBLIC RELEASE
UNDER DOD DIRECTIVE 5200.20 AND
NO RESTRICTIONS ARE IMPOSED UPON
ITS USE AND DISCLOSURE.

DISTRIBUTION STATEMENT A

APPROVED FOR PUBLIC RELEASE;
DISTRIBUTION UNLIMITED.

BRL R 1758

BRL

AD

ADB002628

REPORT NO. 1758

WIND TUNNEL MAGNUS TESTS OF CYLINDRICAL AND
BOATTAIL ARMY-NAVY SPINNER PROJECTILES WITH
SMOOTH SURFACE AND 20MM EQUIVALENT ENGRAVING
(RIFLING GROOVES)

Maurice A. Sylvester

February 1975

Distribution limited to US Government agencies only; Test and
Evaluation; Feb 75. Other requests for this document must be
referred to Director, USA Ballistic Research Laboratories,
ATTN: AMXBR-SS, Aberdeen Proving Ground, Maryland 21005.

USA BALLISTIC RESEARCH LABORATORIES
ABERDEEN PROVING GROUND, MARYLAND



Destroy this report when it is no longer needed.
Do not return it to the originator.

Secondary distribution of this report by originating
or sponsoring activity is prohibited.

Additional copies of this report may be obtained
from the Defense Documentation Center, Cameron
Station, Alexandria, Virginia 22314.

The findings in this report are not to be construed as
an official Department of the Army position, unless
so designated by other authorized documents.

UNCLASSIFIED

SECURITY CLASSIFICATION OF THIS PAGE (When Data Entered)

REPORT DOCUMENTATION PAGE		READ INSTRUCTIONS BEFORE COMPLETING FORM
1. REPORT NUMBER BRL Report No. 1758	2. GOVT ACCESSION NO.	3. RECIPIENT'S CATALOG NUMBER
4. TITLE (and Subtitle) WIND TUNNEL MAGNUS TESTS OF CYLINDRICAL AND BOATTAIL ARMY-NAVY SPINNER PROJECTILES WITH SMOOTH SURFACE AND 20MM EQUIVALENT ENGRAVING (RIFLING GROOVES)		5. TYPE OF REPORT & PERIOD COVERED Final
		6. PERFORMING ORG. REPORT NUMBER
7. AUTHOR(s) Maurice A. Sylvester		8. CONTRACT OR GRANT NUMBER(s)
9. PERFORMING ORGANIZATION NAME AND ADDRESS USA Ballistic Research Laboratories Aberdeen Proving Ground, Maryland 21005		10. PROGRAM ELEMENT, PROJECT, TASK AREA & WORK UNIT NUMBERS RDT&E 1T161102A33D
11. CONTROLLING OFFICE NAME AND ADDRESS US Army Materiel Command 5001 Eisenhower Avenue Alexandria, Virginia 22333		12. REPORT DATE FEBRUARY 1975
		13. NUMBER OF PAGES 99
14. MONITORING AGENCY NAME & ADDRESS (if different from Controlling Office)		15. SECURITY CLASS. (of this report) UNCLASSIFIED
		15a. DECLASSIFICATION/DOWNGRADING SCHEDULE
16. DISTRIBUTION STATEMENT (of this Report) Distribution limited to US Government agencies only; Test and Evaluation; Feb 1975. Other requests for this document must be referred to Director, USA Ballistic Research Laboratories, ATTN: AMXBR-SS, Aberdeen Proving Ground, MD 21005.		
17. DISTRIBUTION STATEMENT (of the abstract entered in Block 20, if different from Report)		
18. SUPPLEMENTARY NOTES		
19. KEY WORDS (Continue on reverse side if necessary and identify by block number)		
Magnus Characteristics Spinning Projectiles Bullet Engraving Effects		Wind Tunnel Tests Boundary Layer Effects on Magnus Magnus Effects on Stability
20. ABSTRACT (Continue on reverse side if necessary and identify by block number) (1ca) Supersonic wind tunnel and range tests on Army-Navy Spinner models with and without 20mm equivalent engraving (rifling grooves) indicate that a previously noted "offset" effect of deep grooves on Magnus data is also quite persistent for more practical depth engraving. However, the existence of any correspond- ing nonlinearities with spin mismatch is much less certain. A mechanism whereby the grooves affect the Magnus data by rotating the boundary layer is illustrated by oil flow results. The implications for bullet stability may (Continued)		

DD FORM 1473
1 JAN 73

EDITION OF 1 NOV 65 IS OBSOLETE

UNCLASSIFIED

SECURITY CLASSIFICATION OF THIS PAGE (When Data Entered)

UNCLASSIFIED

SECURITY CLASSIFICATION OF THIS PAGE(When Data Entered)

20. ABSTRACT (Continued):

be either adverse or beneficial, depending on the other physical and aerodynamic parameters involved, but are probably significant only for large underspin. Related smooth body results suggest that mixed boundary layer conditions and skewed transition may be more important contributors to erratic stability behavior for a wider range of spin.

UNCLASSIFIED

SECURITY CLASSIFICATION OF THIS PAGE(When Data Entered)

TABLE OF CONTENTS

	Page
LIST OF ILLUSTRATIONS	5
I. INTRODUCTION	7
II. TEST EQUIPMENT	10
A. Facilities	10
B. Models and Equipment	10
III. TEST TECHNIQUES AND DATA REDUCTION	12
IV. TEST CONDITIONS	13
V. BOUNDARY LAYER SIMULATION IN MAGNUS TESTING	14
VI. PRESENTATION OF DATA	16
VII. DISCUSSION OF RESULTS	16
A. Wind Tunnel Magnus Tests	16
B. Stability Considerations	18
C. Comparisons of Wind Tunnel and Range Magnus Data	20
D. Pitching Moment Data	20
VIII. CONCLUSIONS	22
REFERENCES	23
APPENDIX	45
LIST OF SYMBOLS	94
DISTRIBUTION LIST	97

LIST OF ILLUSTRATIONS

Figure	Page
1. Smooth and Engraved A-N Spinner Models	26
2. Models Installed in Wind Tunnels	27
a. NASA Ames	27
b. BRL	27
3. Overall Installation in BRL Wind Tunnel	28
4. Magnus Test Procedure Summary for Grooved Models	29
5. Some Factors and Assumptions Involved in Magnus Data Reduction and Interpretation	30
6. Test Condition Summary	31
7. Typical Magnus Data	32
a. Smooth Model Without Boundary Layer Trip	32
b. Smooth Model With Boundary Layer Trip	33
c. Grooved Model With Boundary Layer Trip	34
8. Oil Streak Results	35
a. Oil Streak Angle	35
b. Approximate Surface Streamlines	36
9. $C_{np\alpha}$ vs. pd/V	37
a. Smooth Model	37
b. Grooved Model	38
10. $C_{np\alpha}$ vs. α	39
a. Grooved Model	39
b. Smooth Model	40
11. Effect of $C_{np\alpha}$ on Dynamic Stability	41
12. Effect of $C_{np\alpha}$ on Exponential Damping Coefficients	42

LIST OF ILLUSTRATIONS (Continued)

Figure		Page
13.	Summary of Wind Tunnel and Range Magnus Moment Coefficient Data Comparisons	43
a.	Cylindrical and Boattail Models With Predominantly Turbulent Boundary Layers or Fixed Transition . . .	43
b.	Smooth, Boattail Models With Probable Mixed Boundary Layer Conditions and Skewed Transition . .	44

APPENDIX

A1.	Basic Magnus Force Data	46
A2.	Basic Magnus Moment Data	64
A3.	Magnus Force and Moment Coefficients vs. Angle of Attack .	82
A4.	Comparison of Wind Tunnel Data With Range Check Points for Similar Test Conditions	89
A5.	Typical Pitching Moment Data	92

I. INTRODUCTION

The stability of bullets sometimes shows unexplained behavior at longer ranges. This has resulted in several studies¹⁻³ to determine the cause. One of these studies, sometimes referred to as "Spin Mismatch Magnus Moment," has continued because of the results obtained in early experiments. These initial wind tunnel and range tests showed that rifling or helical serrations could affect the aerodynamic properties of a bullet. The wind tunnel Magnus data indicated strong nonlinearities with spin mismatch and also an "offset" in the Magnus data for models with accentuated helical serrations; while the range results showed some effect on the Magnus coefficient of bullets with typical engraving (rifling grooves). Because of wide differences in model and test parameters in the wind tunnel and range, no meaningful correlations could be made and the possible implications regarding stability were not clear. Also, the valid question was raised as to whether the deep grooved models (used in the initial wind tunnel tests to assure measurable data) would produce results in a different phenomenological regime than that associated with more practical engraving. Therefore, it was felt necessary to extend the tests: (1) to determine whether more practical bullet-like engraving could cause similar, although less severe, effects; (2) to provide better coordination with free-flight range tests; and (3) to extend the range of test variables particularly to include lower supersonic Mach numbers and boattail models. Incident-

-
1. M. J. Piddington, "Deformation Characteristics of One Lot (LC SP412) of 5.56 mm M-193 Ammunition," U.S. Army Ballistic Research Laboratories Memorandum Report No. 2016, Aberdeen Proving Ground, Maryland, October 1969. AD 862966.
 2. M. A. Sylvester and W. F. Braun, "The Influence of Helical Serrations and Bullet Engraving on the Aerodynamic and Stability Properties of a Body of Revolution With Spin," U.S. Army Ballistic Research Laboratories Report No. 1514, Aberdeen Proving Ground, Maryland, November 1970. AD 719235. Also, AIAA Paper No. 70-557, AIAA Atmospheric Flight Mechanics Conference, Tullahoma, Tennessee, May 1970.
 3. Maurice A. Sylvester, "Influence of Helical Serrations on the Aerodynamic Properties of a Spinning Body," *AIAA Journal*, Vol. 10, No. 2, February 1972, pp. 223-225.

ally, the smooth "control" models would also provide added results for the growing data bank on the Army-Navy (A-N) Spinner from various facilities⁴⁻⁷.

Little related information on studies of this type existed at the time of the earlier work and this is still the case. However, a recent investigation⁸ at low speeds showed no significant effect of N-vanes (small, canted fins) and rotating-band rifling grooves on the Magnus characteristics although boattail-mounted N-vanes did reduce the Magnus moment somewhat. Also, a reduction in Magnus moment by small boattail-fins (with and without cant) has been noted by other investigators^{9,10} but these effects on Magnus are probably mostly caused by a different mechanism¹¹ (blanked out fin and/or differential drag effects) than that involved in the present study. More directly related is the recent

4. C. H. Murphy and L. E. Schmidt, "The Effect of Length on the Aerodynamic Characteristics of Bodies of Revolution in Supersonic Flight," U.S. Army Ballistic Research Laboratories Report No. 876, Aberdeen Proving Ground, Maryland, August 1953. AD 23468.
5. J. B. Carmen, J. C. Uselton and W. E. Summers, "Experimental Magnus Characteristics of Basic and Boattail Configurations of 3- and 5-Caliber Army-Navy Spinner Projectiles at Subsonic and Transonic Mach Numbers," AEDC-TR-70-36, April 1970.
6. J. B. Carmen and James Uselton, "Experimental Magnus Characteristics of Basic and Boattail Configurations of 3- and 5-Caliber Army-Navy Spinner Projectiles at Supersonic Mach Numbers," AEDC-TR-69-178, November 1969.
7. G. L. Winchenbach, R. M. Watt and A. G. Skinner, "Free Flight Range Tests of Basic and Boattail Configurations of 3- and 5-Caliber Army-Navy Spinner Projectiles," AEDC-TR-70-12, March 1970.
8. C. W. Ingram, R. J. Lusardi and J. C. Nicolaidis, "Effects of Rifling and N-Vanes on the Magnus Characteristics of Bodies of Revolution," AIAA Paper No. 72-970, AIAA 2nd Atmospheric Flight Mechanics Conference, Palo Alto, California, September 1972.
9. G. I. T. Nielsen and Anders S. Platou, "The Effect of Conical Boattails on the Magnus Characteristics of Projectiles at Subsonic and Transonic Speeds," U.S. Army Ballistic Research Laboratories Report No. 1720, Aberdeen Proving Ground, Maryland, June 1974.
10. Leroy M. Jenke, "Experimental Magnus Characteristics of Ballistic Projectiles With and Without Anti-Magnus Vanes at Mach Numbers 1.5 Through 2.5," AEDC-TR-73-162 (AFATL-TR-73-188), December 1973.
11. Anders S. Platou, "Magnus Characteristics of Finned and Nonfinned Projectiles," AIAA Journal, Vol. 3, No. 1, January 1965, pp. 83-90.

finding¹² that forward-mounted canted bore-riders on an artillery shell cause an offset in the Magnus data similar to that obtained in the results for models with helical serrations.

Smooth and engraved A-N Spinner models with and without boattails were used in the present wind tunnel and range test programs. The engraving was equivalent to that of a 20mm shell and a compromise twist of 1 turn in 20 calibers was selected to provide some overlap of the wind tunnel and range data in an appropriate spin regime. This overlap region tends to be limited by the maximum spin attainable in the wind tunnel and the minimum spin required for stability in the range. However, it was possible to obtain conditions of underspin, matchspin and overspin. A bullet has matchspin as it leaves a stationary gun barrel and then becomes overspun down range as it slows down faster in velocity than spin. A bullet fired from a forward moving gun (on an aircraft, for example) is initially underspun.

The tests were run at both high subsonic and low supersonic Mach numbers and for a range of Reynolds numbers. In addition, artificial boundary layer trips were used to fix transition or further extend the apparent Reynolds number. Attempts to obtain transonic wind tunnel data (an area of particular pertinence for bullets at long range) have so far met with little success. Several tests have been scheduled in facilities which provide services in this Mach number regime but each test has been cancelled, postponed or aborted for one reason or another. Further testing is not now contemplated and, even if resumed, the nature of the tests coupled with the characteristics of transonic wind tunnels might continue to make it impractical or make any data obtained of doubtful value. The results of planned firings in the range at transonic Mach number may help decide if further wind tunnel testing is required. In the meantime, it seems appropriate to present the test data presently available. Although this report is mainly concerned with the wind tunnel tests and data some range results are included.

12. Klaus O. Opalka, "Wind Tunnel Test of a Spinning, Low-Drag Projectile With Canted Bore Riders at Mach Numbers From 1.75 to 2.5," U.S. Army Ballistic Research Laboratories Memorandum Report No. 2349, Aberdeen Proving Ground, Maryland, January 1974. AD 774804.

11. TEST EQUIPMENT

A. Facilities

The tests were conducted in the Ballistic Research Laboratories (BRL) 13" x 15" Supersonic Tunnel No. 1¹³ and the NASA Ames 12-Foot Subsonic Pressure Tunnel¹⁴. The tunnels are of the continuous-flow, variable-density type and operate over a range of subsonic or supersonic Mach numbers. However, these tests were run only at Mach numbers of 0.9 in the NASA tunnel and 1.5 and 2.0 in the BRL tunnel. Although the flow environment was otherwise satisfactory for Magnus measurements in both tunnels, Mach number 1.5 was somewhat critical for this model and neither tunnel was designed to test in the lower supersonic or transonic region ($M = 1.1$ to 1.3) which, as mentioned previously, is of particular interest in this study.

Shadowgraph equipment, an auxiliary air supply for spinning the model and a high speed data acquisition system¹⁵ are available at the BRL facility but must be provided by the test contractor at the NASA facility. Therefore, only a temporary shadowgraph system with limited capability was used and the analog data signals were collected on x-y plotters and magnetic tape. The BRL tunnel model support is also equipped with a mini-yaw device (± 0.8 degree) which can be used to neutralize any initial malalignment or flow inclination in the yaw plane. However, frequent changes in some of these quantities (with M , Re , etc.) plus a lack of sensitivity in the mechanism tends to make this adjustment somewhat impractical or, at least, overly time consuming for general use.

B. Models and Equipment

The smooth and engraved A-N Spinner models are illustrated in Figure 1. The models are all five caliber long and have reference diameters of 2.00 and 4.25 inches for the BRL and NASA tunnel tests, respectively. The two-caliber ogive nose is followed by either a three caliber cylindrical body or a two and one-half caliber cylindrical

13. J. C. McMullen, "Wind Tunnel Testing Facilities at the Ballistic Research Laboratories," U.S. Army Ballistic Research Laboratories Memorandum Report No. 1292, Aberdeen Proving Ground, Maryland, July 1960. AD 244180.
14. C. S. Pirrello, R. D. Hardin, M. V. Heckart and K. R. Brown, "An Inventory of Aeronautical Ground Facilities, Vol. 1--Wind Tunnels," NASA CR-1874, November 1971.
15. L. D. Kayser, "The BRL Wind Tunnel High Speed Analog-to-Digital Data Acquisition System," U.S. Army Ballistic Research Laboratories Memorandum Report No. 2142, Aberdeen Proving Ground, Maryland, December 1971. AD 737180.

section and a one-half caliber, seven-degree boattail. The 20mm equivalent engraving consists of 9 equally spaced grooves 0.115 caliber wide by 0.0205 caliber deep and is provided on the cylindrical surface only, running out on the nose and boattail. The twist of one turn in 20 calibers results in a groove angle of approximately nine degrees with respect to the longitudinal model axis. The right-hand twist of the grooves is in the direction to cause a clockwise (looking upstream) torque or spin when the model is in the tunnel flow.

The configuration identification is shown in the figure and listed in Table 1.

Table 1. Configuration Identification

<u>Code</u>	<u>Description</u>
02000	Smooth, cylindrical tail
03000	Grooved, cylindrical tail
06000	Smooth, boattail
07000	Grooved, boattail

Note that non-zeros in any of the last three digits indicates a boundary layer trip. This trip (when used) was a 0.125 caliber wide band of sparsely populated number 80 grit (or equivalent) located one-half caliber from the nose.

Typical models are shown installed in the BRL tunnel in Figure 2a and in the NASA tunnel in Figure 2b. The models are free to rotate on grease-plated precision ball bearings and may be spun up in the clockwise direction by the primary air turbine located inside the model base, or braked (or spun in the opposite direction) by a reverse air jet located externally at the model base. The primary spin-up air supply is brought into the model through a hollow strut and then exits through nozzles and blades into the base area behind the model. Converging sonic nozzles have proved to be most efficient. The reversing air supply is routed through tubes on the top and bottom of the support strut and is then directed onto notches cut in the model base retainer. The overall installation in the BRL tunnel is shown in Figure 3. The primary spin-up turbine is capable of rotating the models to at least 45,000 rpm in the BRL facility and 15,000 rpm in the NASA tunnel using air supply pressures of about 120-150 psia. The reversing nozzle was considerably less effective but adequate for use as a brake to speed up tests or to stop auto-spin of the grooved models. This was fortunate since other attempts at braking have been unsuccessful or impractical. The models could be locked at roll angles of 0, 90, 180 and 270° for static tests.

The spin rate of the models was determined from the pulses induced in a stationary coil by two small magnets rotating with the model. This device works well at spin rates greater than about 1,000 rpm but is unreliable at lower speeds.

The aerodynamic forces in the pitch and yaw planes were detected by appropriately-sized four-component internal strain-gage balances plus an additional yaw component located on the strut behind the model. This redundant gage was shielded from the air flow and used to improve the accuracy of the Magnus determination. Its use assures that the rearward Magnus centers of pressure will generally remain between, rather than outside, the yaw gage positions.

III. TEST TECHNIQUES AND DATA REDUCTION

The static (non-spinning) tests were made with the model locked in a reference roll position and the data were recorded as the angle of attack was varied.

The Magnus (spinning) tests were made with the model at constant angle of attack. For the smooth models, the procedure was to spin the model up to the maximum rotational speed, shut off the air to the turbine and then record strain gage data as functions of time and rpm as the model coasted to a stop. For the grooved models, the Magnus test procedure was basically the same except for the free spinning tendency caused by the helical serrations. For these tests, the reversing nozzle was used to brake the model spin back to zero and then the data were obtained as the model was spun up to its experimental free-spin rate by the effect of the serrations. The air turbine was then actuated to spin the model to the maximum rotational speed and the data for the remaining spin range were obtained as the spin decayed to the experimental free-spin value. The reversing nozzle was also sometimes used to brake both the smooth and grooved models to save testing time. However, data were collected only when the air supply to the nozzle was off to prevent interference with the measurements. (There also was a brief transient period after shutting the air off during which the data were unreliable. This was of little consequence in the present tests but can be very troublesome for models with high roll damping or short spin down times by causing loss of a substantial portion of data.) The test procedures are summarized in Figure 4.

The accurate determination of relatively small Magnus forces and moments, which is an exacting process with smooth models, is made even more difficult by the effects of the grooves. Therefore, certain precautions and checks not normally employed are necessary to provide reliable and reduceable data. Essentially, this involves provisions to allow the separation of the groove effects in the data from several unwanted effects such as flow inclinations, interactions, zero shift, strut and model malalignments, angle of attack skew, etc. These effects, though small, can frequently be of the same order as the perturbations on the Magnus data caused by the grooves. Careful calibration checks, no-flow zero knowledge, minimum instrumentation drift, smooth "control"

model data and yaw data from corresponding pitch polars are essential for proper data reduction and interpretation. Some of these factors and assumptions are listed in Figure 5 to indicate the basis for the Magnus data reduction procedure.

For the smooth models, the usual assumption of zero forces and moments at zero spin for all angles of attack is sufficient to eliminate the unwanted effects and provide the typical Magnus data going through the origin. However, this assumption is too liberal for the grooved model data and the more restrictive assumption of zero force and moment only at zero angle of attack must be used, if the groove effects (along with, unfortunately, many unwanted effects) are to be preserved. The groove effects are then isolated from the other extraneous effects by the measures outlined in Figure 5. The difference in Magnus and normal force centers of pressure and comparisons of smooth and grooved body yaw data from pitch polars are also frequently helpful in interpreting the data or sorting out some of the undesirable effects¹⁶. (Although this discussion and Figures 4 and 5 are primarily concerned with the present grooved model, data from any configuration with minor departures from mirror symmetry may require special attention lest the subtle effects one is seeking be obscured or removed in the testing and reduction processes. Small canted fins and canted bore riders are other common examples which may fall in this category.) However, these special testing and reduction techniques are time consuming and should not be applied routinely in general testing but used only when the departure from mirror symmetry reasonably suggests a significant effect.

IV. TEST CONDITIONS

The wind tunnel test conditions are listed in Table 2 and are summarized in Figure 6 along with some typical sea level bullet conditions.

Table 2. Wind Tunnel Test Conditions

<u>Tunnel</u>	<u>Mach No.</u>	<u>Re_q x 10⁻⁶</u>
NASA Ames	0.90	2.0
BRL	1.50	1.8, 3.5
BRL	2.00	2.0, 4.5 ^a , 6.0

a Range check points obtained only for this condition.

16. Anders S. Platou, "Wind-Tunnel Magnus Testing of a Canted Fin or Self-Rotating Configuration," *AIAA Journal*, Vol. 10, No. 7, July 1972, pp. 965-967.

As pointed out previously, wind tunnel data could be obtained essentially from maximum design spin rate to zero. However, since the range check points were obtained at specific values of spin some of the wind tunnel data presented also favor these values which are specified in the listing in Table 3.

Table 3. Representative Spin Conditions

pd/V	$\frac{pd/V}{2 \tan \delta_g}$ ^a	rpm		
		NASA	BRL	
		M = 0.9	M = 1.5	M = 2.0
0	0 (Underspin)	0	0	0
.270 ^b	.86 (Underspin)	7,100	22,300	27,000
.314 ^b	1.00 (Matchspin)	8,300	25,900	31,400
.430 ^b	1.37 (Overspin)	11,400	35,500	43,000
--	--	18,000 ^c	45,000 ^c	45,000 ^c

a Has significance for grooved models only.

b Range check points (M = 2.0 only)

c Maximum design spin rate.

V. BOUNDARY LAYER SIMULATION IN MAGNUS TESTING

Since Magnus forces are basically a boundary-layer caused phenomenon, it follows that the boundary layer characteristics (laminar, turbulent, transitional, thickness, growth, etc.) must be accurately known and appropriately duplicated before results from various tests can be expected to show more than chance agreement. Equating Reynolds numbers is not usually sufficient to give similar boundary layer conditions because of facility and surface finish variables. Also, artificial trip devices must be employed with great care since they can also effect Magnus results¹¹. The boundary layer is sensitive to these (and other) factors even when the model is not spinning and is at zero angle of attack; and it is further modified by cross flows induced by angle of attack and also distorted by spin during Magnus testing. Transition on a model with subsequent skewing by angle of attack and spin is a particularly

sensitive situation¹⁷⁻¹⁹. There is also some indication that body vortices may interact with the boundary layer²⁰ to further confuse the picture. Because of the many complications in simulating and determining the actual boundary layer conditions, it is not surprising that, even though the effects of various factors have been individually demonstrated and are generally known, their collective impact is not always fully appreciated or cannot be properly accounted for. As a result, difficulties in interpreting or comparing Magnus data may occur or, worse yet, model tests may not accurately predict prototype Magnus characteristics. Increased attention must be focused on this area of difficulty to insure compatible results.

As already mentioned, mixed boundary layer conditions and skewed transition present a particularly sensitive situation where simulation may not be practically attainable. Unfortunately, however, small bullets fly in this confused regime and, therefore, the present tests emphasize this region. As a result, the boundary layer conditions are quite variable. For the smooth wind tunnel model at zero angle of attack and $M = 2.00$, transition occurred near (but usually aft of) the model base at a Reynolds number of 4.5×10^6 . At a lower Reynolds number of 2×10^6 , transition occurred further downstream in the wake and, at higher Reynolds number of 6×10^6 , it occurred forward of the base on the latter half of the cylinder. At angle of attack, transition moved forward on the lee side to cause considerable skewing of the transition position around the model. In contrast to the smooth models, transition on the grooved models (for the same test conditions) was forced by the front of the grooves and tended to remain less skewed at angles of attack. With a boundary layer trip transition was, of course, fixed at the trip position near the nose for both the smooth and grooved wind tunnel models. In the range, boundary layer transition occurred naturally somewhat forward of the grooves (but with considerable variation) for low angles of attack and $Re = 4.5 \times 10^6$. This most closely approximates the wind tunnel tripped boundary-layer condition. At Mach number 0.9, the wind-tunnel model boundary-layer conditions were

17. W. B. Sturek, "Boundary Layer Studies on a Spinning Cone," U.S. Army Ballistic Research Laboratories Report No. 1649, Aberdeen Proving Ground, Maryland, May 1973. AD 762564.
18. Walter B. Sturek, "Boundary Layer Studies on Spinning Bodies of Revolution," U.S. Army Ballistic Research Laboratories Memorandum Report No. 2381, Aberdeen Proving Ground, Maryland, May 1974. AD 920069L.
19. Edwin P. Birthwell, "Magnus Forces and Sting Interference on Magnetically-Suspended Ogive Cylinders," Masters Thesis, Massachusetts Institute of Technology, May 1974.
20. J. M. Martin and C. W. Ingram, "Experimental Correlation Between the Flow and Magnus Characteristics of a Spinning Ogive-Nose Cylinder," *AIAA Journal*, Vol. 11, July 1973, pp. 901-902.

not well defined but transition apparently occurred on the forward portion of the model whether tripped or not.

VI. PRESENTATION OF DATA

Some limited but typical Magnus results at $M = 2.0$ are presented in Figures 7-13 to illustrate significant points in the results and discussion, and a summary of pitching moment data is shown in Table 4. In addition, all of the basic Magnus data are included in Figures A1 and A2 of the Appendix, and these Magnus data are summarized for a particular value of $pd/V = 0.314$ in Figure A3. Comparisons of wind tunnel and range data are presented in Figure A4. Figure A5 shows an example of some basic pitching moment data.

VII. DISCUSSION OF RESULTS

The discussion of results emphasizes the Magnus data at Mach number 2.0 where most of the testing was done. The Mach number 0.9 data included in the Appendix have not been thoroughly analyzed but, with somewhat less clarity and consistency, show some of the same trends evidenced at the higher Mach number. This was more true for the boat-tail than the cylindrical tail model.

A. Wind Tunnel Magnus Tests

The wind tunnel Magnus data in Figures 7-13 are mainly presented as the moment coefficient, C_n (or its derivatives), where the moment is referred to a point two calibers forward of the model base. These coefficients are derived from the moments induced in the yaw plane by spin and angle of attack. The corresponding force coefficients are not shown since they generally (with a few exceptions) show similar trends.

Some typical wind tunnel Magnus moment data at $M = 2.0$ are presented in Figure 7 for the boattail model at a Reynolds number of 4.5×10^6 . The similarity of the data at positive and negative angles of attack is a favorable indication of data quality. In this connection, it is also interesting to note the good check (after accounting for sign change) between the data of Figure 7a and that in Appendix Figure 2A-30 where the model is spinning in the opposite direction. For the smooth model without boundary layer trip (Figure 7a), the Magnus moment data are seen to be nonlinear, especially at the lower angles of attack. This is primarily caused by mixed boundary layer conditions and skewed transition discussed previously. This condition is very sensitive to Reynolds number and the nonlinearities (Appendix Figures A2-28 and 31) are quite different in appearance at $Re_\ell = 2$ and 6×10^6 . (The force coefficients were not so strongly nonlinear which implies a center of pressure shift.) In contrast, the smooth model with boundary layer trip (Figure 7b) shows

well-behaved nearly-linear data which is typical for the fixed transition case. Figure 7c shows Magnus data for the grooved model with boundary layer trip. The "offset" effect of the grooves on the Magnus data is similar to that previously reported^{2,3} for models with accentuated helical serrations and, surprisingly, of comparable magnitude. However, no corresponding strong nonlinearities with spin mismatch are evident. The "offset" effect referred to is the moment at zero spin which opposes the Magnus moment and causes an apparent origin at $pd/V \approx 0.1$. Otherwise, the grooved body data is very similar to that of the smooth body since the slopes are about comparable. The data for the models without boattails showed similar, although not identical, trends.

In order to investigate the nature of the "offset" effect, vapor screen, shadowgraph and oil streak photographs were obtained at zero rpm with the models locked in various roll positions. Although results from the first two methods were inconclusive, the latter yielded some interesting qualitative information. This is summarized in Figure 8 and indicates that the boundary layer (or at least the surface flow) is rotated somewhat in the direction of the groove twist. The easiest way to visualize the data in Figure 8a is to imagine the model as having been run at the conditions indicated. Then, with the oil pattern frozen, the oil streak angle is measured with respect to the model axis as each of the positions noted is rotated to face the viewer. These data indicate that the local oil streak angle of the grooved model tends away from that for the smooth model and in the direction of the groove angle, δ_g , for each viewing position, ϕ , except 90° where all angles are coincidentally the same. Figure 8b shows the approximate surface streamlines interpreted from the oil-streak-angle data. This rotation of angle-of-attack-distorted boundary layer is in the opposite direction to that caused by spin and, thus, could explain the offset effect.

It is interesting to note that the center of pressure of the force induced by the grooves on the non-spinning body is generally at about the same location as that of the Magnus force. This lends added weight to the speculation of an oppositely-rotated boundary layer, the effects of which would be cumulative along the body and, thus, most effective over the rear part where the Magnus force also acts. A possible added contribution to the offset effect is the thickening of the boundary layer on one side of the model and a thinning on the other as a result of geometric asymmetries when the model is at an angle of attack (groove angles with respect to the flow differ on opposite sides of the model.)

The main effect of the offset in the Magnus data is to cause a reduction in $C_{np\alpha}$ which is one of the parameters affecting bullet stability. As an example, $C_{np\alpha} = C_n / \left(\frac{pd}{V} \alpha \right)$ has been calculated from the data in Figures 7b and c and is presented as a function of pd/V in Figure 9. Although not specifically identified the various symbols represent different angles of attack from -4 to 13 degrees. Part "a" indicates the relatively constant $C_{np\alpha}$ of the smooth body and the average value (dashed

line) is reproduced on part "b" of the figure for reference. The grooved body shows a moderate reduction in $C_{np\alpha}$ for the overspin condition. At lower values of spin, the reduction is more severe and for sufficient underspin the sign of the Magnus moment becomes negative and then "blows up". The relatively close grouping of the data points for these two models indicates that the Magnus moments for these particular configurations are approximately linear with angle of attack. This is shown more clearly in Figure 10 where the data are cross plotted (heavy solid line) for a constant value (0.31) of the spin parameter.

Also shown in Figure 10 are range check points and wind tunnel data for the models with no trip at Reynolds numbers of 2, 4.5 and 6 x 10⁶. (It will be recalled that the range boundary layer characteristics were intermediate between those of the tripped and untripped wind tunnel model but closer to the tripped case. More detailed comparison of wind tunnel and range data will be made in a later section.) In Figure 10a, the $C_{np\alpha}$ for models with a boundary layer trip is probably higher because of the thicker boundary layer¹¹. However, the data for models without trips is quite consistent for the various Reynolds numbers. This implies a tendency for the boundary layer to be tripped relatively uniformly by the front of the grooves, thus minimizing skewed transition effects. In contrast, smooth models without boundary layer trips (Figure 10b) indicate the strong influence of skewed boundary layer transition. Considering the extreme sensitivity of this condition to Reynolds number, the repeatability of the data for positive and negative angles of attack is quite remarkable.

B. Stability Considerations

The effects of Magnus moment on stability can be examined by assuming typical aerodynamic and physical "constants" and computing the dynamic stability, S_d , or exponential damping coefficients, λ_1 and λ_2 , as linear functions of $C_{np\alpha}$ ^{21,22}. Figures 11 and 12 show the results of such calculations (diagonal lines) where the aerodynamic and physical constants used were averages of those for the range firings associated with this program. The range data are included in the figures to verify the calculated curves. The stability boundaries in Figure 11 were determined by using the range value for gyroscopic stability, S_g , and the generalized stability plot of reference 21. Ordinarily, these boundaries

21. C. H. Murphy, "Free Flight Motion of Symmetric Missiles," U.S. Army Ballistic Research Laboratories Report No. 1216, Aberdeen Proving Ground, Maryland, July 1963. AD 442757.
22. Anders S. Platou, "The Influence of the Magnus Moment on the Dynamic Stability of a Projectile," U.S. Army Ballistic Research Laboratories Memorandum Report No. 2155, Aberdeen Proving Ground, Maryland, January 1972. AD 738016.

would tend to move toward each other as the spin rate reduces but, in this case, the bullet physical properties were adjusted to approximately compensate for the spin reduction. It will be noted that if $C_{np\alpha}$ varies sufficiently in magnitude (< -0.1 or > 0.8) then either the slow or fast mode motion undamps and dynamic instability is encountered.

The wind tunnel data are shown as heavy bars superposed on the calculated data and are for both cylindrical and boattail models and for the range of spin and angle of attack indicated. A comparison of the results for the smooth and grooved models with boundary layer trip indicates that the reduction in $C_{np\alpha}$ caused by the grooves is not particularly significant for moderate amounts of overspin and underspin, $pd/V = 0.27 - 0.43$. This would probably also be true for even greater overspin since an extrapolation of the results of Figure 9b would imply increasingly closer coincidence for the smooth and grooved model Magnus moments. This overspin region is pertinent to bullets in the down range portion of flight. On the other hand, bullets with gross underspin might become unstable because of the sharp reduction in Magnus moment (see Figure 9b). This is the case of bullets fired from a moving airplane. (In range experiments, bullets fired from a stationary gun cannot be despun to provide such large underspin because they become gyroscopically unstable. This implies that, if free flight investigations are to be made in this region, a forward moving platform must be used to reduce pd/V rather than a reduction in spin as is done in the wind tunnel.)

Also shown on Figure 11 are the wind tunnel results for the grooved models with no trip. Corresponding results for the smooth models without trip are not shown but would range from one stability boundary to the other because of the mixed boundary layer and skewed transition effects mentioned previously. This further emphasizes the importance of boundary layer simulation if experimental Magnus data are to be used for stability predictions. However, mixed boundary layer conditions present a particularly sensitive situation where simulation may not be reasonably attainable. Unfortunately, smaller bullets frequently fly in this sensitive region and it would appear likely that mixed boundary layer conditions and skewed transition, rather than groove effects, might be the cause of erratic stability behavior of bullets at longer ranges. As pointed out previously, the grooves may even have a beneficial effect in tending to fix transition so that skewing is reduced.

Figure 12 presents information similar to that just discussed for Figure 11 except that the exponential damping coefficients are used as the stability criteria and the data are for a single pd/V value rather than for a range of this parameter. The dashed lines are used to identify the data bars, not to indicate a specific value.

It should be pointed out that most of the previous stability considerations are for the specific conditions associated with these particular models and that other bullet models could present a somewhat different picture. For instance, variations in $C_{np\alpha}$ might be either

adverse or beneficial depending on the other physical and aerodynamic properties involved. However, it would still appear that minor variations in $C_{np\alpha}$ (such as those caused by the groove effects in the overspin condition) would not be serious; while larger variations (such as those caused by the groove effects at large underspin or by mixed boundary layer conditions) could have significant implications for bullet stability.

C. Comparisons of Wind Tunnel and Range Magnus Data

A number of grooved models were fired in support of the present test program. However, after these were divided up for various test conditions only a few rounds at each specific test condition were available. Comparisons of range and wind tunnel data for grooved models with predominantly turbulent boundary layer or fixed transition are shown in Appendix Figures 4A-1 through 6 and are summarized in Figure 13a.

The comparisons are quite good even though much of the range data is at too low angle of attack to be useful. The smooth model results are shown for reference and the results for the grooved model without trip, although not shown, would fall somewhat erratically below the presented data. As mentioned previously, the range boundary layer conditions favored those of the grooved wind-tunnel model with trip. Although planned, no range data are presently available for the smooth model with fixed transition.

For the more sensitive case of smooth models with mixed boundary layer conditions, simulation becomes much more difficult and no match was found between the wind tunnel and range models. Quite surprisingly, natural transition always occurred more forward on the range models. A search of the literature for other appropriate range data was not much more rewarding except for reference 7 which yielded five rounds with approximately comparable boundary layer conditions and Reynolds numbers. A comparison of this range data with that of the present wind tunnel tests is shown in Figure 13b and the agreement is favorable considering the difficulties associated with this mixed boundary layer condition.

D. Pitching Moment Data

The forces and moments in the pitch plane were obtained incidental to the Magnus data. A typical plot of some basic pitching moment data is shown in Appendix Figure A5 and the pitching moment slopes at zero angle of attack, $C_{m\alpha 0}$, are summarized in Table 4 along with some values from several references. The values are in general agreement and any possible groove effects are small and insignificant.

Table 4. Pitching Moment Coefficient Slope Summary

Configuration	$C_{m\alpha}$				
	Wind Tunnel		Range		
	Present ^a Tests	Refs. 5,6 ^b	Present ^a Tests	Ref. 7 ^b	Ref. 4 ^b
a. <u>M = 0.9</u>					
Cylindrical Smooth	3.45	3.3	--	3.2	--
" Grooved	3.46	--	--	--	--
Boattail Smooth	4.23	4.1	--	3.9	--
" Grooved	4.41	--	--	--	--
b. <u>M = 1.5</u>					
Cylindrical Smooth	--	3.9	--	3.8	3.9
" Grooved	4.07	--	--	--	--
c. <u>M = 2.0</u>					
Cylindrical Smooth	3.75	3.6	3.77	3.5	3.7
" Grooved	3.68	--	3.77	--	--
Boattail Smooth	3.82	3.9	--	3.7	--
" Grooved	3.75	--	3.73	--	--

a Average value

b Interpolated, extrapolated and/or average value

VIII. CONCLUSIONS

Magnus tests on smooth and engraved Army-Navy Spinner models have shown, particularly at Mach number 2.0 but to some extent at Mach number 0.9 also, that:

(1) No significant Magnus nonlinearities with spin mismatch are caused by the 20mm equivalent engraving,

(2) The basic Magnus data, C_n , for the grooved (engraved) models are "offset" from that of corresponding smooth models,

(3) The offset in the Magnus data is probably caused by the tendency of the grooves to rotate the boundary layer towards alignment with the grooves,

(4) The offset in the data causes a measurable reduction in $C_{np\alpha}$ for the overspin condition and a much greater reduction for large underspin,

(5) The effect of the grooves on stability is not significant for the overspin condition but is appreciable for sufficient underspin,

(6) Proper boundary layer simulation must be provided if reliable predictions of Magnus characteristics are to be made from experimental results or if other than chance agreement is to be expected from various tests or facilities, and

(7) Magnus results are particularly sensitive to mixed boundary layer and skewed transition effects which are present when natural transition occurs on a model.

REFERENCES

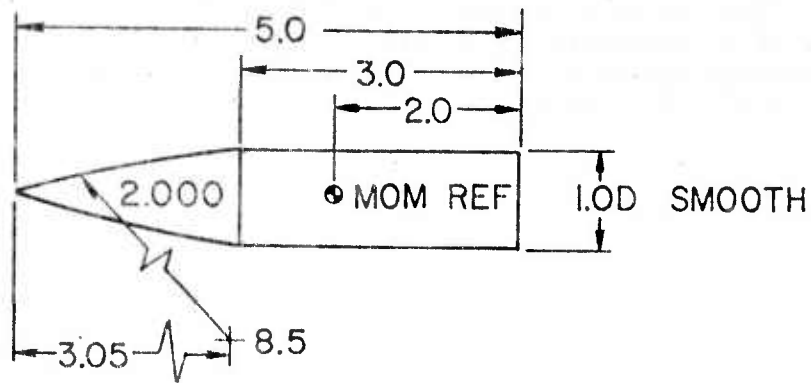
1. M. J. Piddington, "Deformation Characteristics of One Lot (LC SP412) of 5.56 mm M-193 Ammunition," U.S. Army Ballistic Research Laboratories Memorandum Report No. 2016, Aberdeen Proving Ground, Maryland, October 1969. AD 862966.
2. M. A. Sylvester and W. F. Braun, "The Influence of Helical Serrations and Bullet Engraving on the Aerodynamic and Stability Properties of a Body of Revolution With Spin," U.S. Army Ballistic Research Laboratories Report No. 1514, Aberdeen Proving Ground, Maryland, November 1970. AD 719235. Also, AIAA Paper No. 70-557, AIAA Atmospheric Flight Mechanics Conference, Tullahoma, Tennessee, May 1970.
3. Maurice A. Sylvester, "Influence of Helical Serrations on the Aerodynamic Properties of a Spinning Body," *AIAA Journal*, Vol. 10, No. 2, February 1972, pp. 223-225.
4. C. H. Murphy and L. E. Schmidt, "The Effect of Length on the Aerodynamic Characteristics of Bodies of Revolution in Supersonic Flight," U.S. Army Ballistic Research Laboratories Report No. 876, Aberdeen Proving Ground, Maryland, August 1953. AD 23468.
5. J. B. Carmen, J. C. Uselton, and W. E. Summers, "Experimental Magnus Characteristics of Basic and Boattail Configurations of 3- and 5-Caliber Army-Navy Spinner Projectiles at Subsonic and Transonic Mach Numbers," AEDC-TR-70-36, April 1970.
6. J. B. Carmen and James Uselton, "Experimental Magnus Characteristics of Basic and Boattail Configurations of 3- and 5-Caliber Army-Navy Spinner Projectiles at Supersonic Mach Numbers," AEDC-TR-69-178, November 1969.
7. G. L. Winchenbach, R. M. Watt and A. G. Skinner, "Free Flight Range Tests of Basic and Boattail Configurations of 3- and 5-Caliber Army-Navy Spinner Projectiles," AEDC-TR-70-12, March 1970.
8. C. W. Ingram, R. J. Lusardi and V. D. Nicolaidis, "Effects of Rifling and N-Vanes on the Magnus Characteristics of Bodies of Revolution," AIAA Paper No. 72-970, AIAA 2nd Atmospheric Flight Mechanics Conference, Palo Alto, California, September 1972.
9. G. I. T. Nielsen and Anders S. Platou, "The Effect of Conical Boattails on the Magnus Characteristics of Projectiles at Subsonic and Transonic Speeds," U.S. Army Ballistic Research Laboratories Report No. 1720, Aberdeen Proving Ground, Maryland, June 1974.

REFERENCES (Continued)

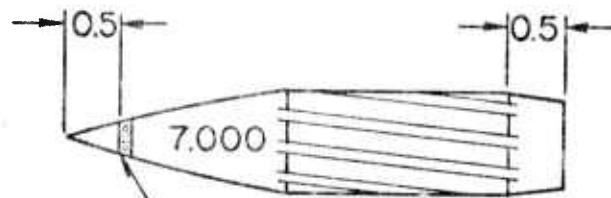
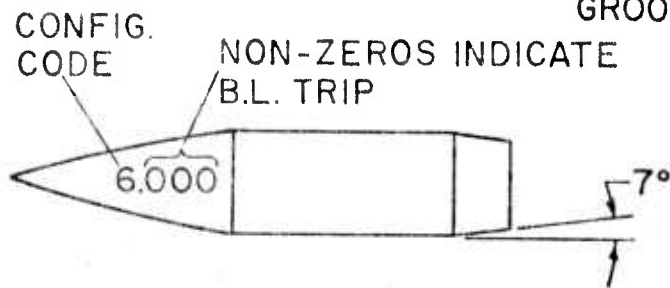
10. Leroy M. Jenke, "Experimental Magnus Characteristics of Ballistic Projectiles With and Without Anti-Magnus Vanes at Mach Numbers 1.5 Through 2.5," AEDC-TR-73-162 (AFATL-TR-73-188), December 1973.
11. Anders S. Platou, "Magnus Characteristics of Finned and Nonfinned Projectiles," *AIAA Journal*, Vol. 3, No. 1, January 1965, pp. 83-90.
12. Klaus O. Opalka, "Wind Tunnel Test of a Spinning, Low-Drag Projectile With Canted Bore Riders at Mach Numbers From 1.75 to 2.5," U.S. Army Ballistic Research Laboratories Memorandum Report No. 2349, Aberdeen Proving Ground, Maryland, January 1974. AD 774804.
13. J. C. McMullen, "Wind Tunnel Testing Facilities at the Ballistic Research Laboratories," U.S. Army Ballistic Research Laboratories Memorandum Report No. 1292, Aberdeen Proving Ground, Maryland, July 1960. AD 244180.
14. C. S. Pirrello, R. D. Hardin, M. V. Heckart and K. R. Brown, "An Inventory of Aeronautical Ground Facilities, Vol. 1--Wind Tunnels," NASA CR-1874, November 1971.
15. L. D. Kayser, "The BRL Wind Tunnel High Speed Analog-to-Digital Data Acquisition System," U.S. Army Ballistic Research Laboratories Memorandum Report No. 2142, Aberdeen Proving Ground, Maryland, December 1971. AD 737180.
16. Anders S. Platou, "Wind-Tunnel Magnus Testing of a Canted Fin or Self-Rotating Configuration," *AIAA Journal*, Vol. 10, No. 7, July 1972, pp. 965-967.
17. W. B. Sturek, "Boundary Layer Studies on a Spinning Cone," U.S. Army Ballistic Research Laboratories Report No. 1649, Aberdeen Proving Ground, Maryland, May 1973. AD 762564.
18. Walter B. Sturek, "Boundary Layer Studies on Spinning Bodies of Revolution," U.S. Army Ballistic Research Laboratories Memorandum Report No. 2381, Aberdeen Proving Ground, Maryland, May 1974.
19. Edwin P. Birtwell, "Magnus Forces and Sting Interference on Magnetically-Suspended Ogive Cylinders," Masters Thesis, Massachusetts Institute of Technology, May 1974.
20. J. M. Martin and C. W. Ingram, "Experimental Correlation Between the Flow and Magnus Characteristics of a Spinning Ogive-Nose Cylinder," *AIAA Journal*, Vol. 11, July 1973, pp. 901-902.

REFERENCES (Continued)

21. C. H. Murphy, "Free Flight Motion of Symmetric Missiles," U.S. Army Ballistic Research Laboratories Report No. 1216, Aberdeen Proving Ground, Maryland, July 1963. AD 442757.
22. Anders S. Platou, "The Influence of the Magnus Moment on the Dynamic Stability of a Projectile," U.S. Army Ballistic Research Laboratories Memorandum Report No. 2155, Aberdeen Proving Ground, Maryland, January 1972. AD 738016.

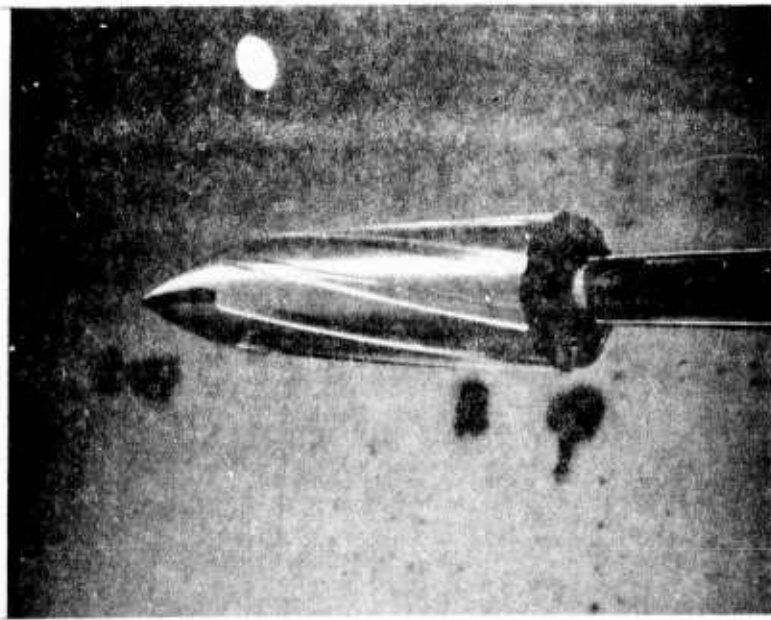


20MM EQUIVALENT ENGRAVING
 9 GROOVES, 0.115 X 0.205
 1 TURN IN 20 CAL. TWIST
 GROOVE ANGLE = 9°

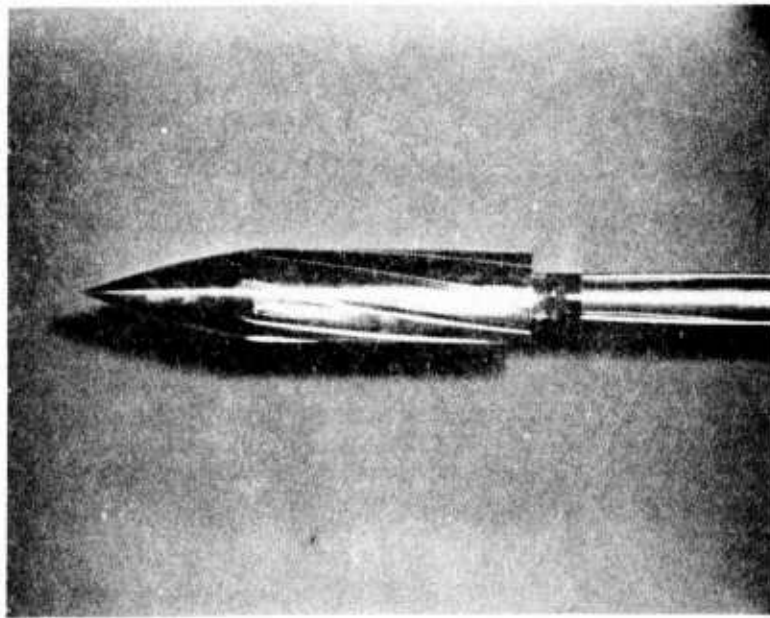


All linear dimensions in calibers; 1 caliber = 2 inches (5.1 cm)
 BRL Tunnel, 4.25 inches (10.8 cm) NASA Ames Tunnel, 0.79 inches
 (2.0 cm) BRL Range.

Figure 1. Smooth and Engraved A-N Spinner Models



a. NASA Ames



b. BRL

Figure 2. Models Installed in Wind Tunnels

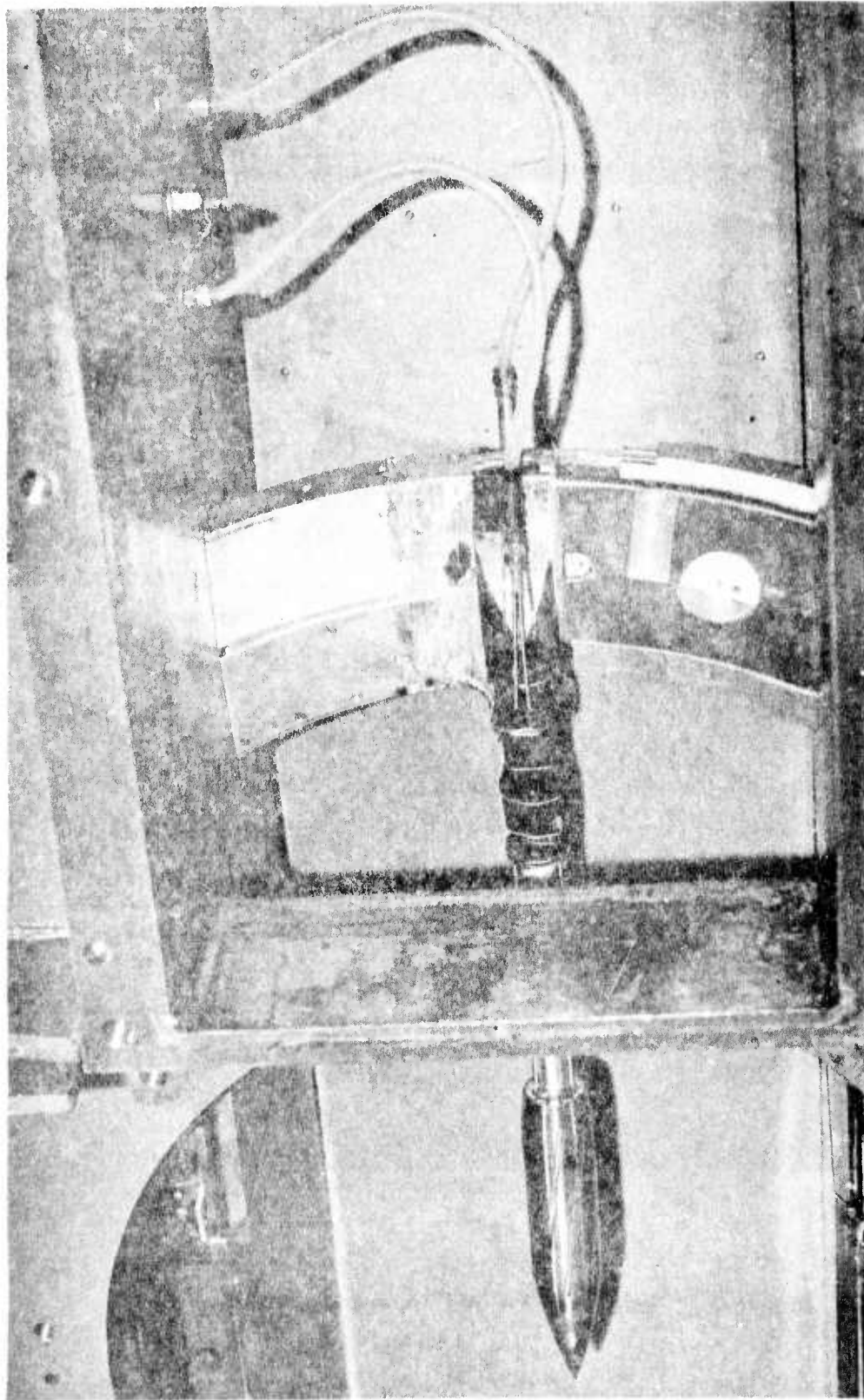


Figure 3. Overall Installation in BRL Wind Tunnel

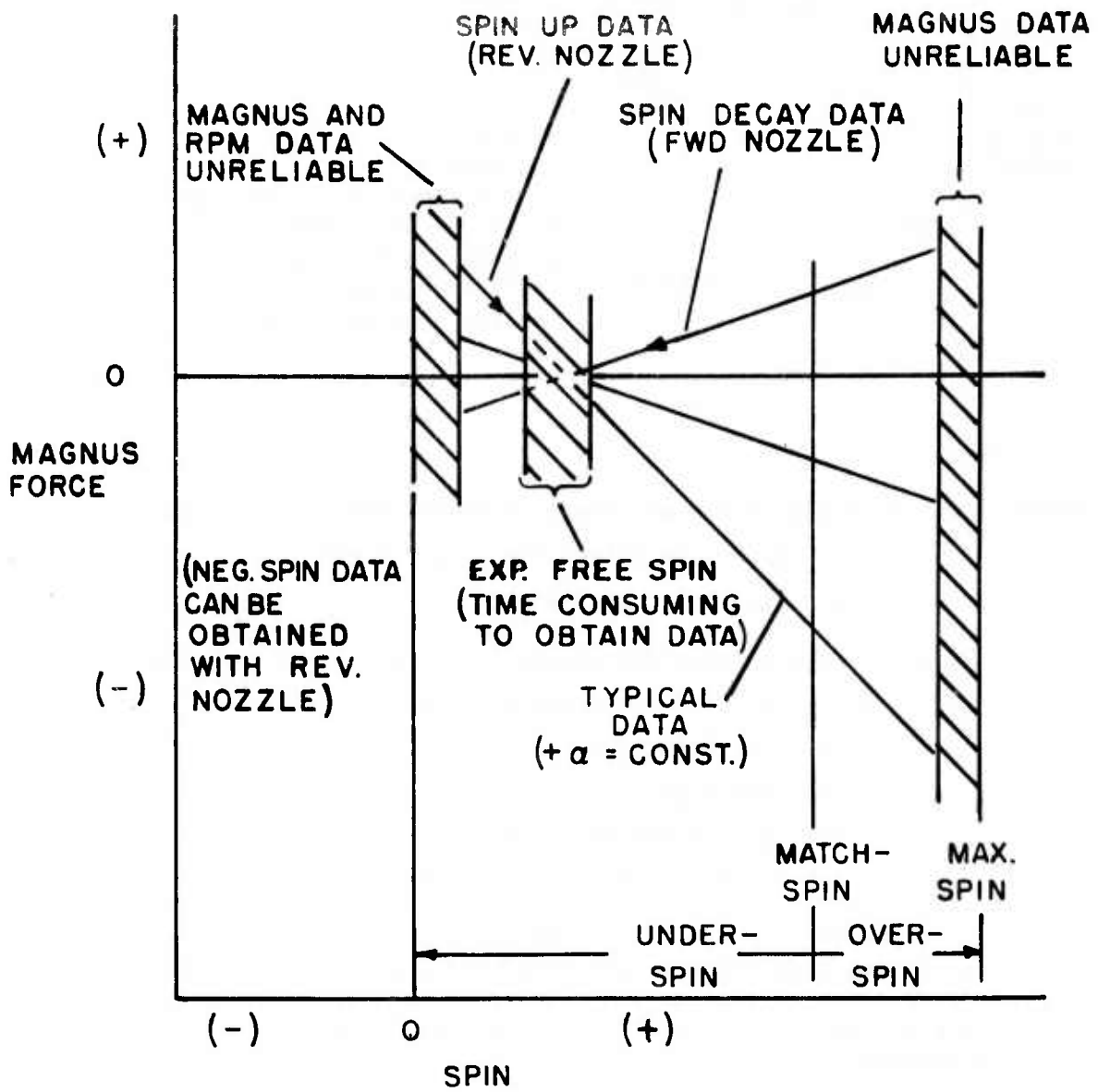
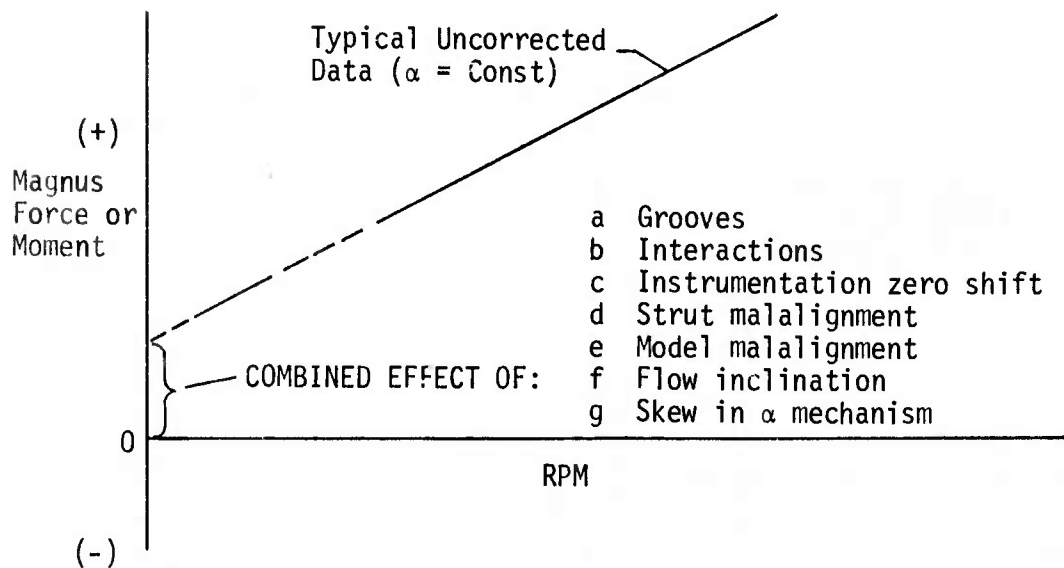


Figure 4. Magnus Test Procedure Summary for Grooved Models



SMOOTH MODEL -- Assume force and moment = 0 when RPM = 0 for each α

- a No groove effect for smooth model
- b-g Eliminated by assumption

GROOVED MODEL -- Assume force and moment = 0 when RPM = 0 only for $\alpha = 0$

- a Desired measurement to be isolated
- b Calibrate out
- c Minimize
- d,e Eliminated by assumption
- f,g Eliminate by assuming same as smooth

NOTE: Yaw plane data from pitch polars at zero spin, difference in normal and Magnus force centers of pressure, and uncanted- or no-groove configuration data are often helpful in reducing data and interpreting Magnus results for configurations with mirror asymmetry.

Figure 5. Some Factors and Assumptions Involved in Magnus Data Reduction and Interpretation

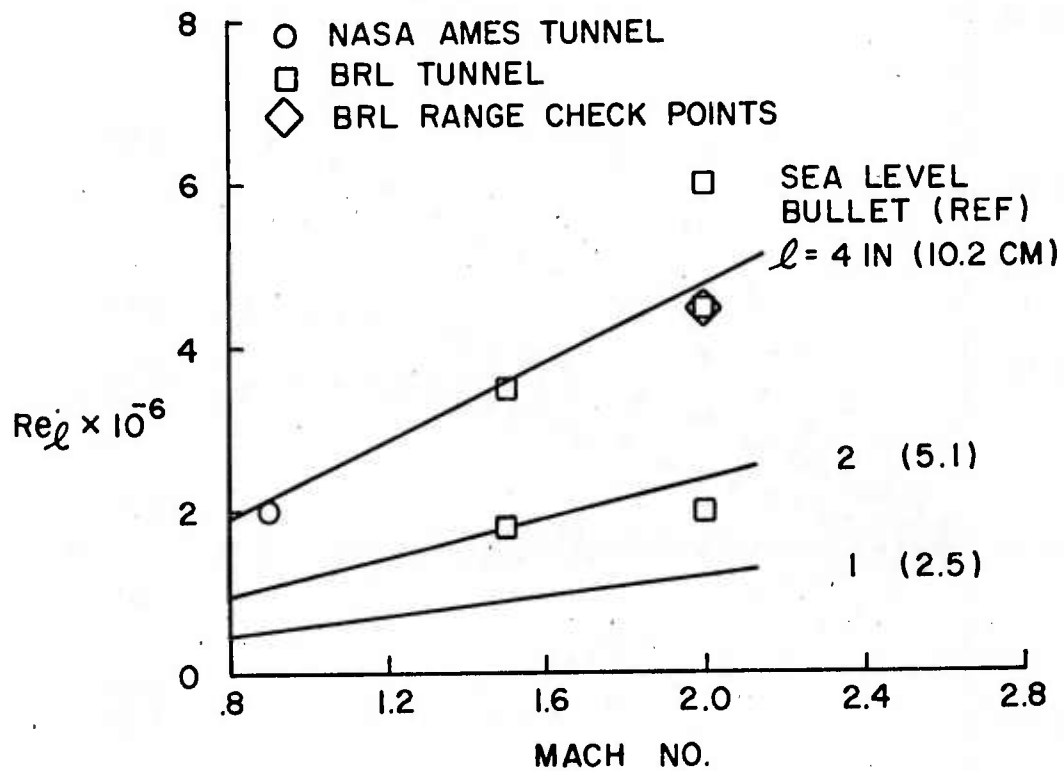
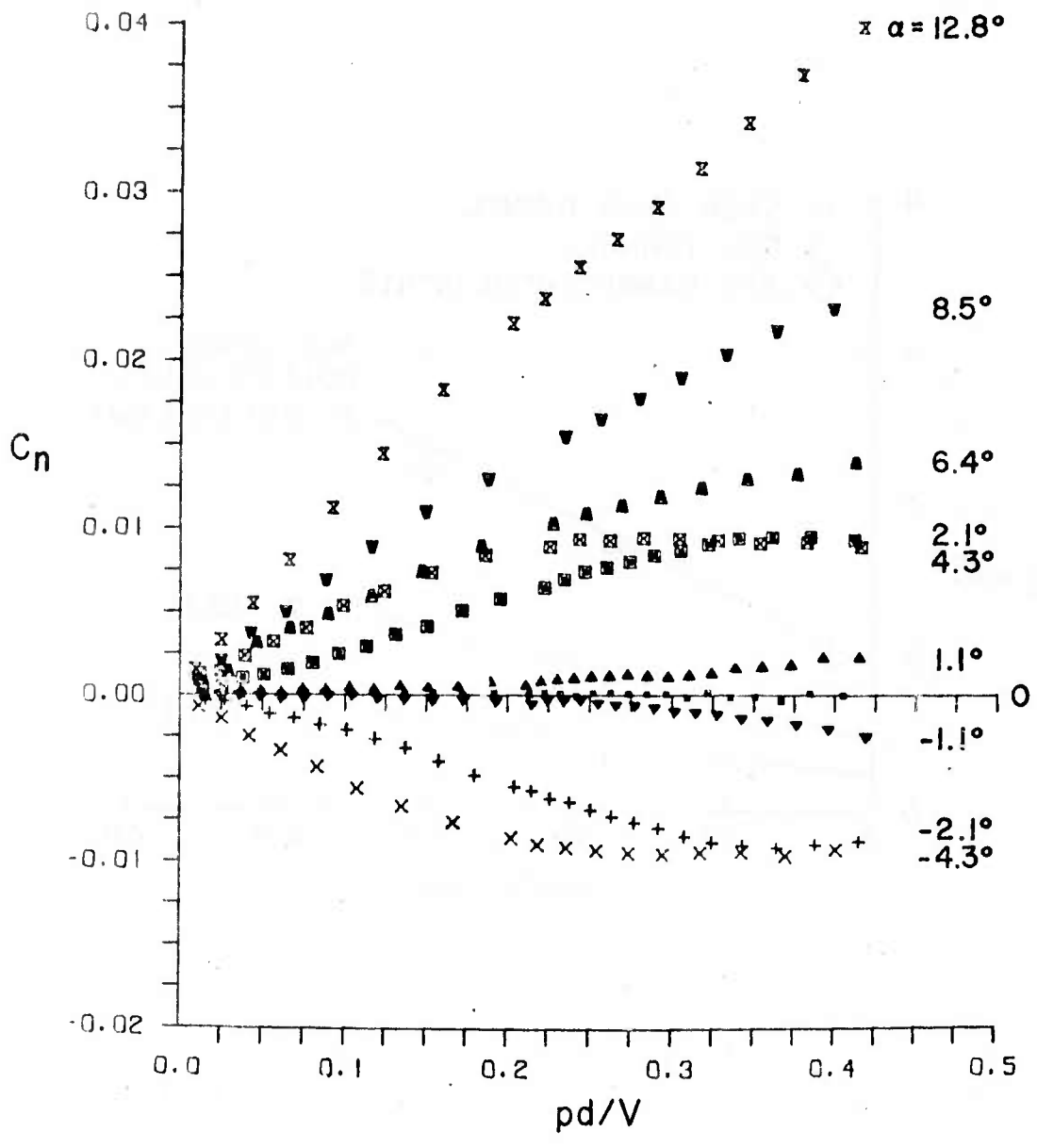
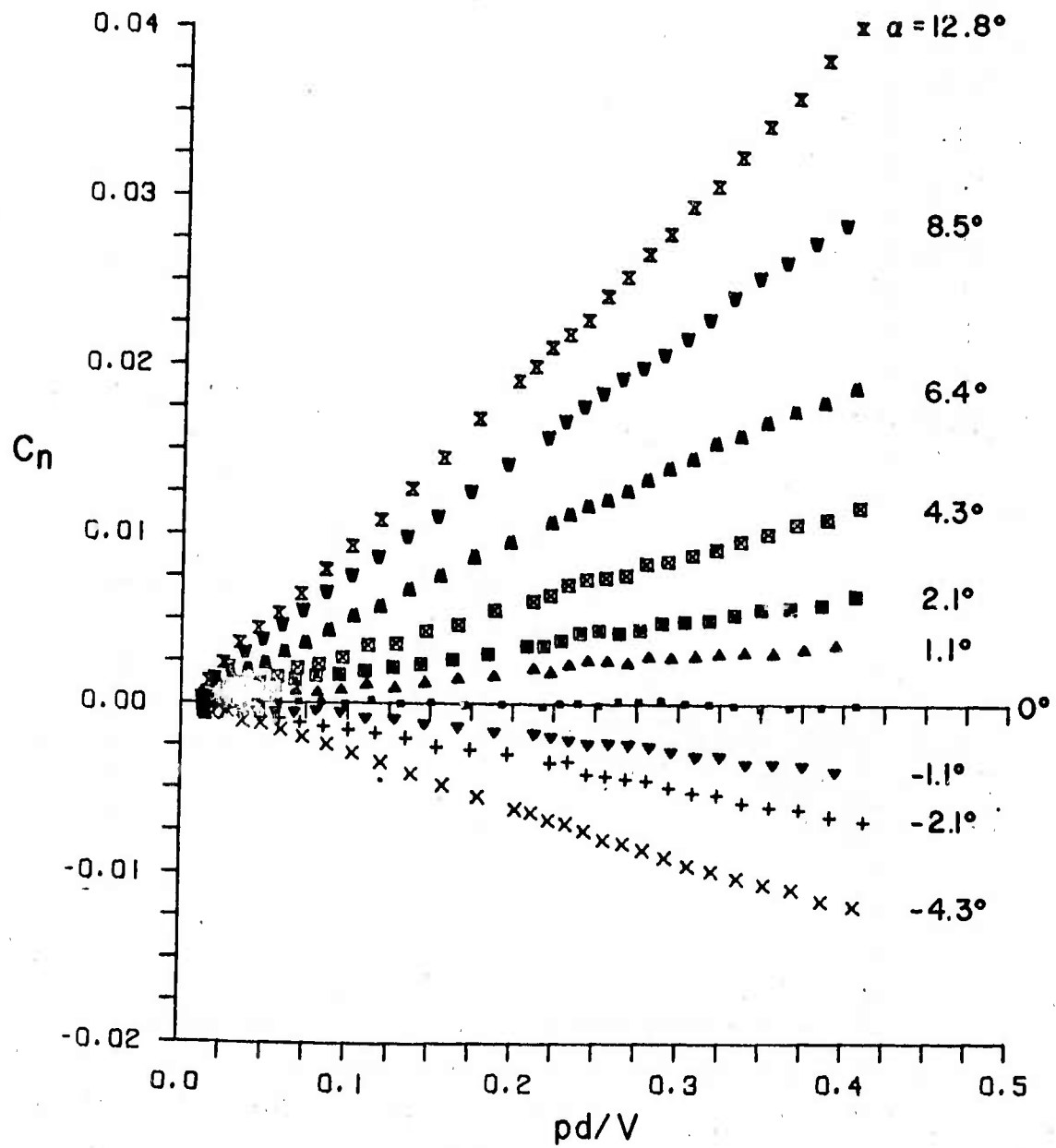


Figure 6. Test Condition Summary



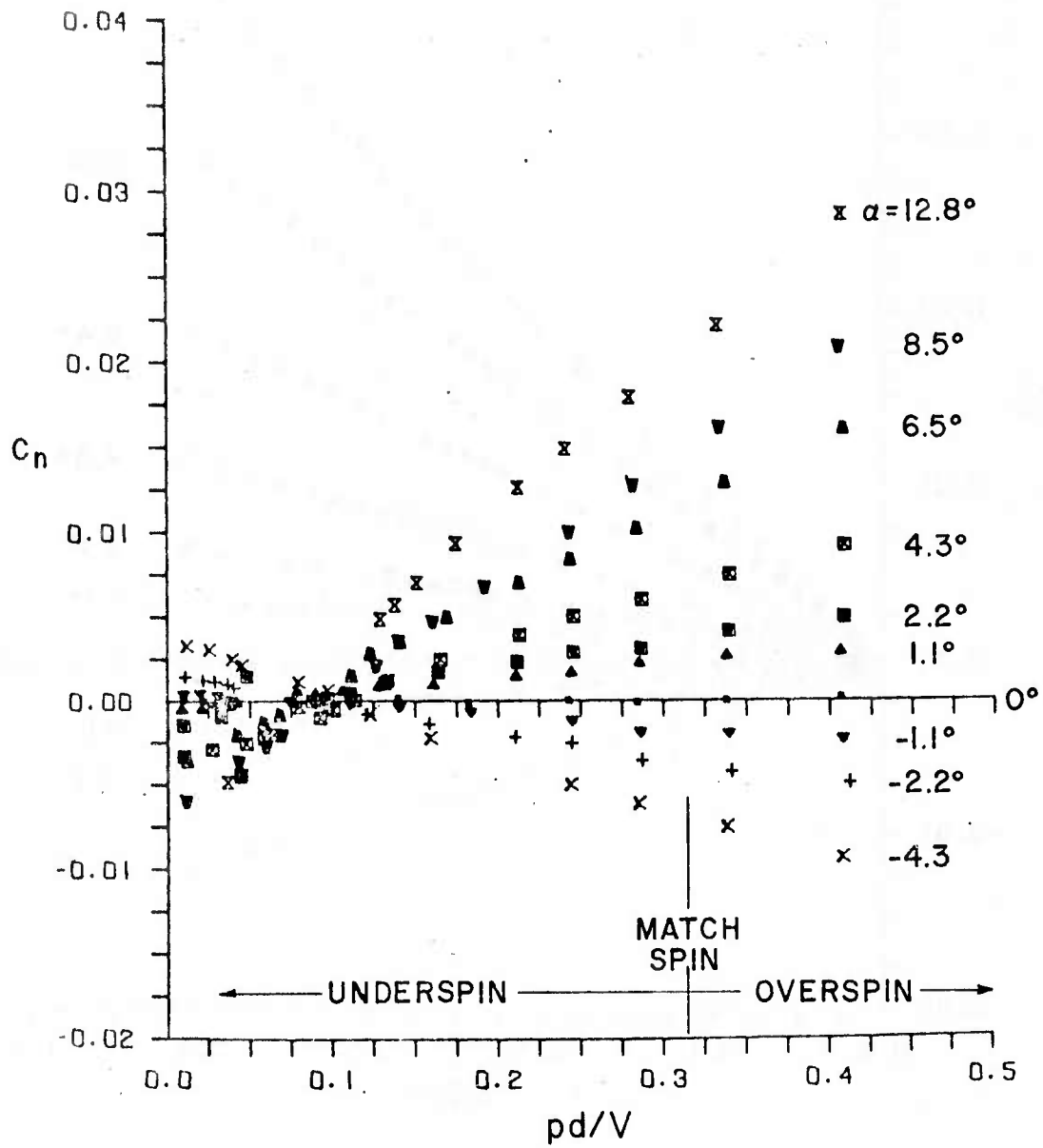
a. Smooth Model Without Boundary Layer Trip

Figure 7. Typical Magnus Data
 (Boattail Model, $M = 2.0$, $Re_{\ell} = 4.5 \times 10^6$)



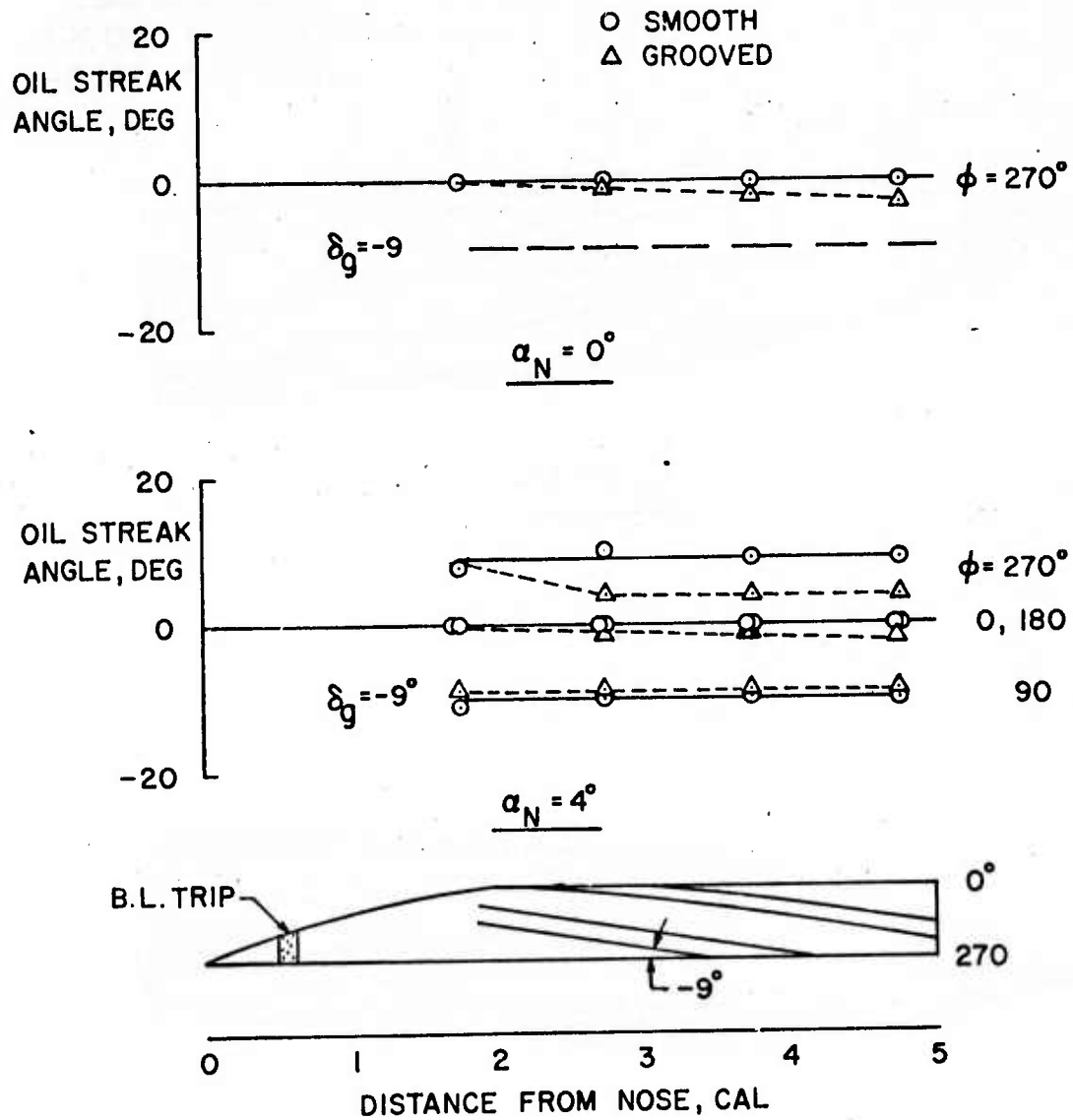
b. Smooth Model With Boundary Layer Trip

Figure 7. Continued



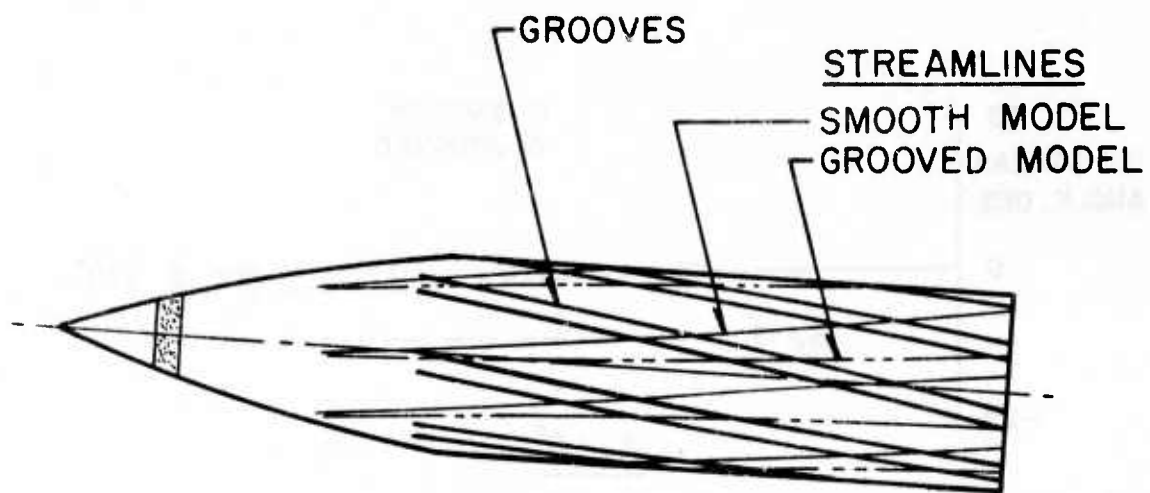
c. Grooved Model With Boundary Layer Trip

Figure 7. Concluded

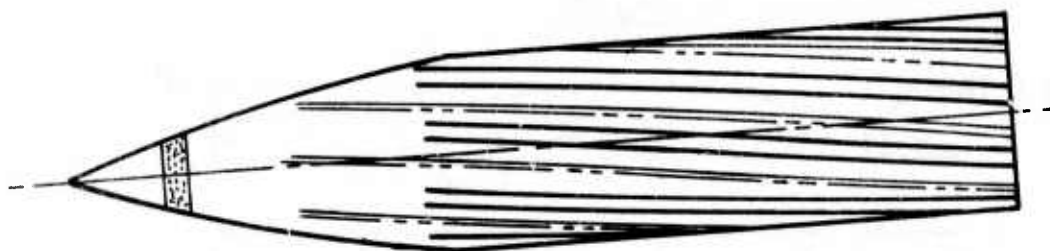


a. Oil Streak Angle

Figure 8. Oil Streak Results Showing Rotation Effect of Grooves on Surface Flow ($M = 2.0$, $pd/V = 0$, $Re_\rho = 4.5 \times 10^6$)



$$\underline{\alpha_N = +4^\circ}$$

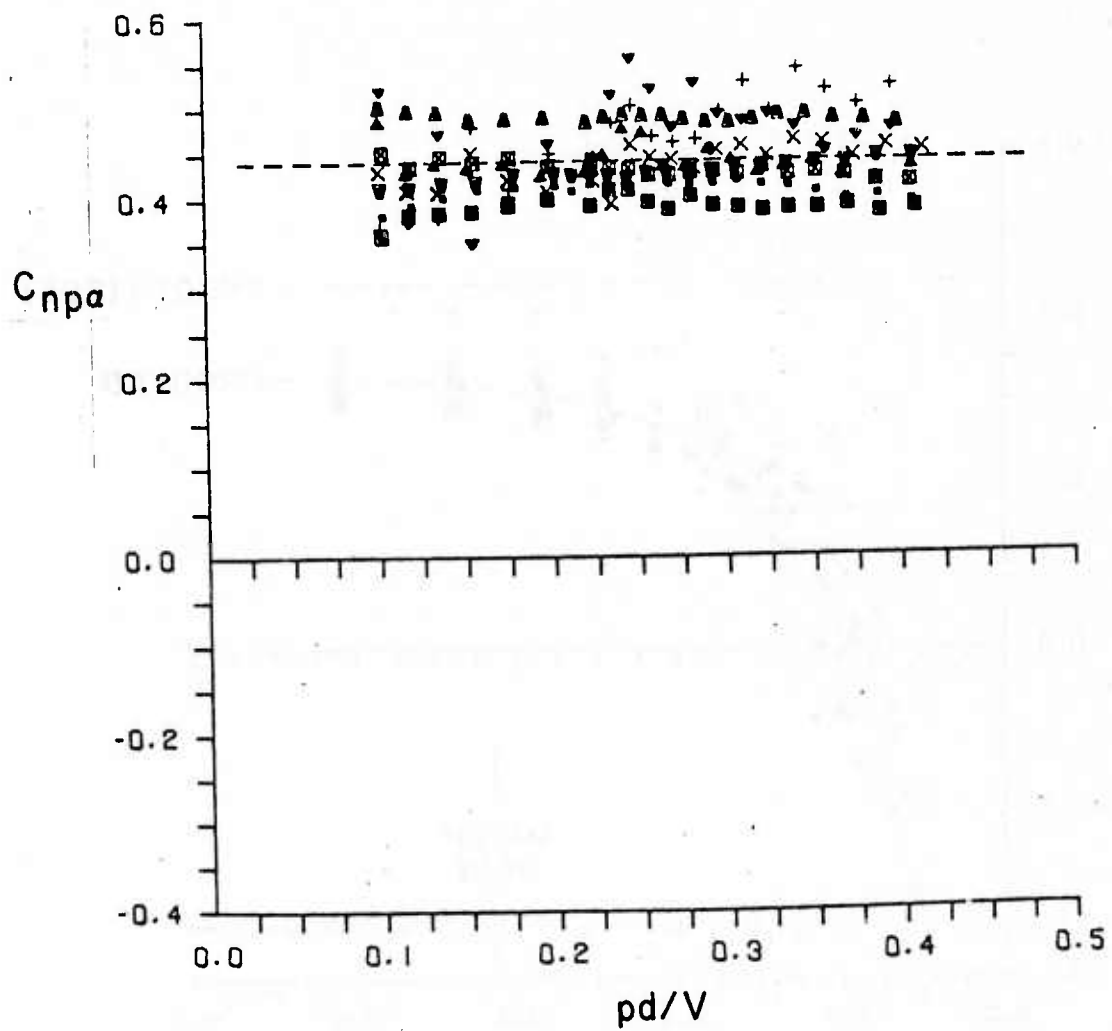


$$\underline{\alpha_N = -4^\circ}$$

(EQUIVALENT TO OTHER SIDE OF MODEL AT $\alpha = +4^\circ$)

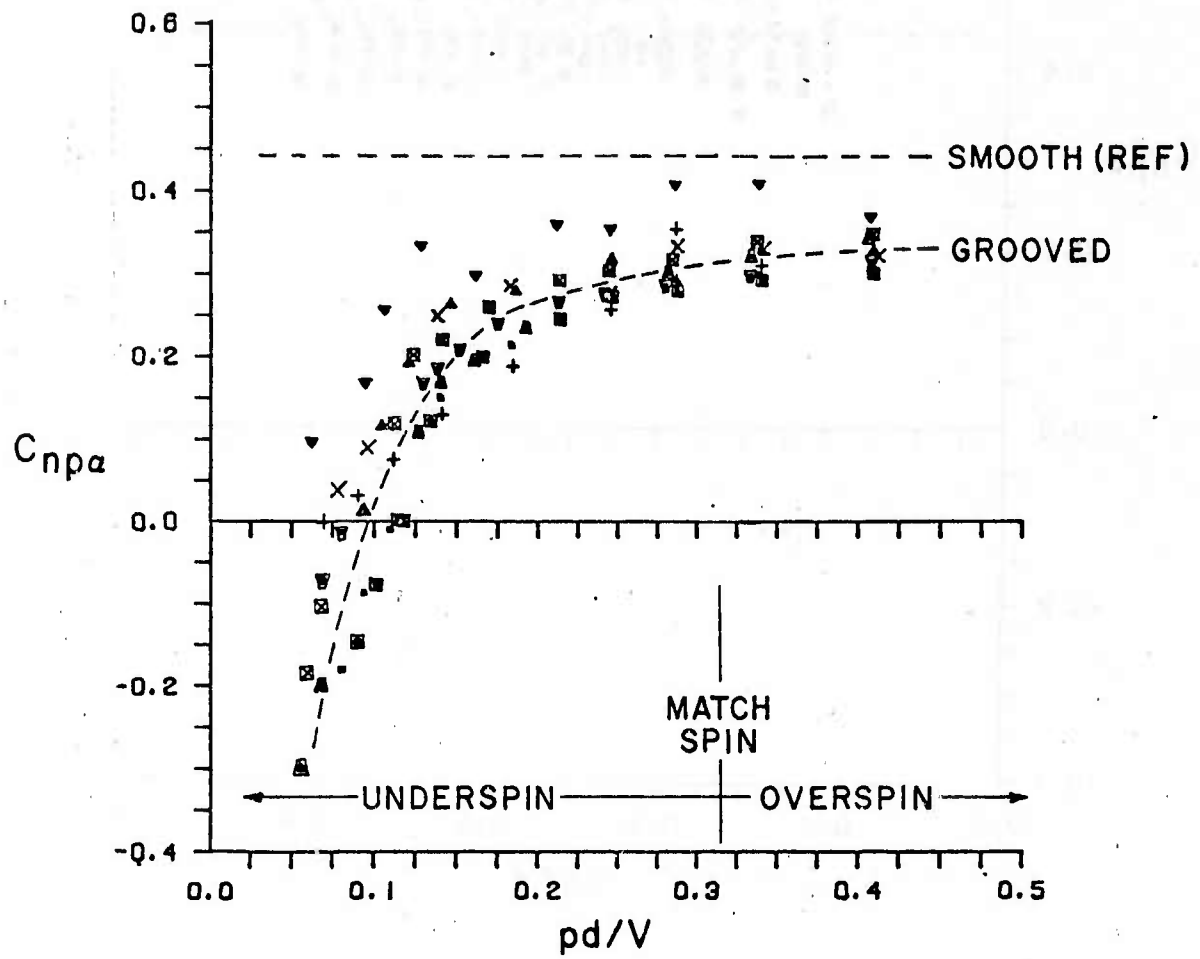
b. Approximate Surface Streamlines

Figure 8. Concluded



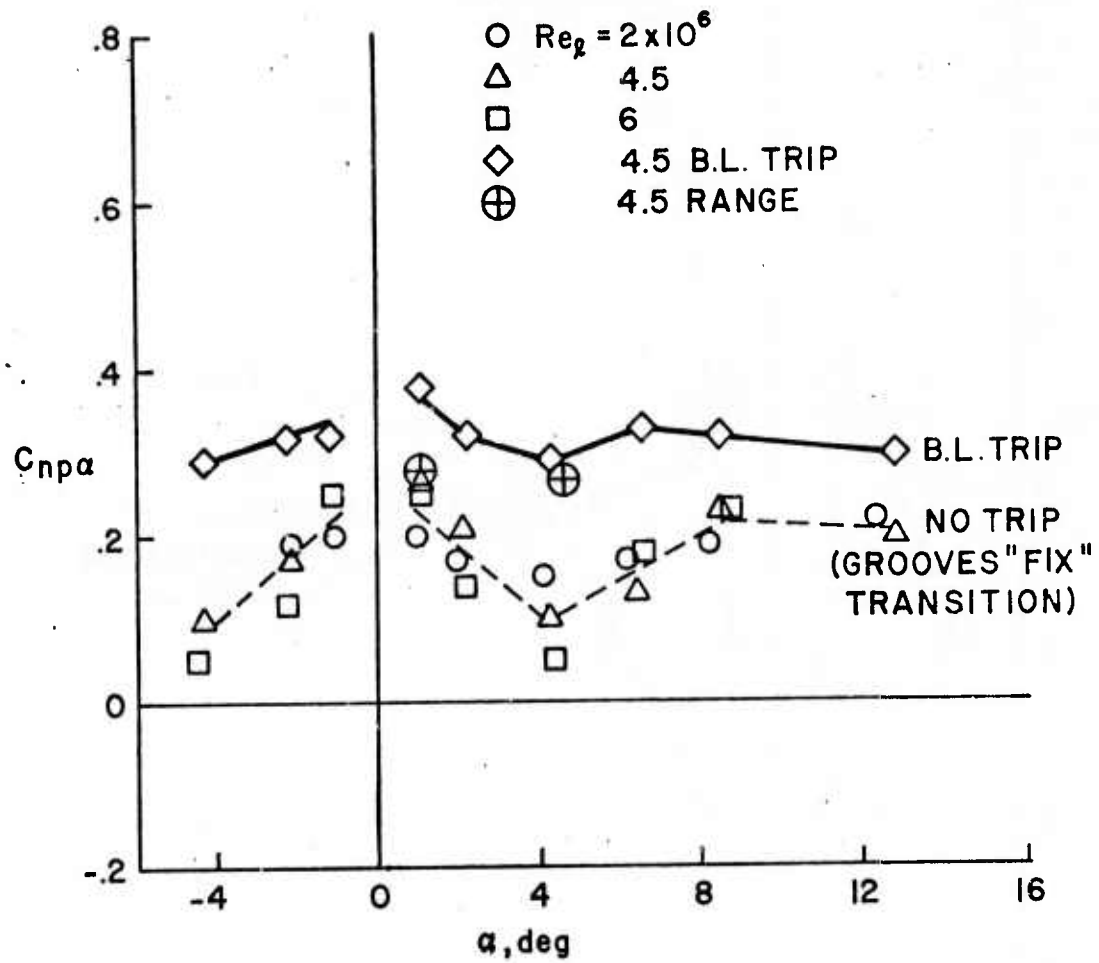
a. Smooth Model Results Showing Constant $C_{np\alpha}$

Figure 9. $C_{np\alpha}$ vs. pd/V ; Boattail Model With Boundary-Layer Trip,
 $M = 2.0$, $Re_{\lambda} = 4.5 \times 10^6$, $\alpha = -4$ to 13°



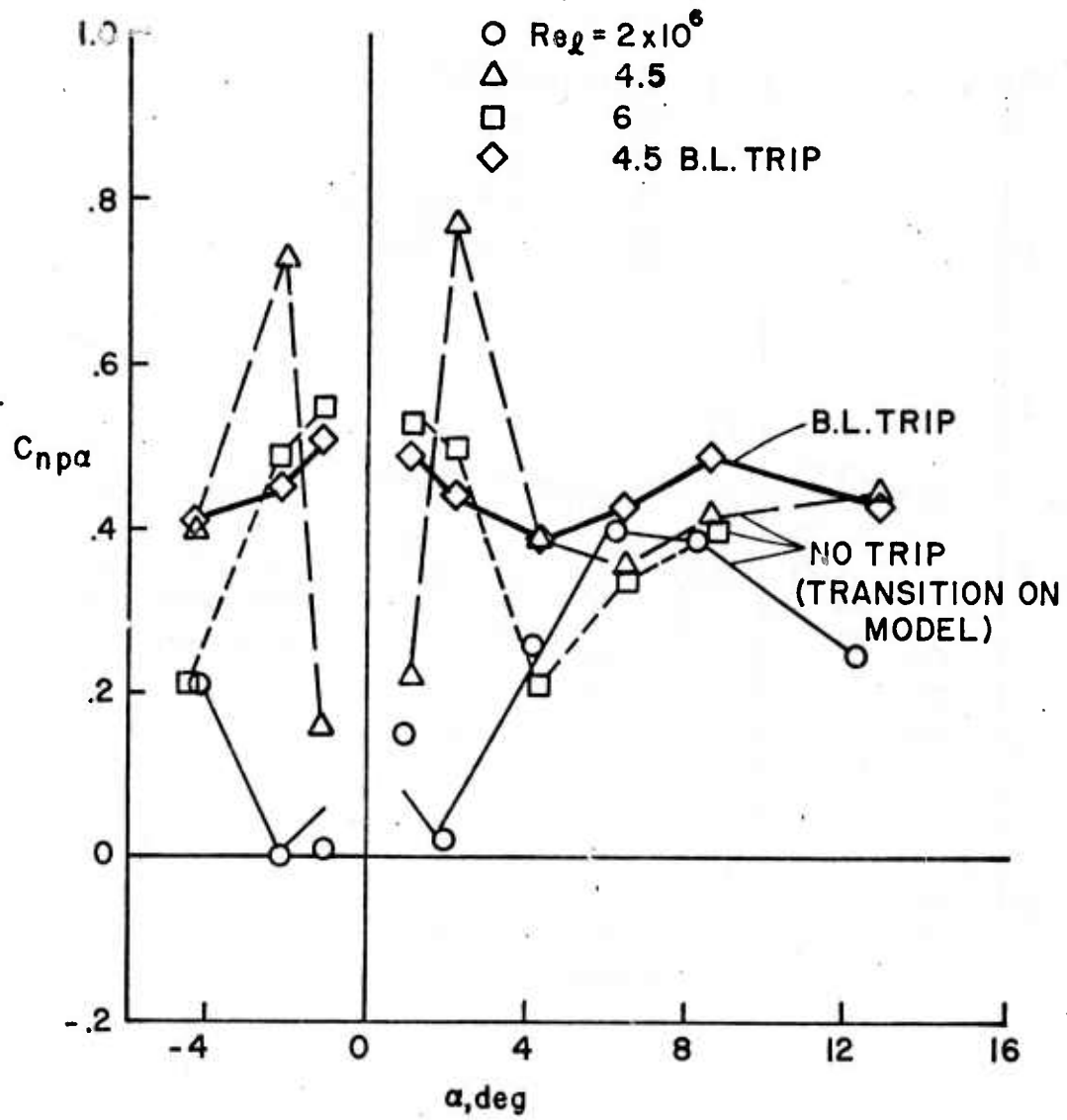
b. Grooved Model Results Showing $C_{np\alpha}$ Reduction Due to "Offset" Effect

Figure 9. Concluded



a. Grooved Model Data Showing Consistent Results With Predominantly Turbulent Boundary Layer or "Fixed" Transition

Figure 10. $C_{np\alpha}$ vs. α ; Boattail Model, $M = 2.0$, $pd/V = 0.31$



b. Smooth Body Data Showing Strong Influence of Mixed Boundary Layer Conditions and Skewed Transition

Figure 10. Concluded

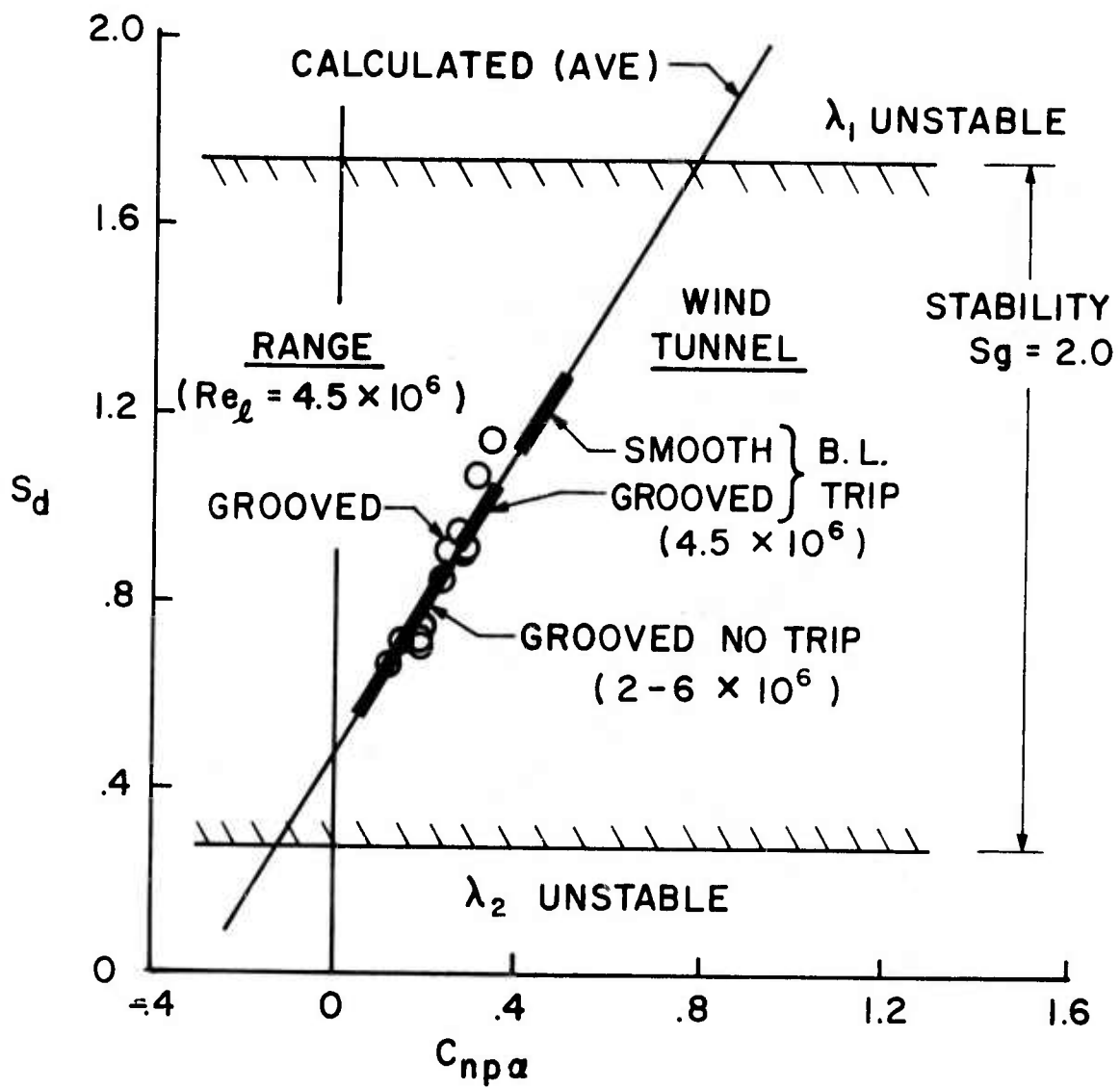


Figure 11. Effect of $C_{np\alpha}$ on Dynamic Stability; Cylindrical and Boattail Models, $M = 2.0$, $pd/V = 0.27-0.43$, $\alpha = 1-13^\circ$ Wind Tunnel, $2-6^\circ$ Range

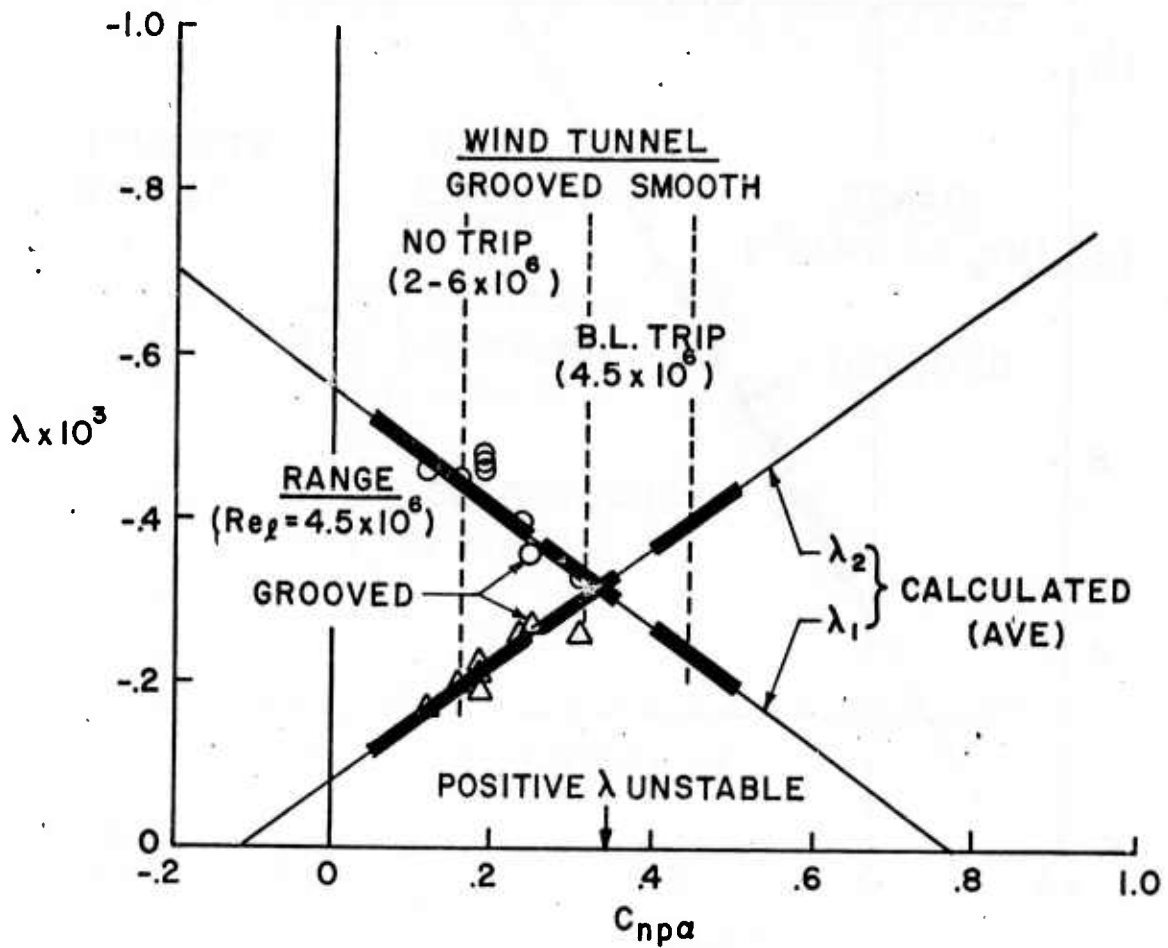
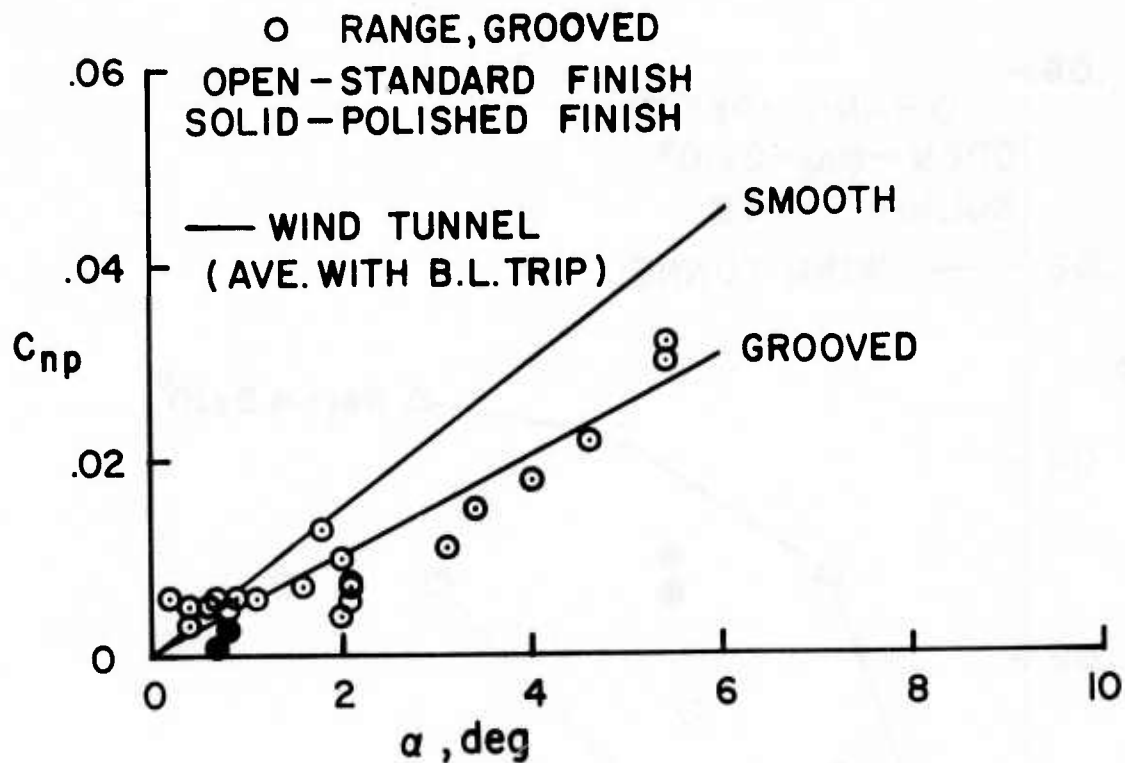
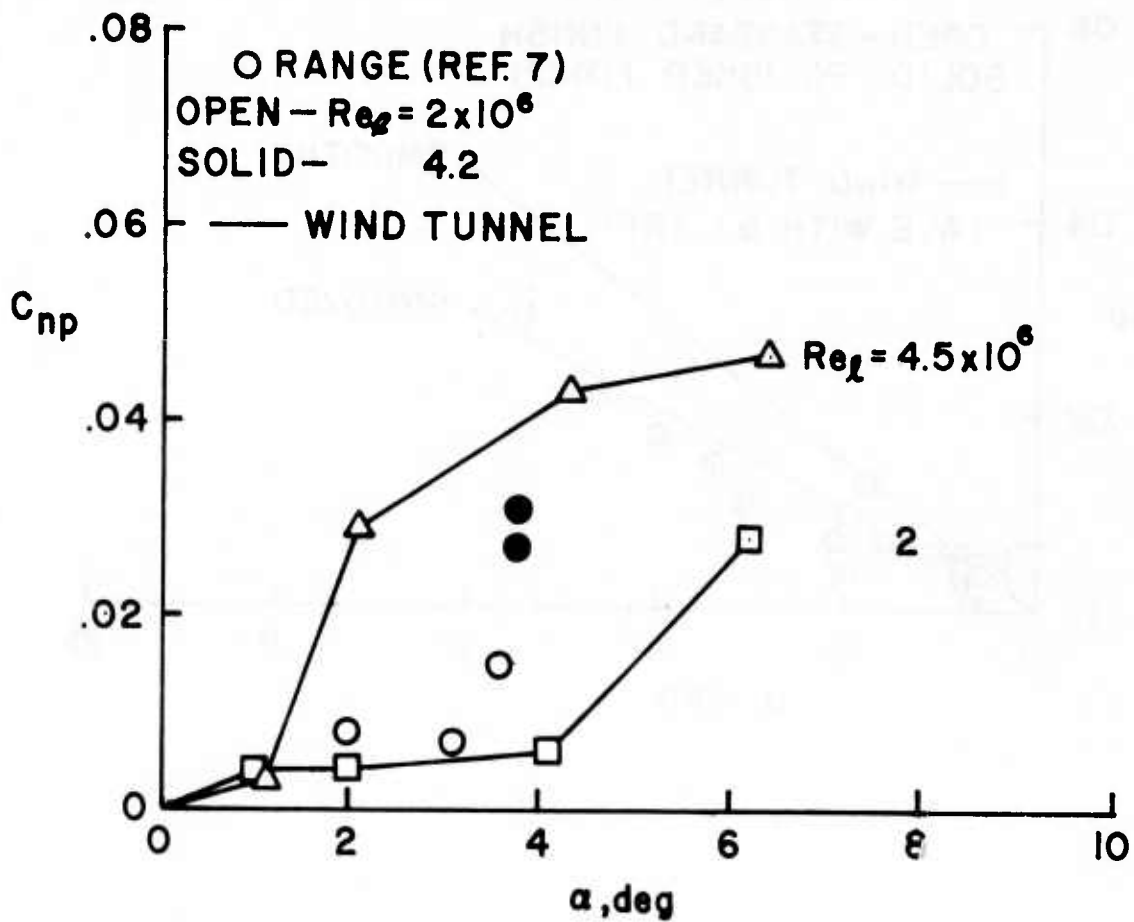


Figure 12. Effect of $C_{np}\alpha$ on Exponential Damping Coefficients; Cylindrical and Boattail Models, $M = 2.0$, $pd/V = 0.43$, $\alpha = 1-13^\circ$ Wind Tunnel, $2-6^\circ$ Range



a. Cylindrical and Boattail Models With Predominantly Turbulent Boundary Layers or Fixed Transition; $Re_{\ell} = 4.5 \times 10^6$, $pd/V = 0.27-0.43$

Figure 13. Summary of Wind Tunnel and Range Magnus Moment Coefficient Data Comparisons; $M = 2.0$



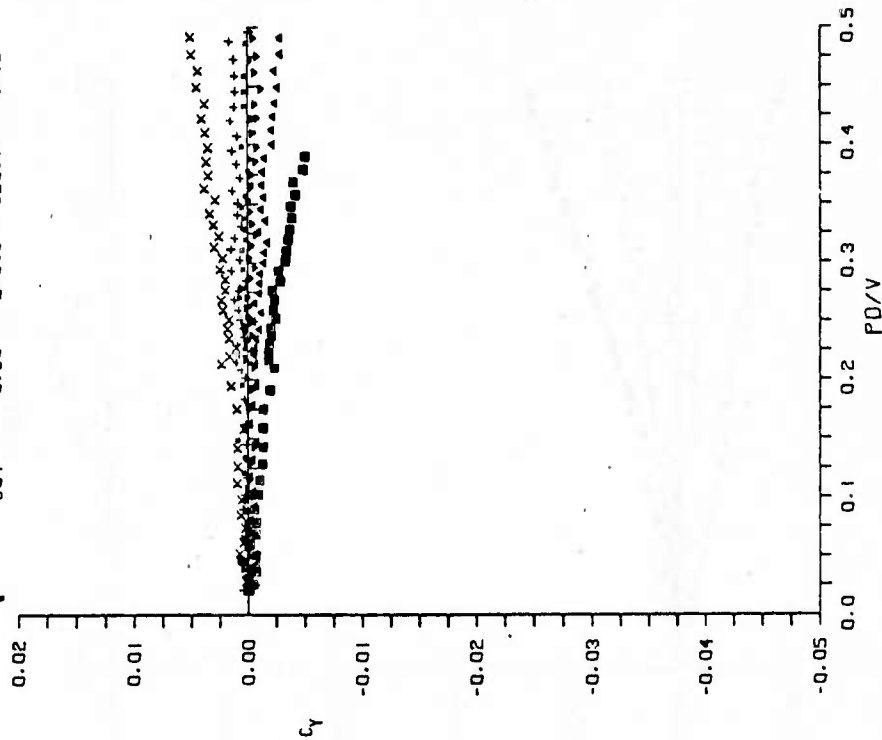
b. Smooth, Boattail Models With Probable Mixed Boundary Layer Conditions and Skewed Transition; $pd/V = 0.21$

Figure 13. Concluded

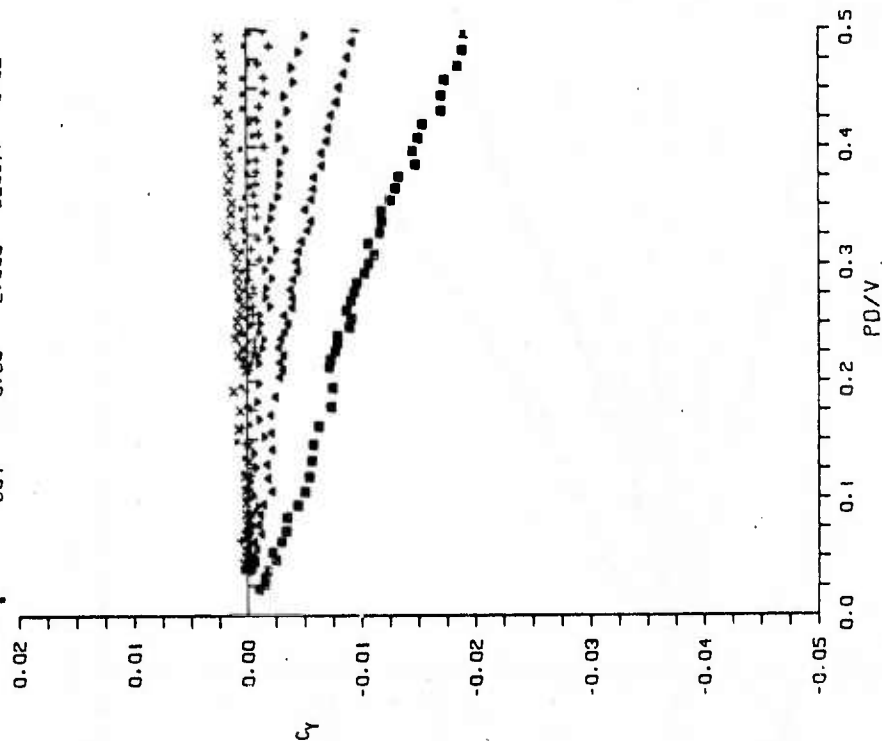
APPENDIX

SYM.	RUN NUMBER	MACH	CONFIG	RE/INCH	ALPHA
■	613	0.90	2.000	92095.	5.19
▲	612	0.90	2.000	92173.	3.10
▼	611	0.90	2.000	92419.	1.07
+	610	0.90	2.000	92661.	-0.97
x	609	0.90	2.000	93363.	-3.04
.	604	0.90	2.000	92067.	0.02

SYM.	RUN NUMBER	MACH	CONFIG	RE/INCH	ALPHA
■	614	0.89	2.000	91996.	8.29
▲	608	0.89	2.000	91877.	6.21
▼	606	0.89	2.000	91914.	4.16
+	605	0.90	2.000	91395.	2.10
x	603	0.90	2.000	92133.	-2.02
.	604	0.90	2.000	92067.	0.02



A1-2

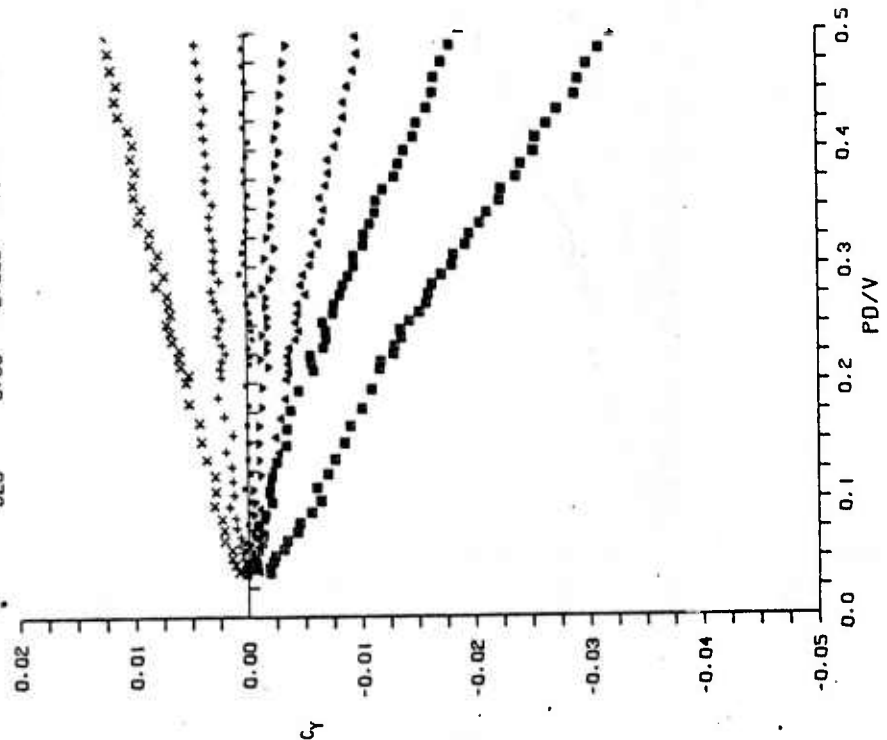


A1-1

Figure A1. Basic Magnus Force Data

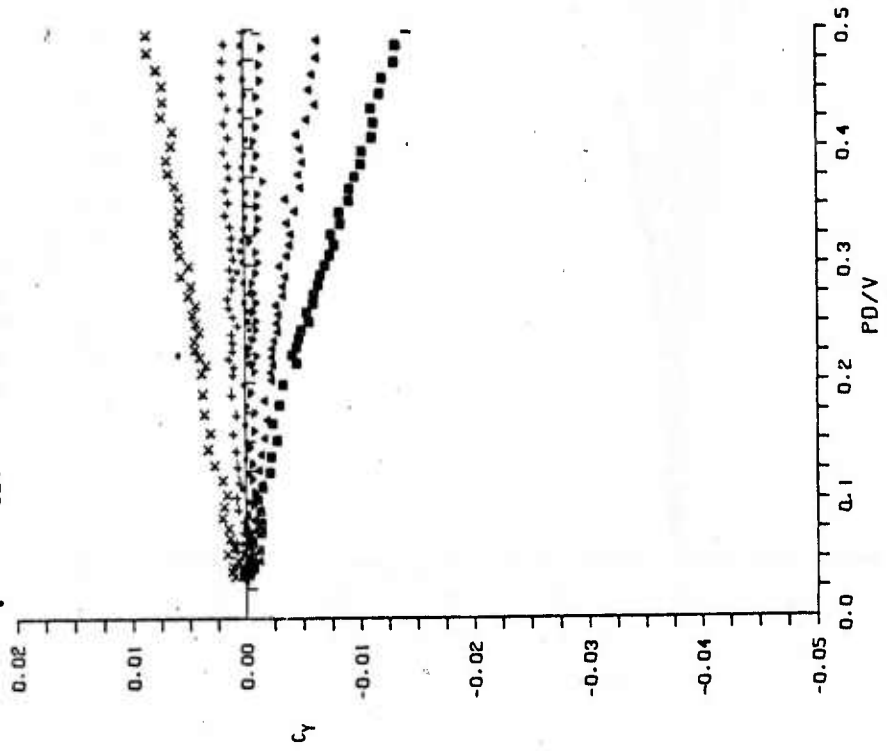
PRECEDING PAGE BLANK-NOT FILMED.

SYN.	RUN NUMBER	MACH	CONFIG	RE/INCH	ALPHA
■	627	0.87	2.008	90775.	8.27
■	628	0.88	2.008	90980.	6.25
■	626	0.87	2.008	90817.	4.17
▲	617	0.88	2.008	91425.	2.13
▼	623	0.87	2.008	90764.	-2.00
×	615	0.89	2.008	92536.	-4.07
×	620	0.88	2.008	91071.	0.08



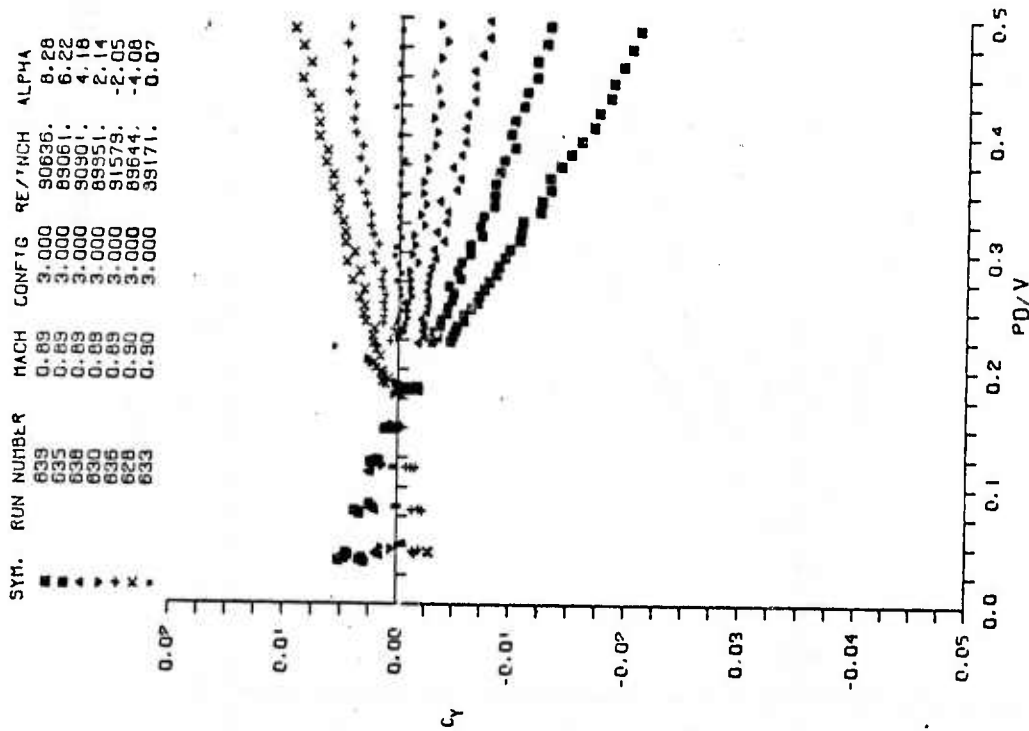
A1-3

SYN.	RUN NUMBER	MACH	CONFIG	RE/INCH	ALPHA
■	618	0.88	2.008	91137.	5.21
■	621	0.88	2.008	91073.	3.15
▲	625	0.87	2.008	90782.	1.09
▼	616	0.88	2.008	91735.	-0.98
×	619	0.88	2.008	90986.	-3.05
×	620	0.88	2.008	91071.	0.08

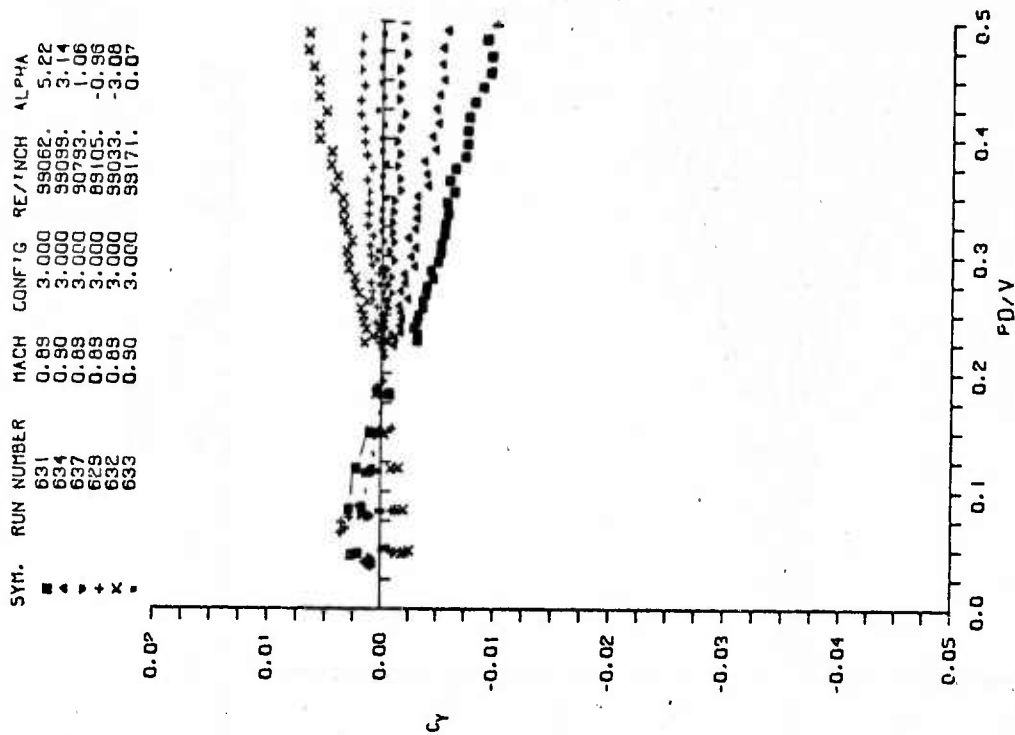


A1-4

Figure A1. Continued



A1-5



A1-6

Figure A1. Continued

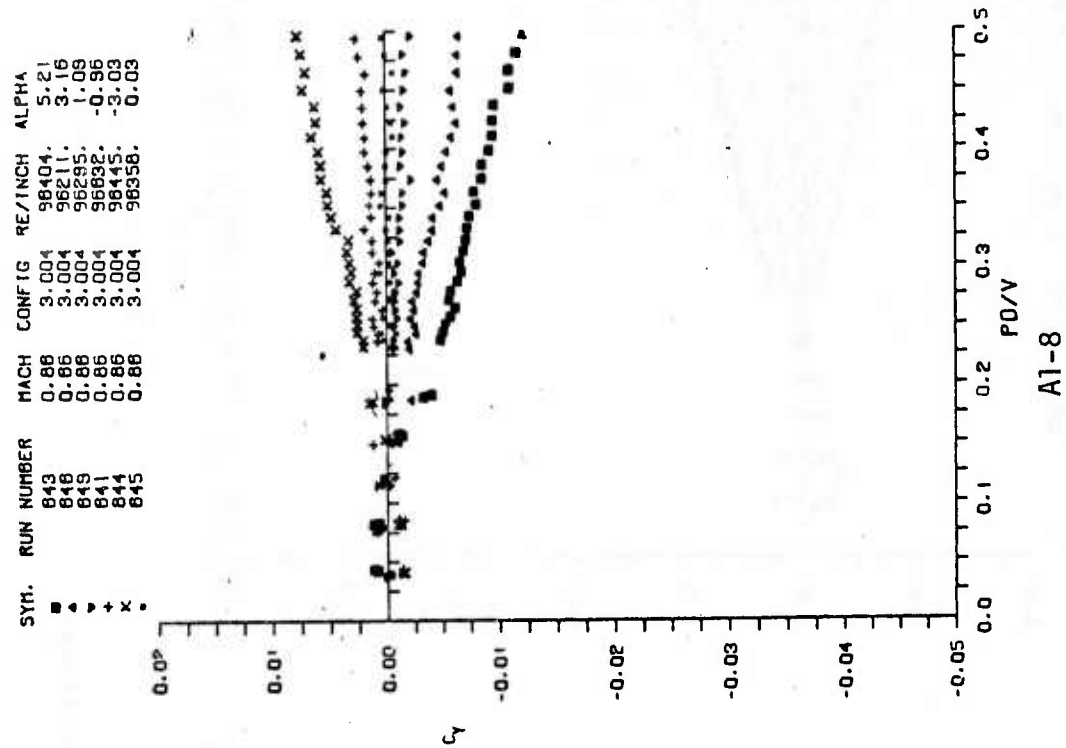
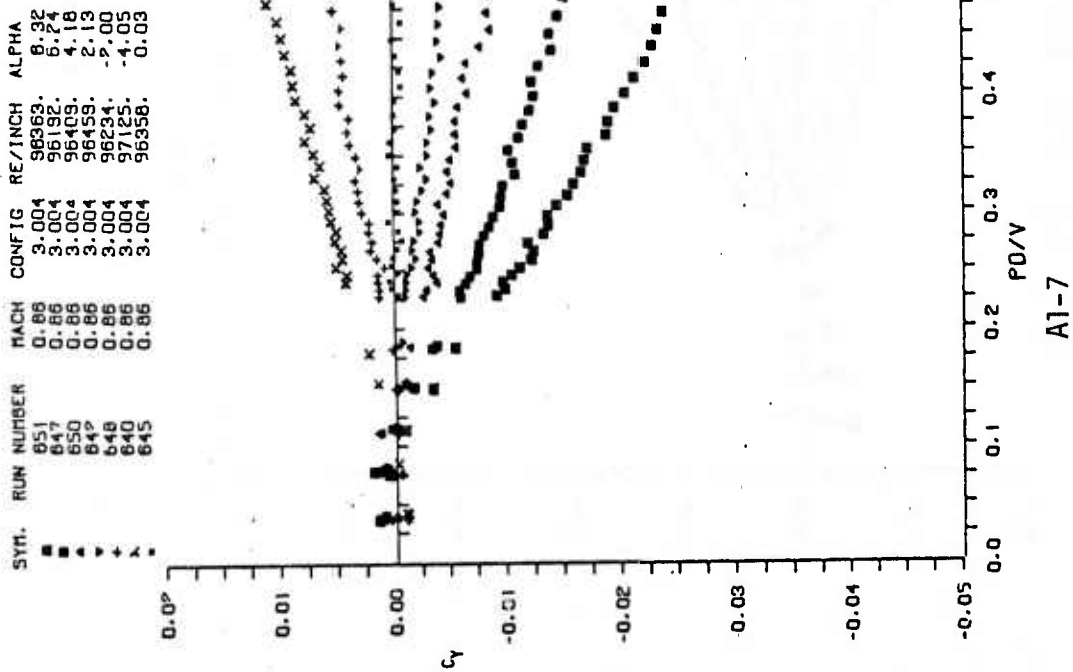
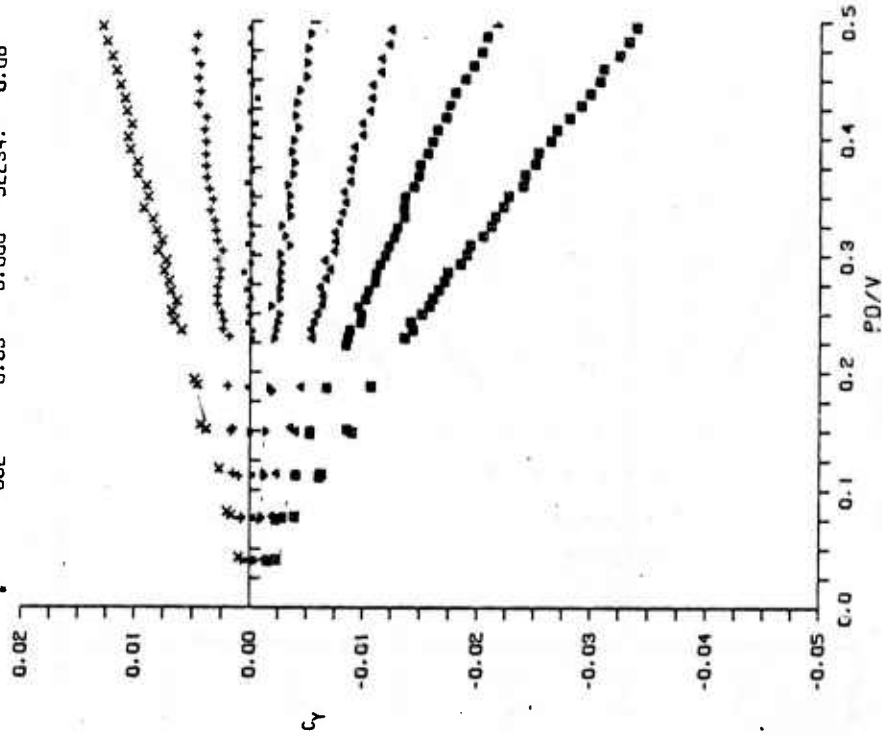


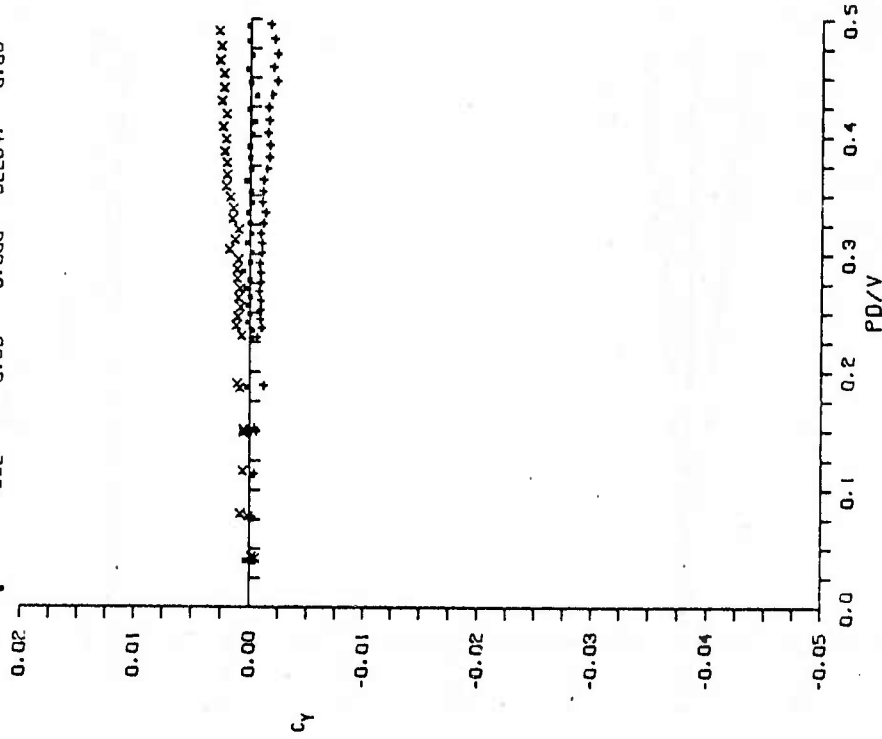
Figure A1. Continued

SYM.	RUN NUMBER	MACH	CONFIG	RE/INCH	ALPHA
■	680	0.89	6.000	92530.	8.24
■	684	0.89	6.000	92026.	6.22
▲	679	0.89	6.000	92702.	4.19
▲	683	0.89	6.000	92185.	2.08
+	681	0.89	6.000	92338.	-1.99
+	678	0.89	6.000	93396.	-4.12
•	682	0.89	6.000	92234.	0.06



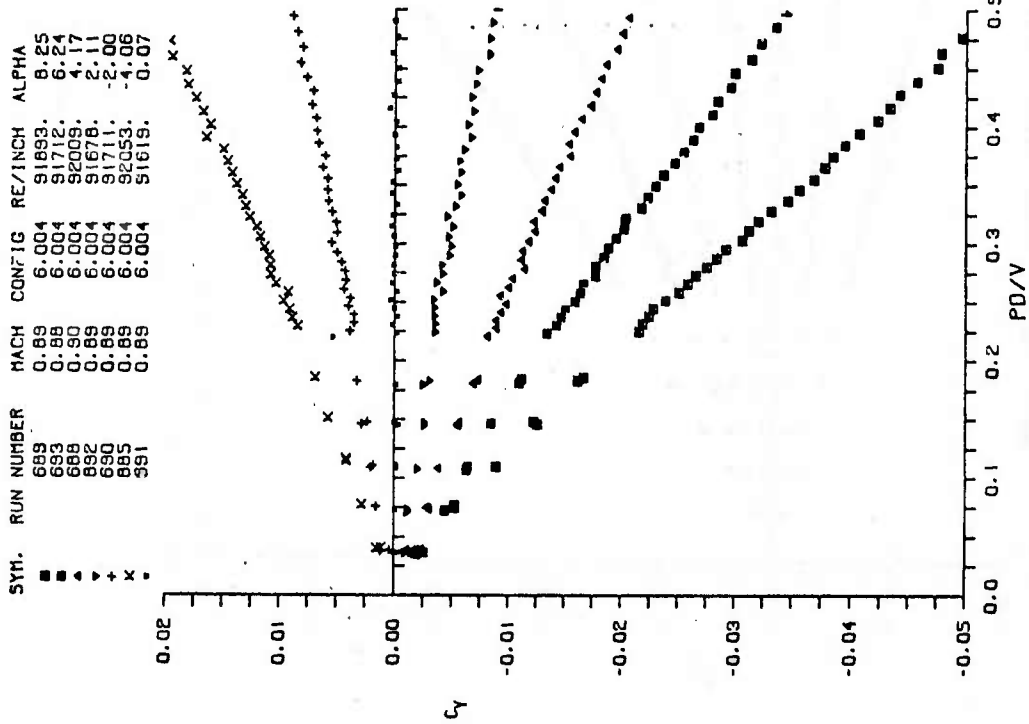
A1-9

SYM.	RUN NUMBER	MACH	CONFIG	RE/INCH	ALPHA
+	678	0.90	6.000	92945.	1.08
x	677	0.90	6.000	93387.	-1.00
•	682	0.89	6.000	92234.	0.06

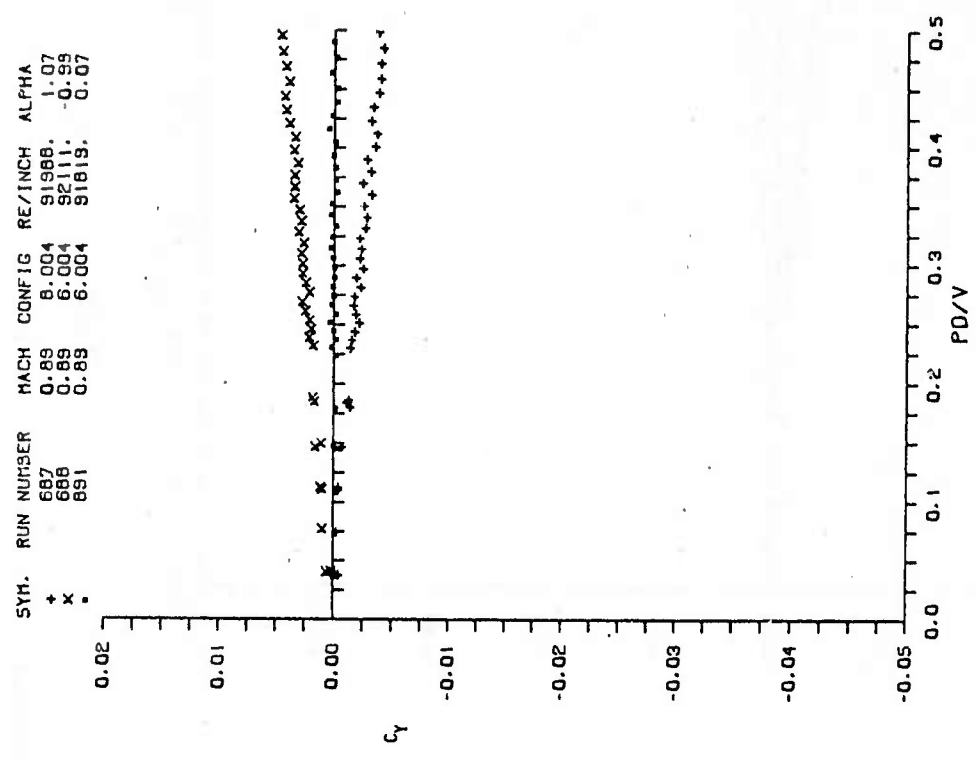


A1-10

Figure A1. Continued



A1-11



A1-12

Figure A1. Continued

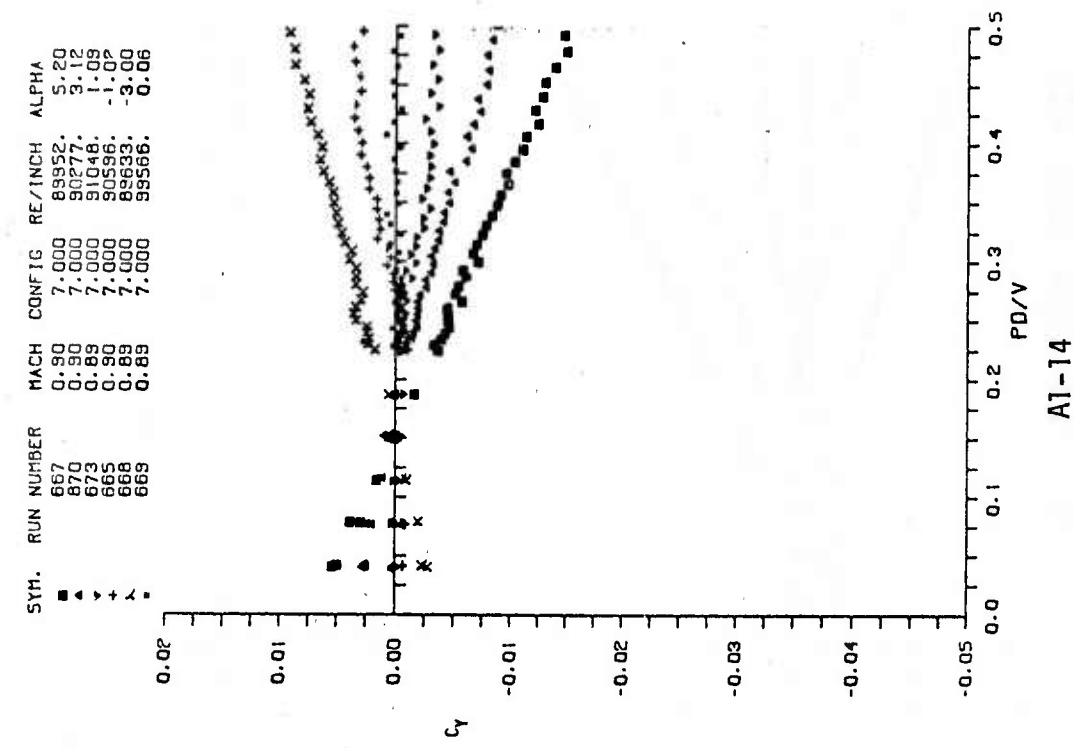
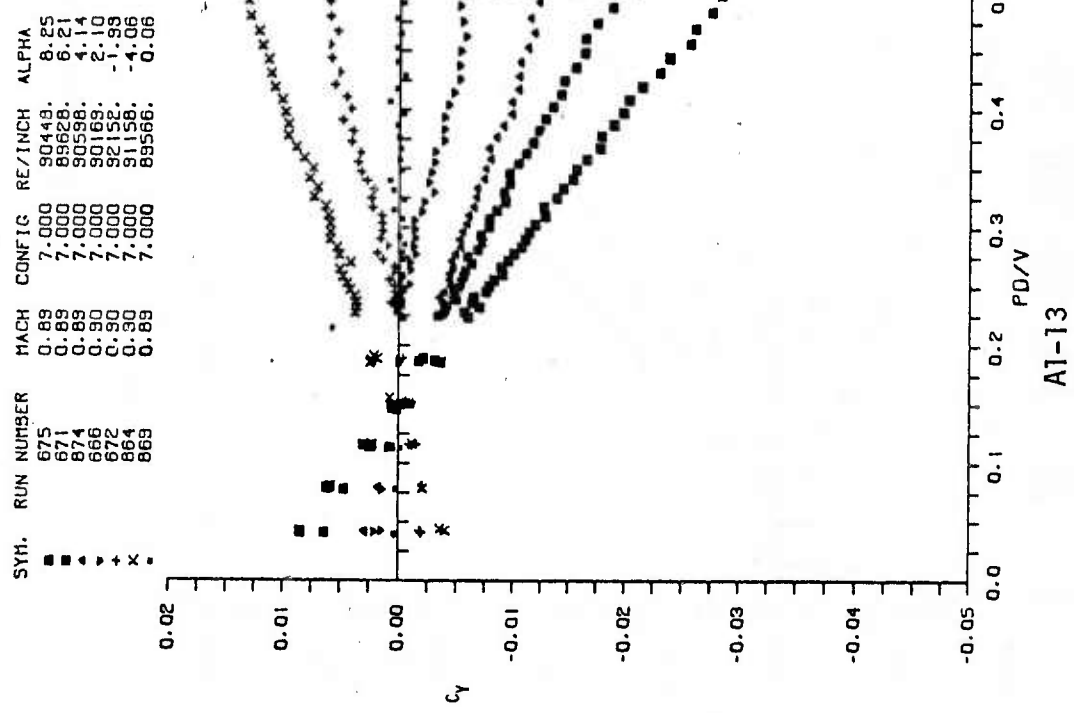


Figure A1. Continued

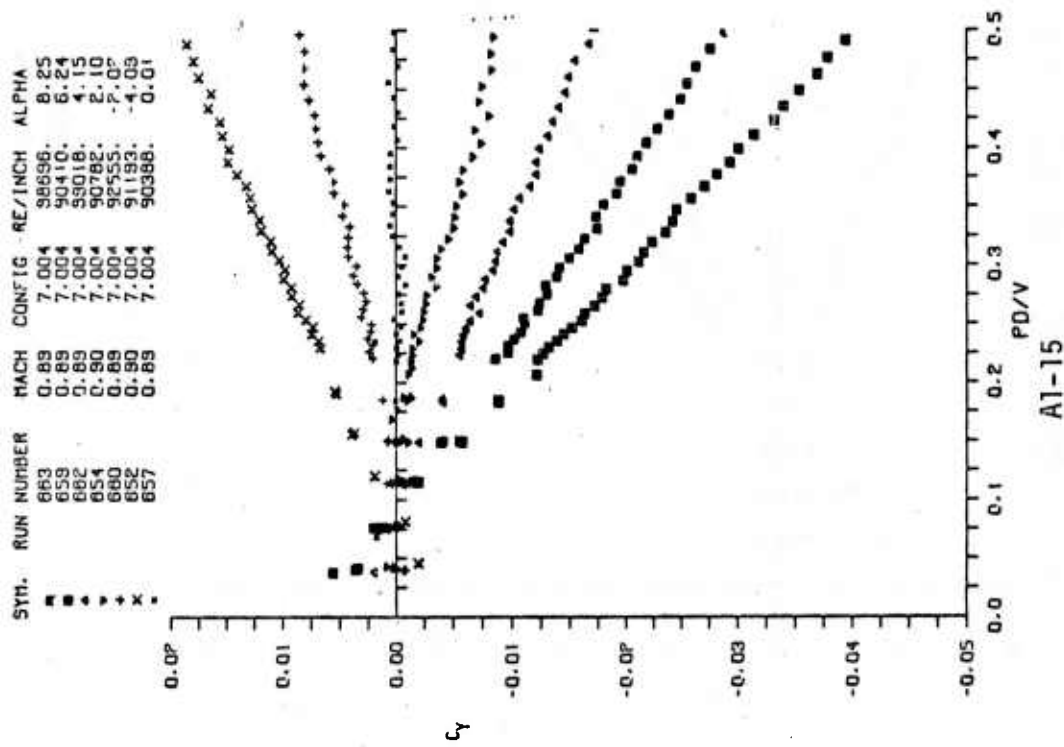
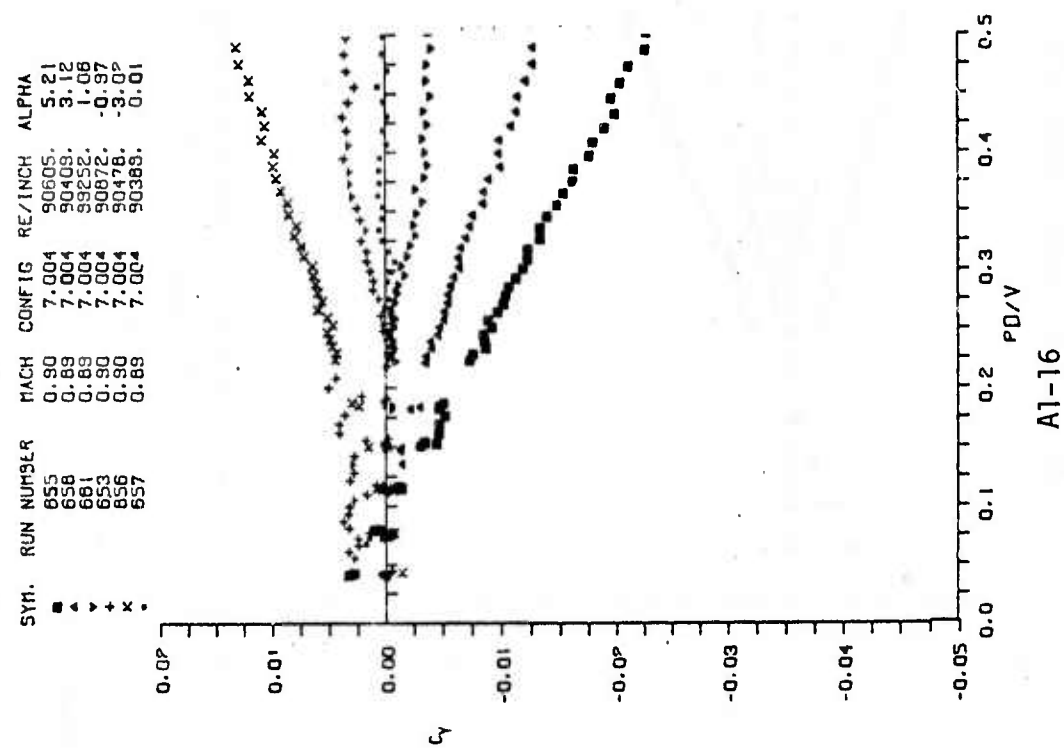
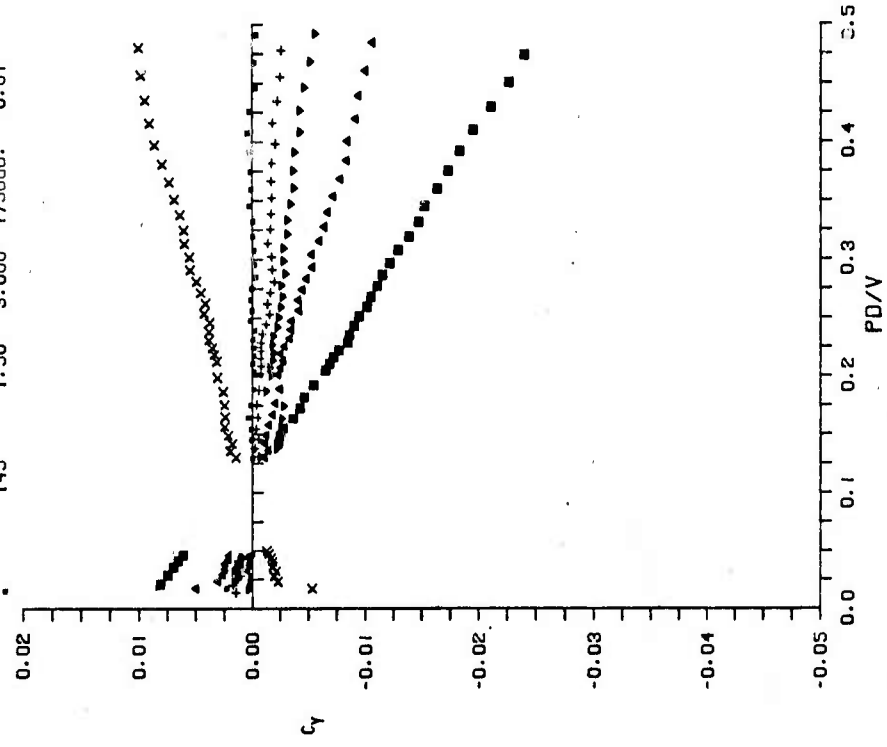


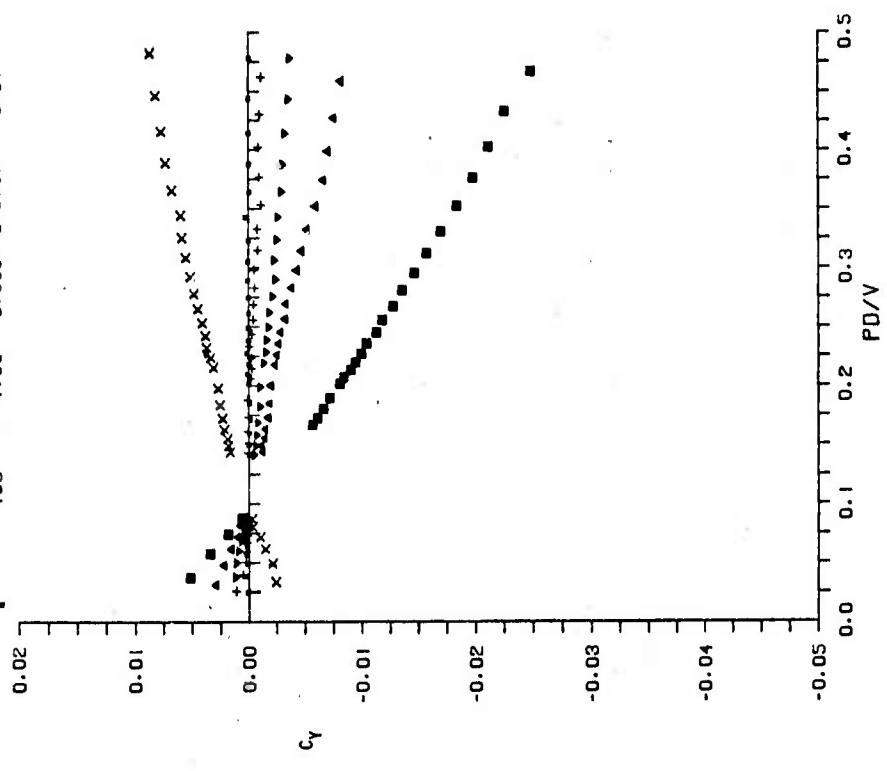
Figure A1. Continued

SYM.	RUN NUMBER	MACH	CONFIG	RE/INCH	ALPHA
■	149	1.50	3.000	175568.	6.19
▲	148	1.50	3.000	175639.	4.09
▼	147	1.50	3.000	175695.	2.03
+	146	1.50	3.000	176233.	1.01
x	144	1.50	3.000	1763.3.	-4.10
.	145	1.50	3.000	175608.	-0.01



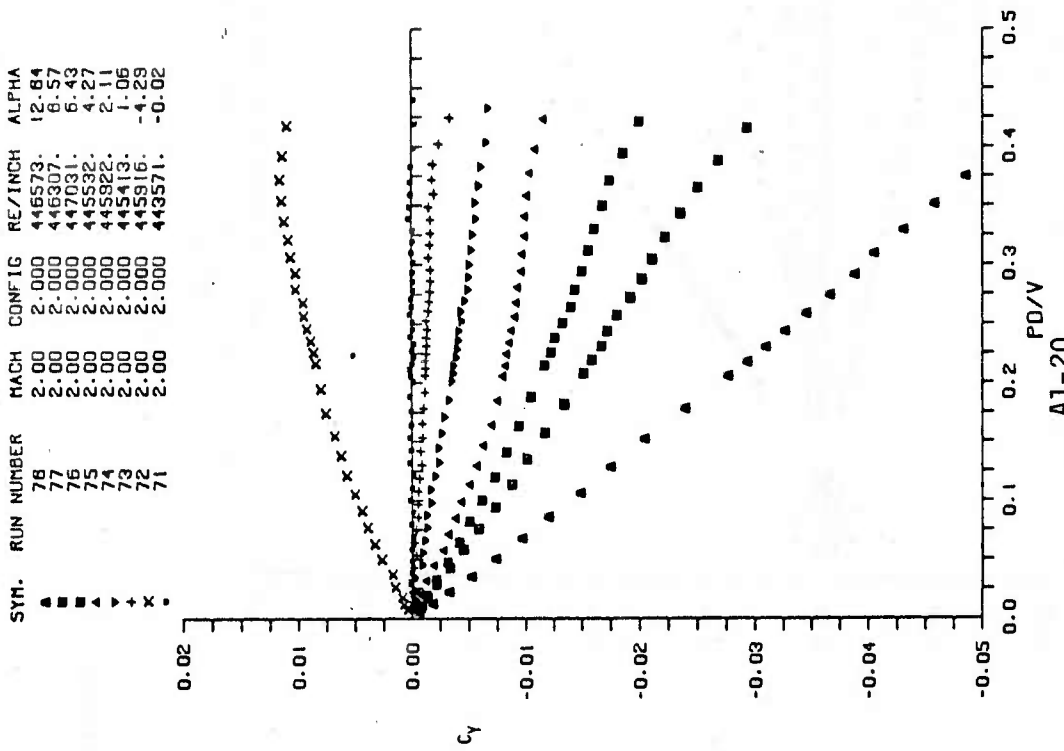
A1-17

SYM.	RUN NUMBER	MACH	CONFIG	RE/INCH	ALPHA
■	143	1.50	3.000	348695.	6.43
▲	142	1.50	3.000	349171.	4.20
▼	141	1.50	3.000	348920.	2.09
+	140	1.50	3.000	348699.	1.05
x	138	1.50	3.000	348728.	-4.21
.	139	1.50	3.000	348757.	0.01

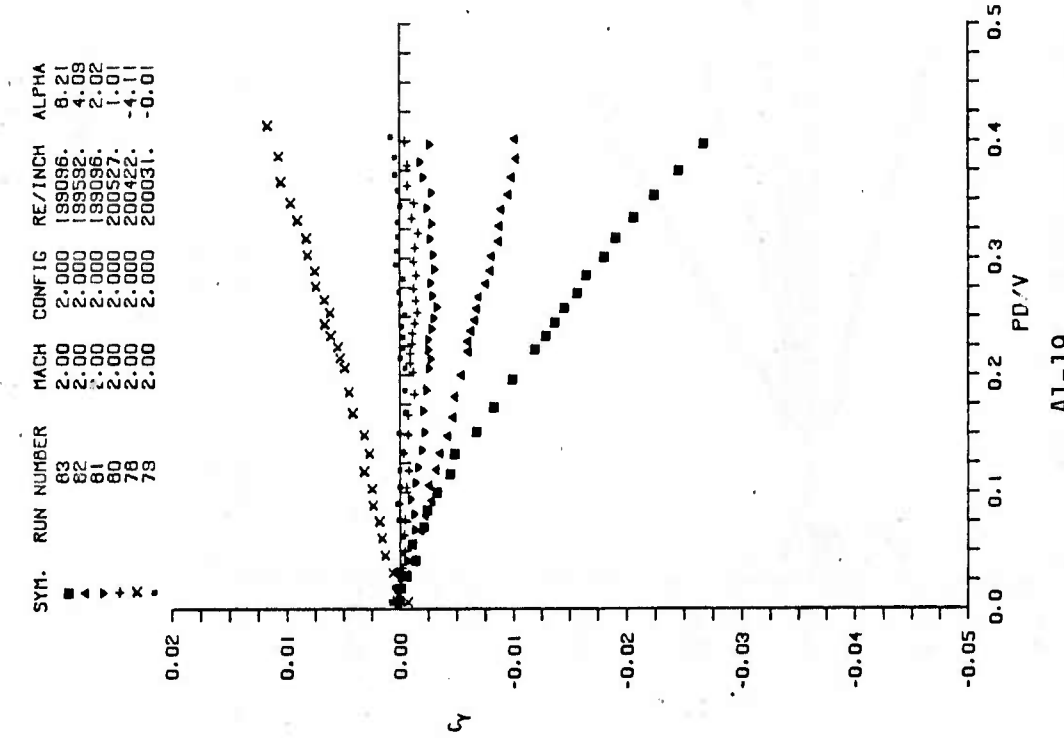


A1-18

Figure A1. Continued



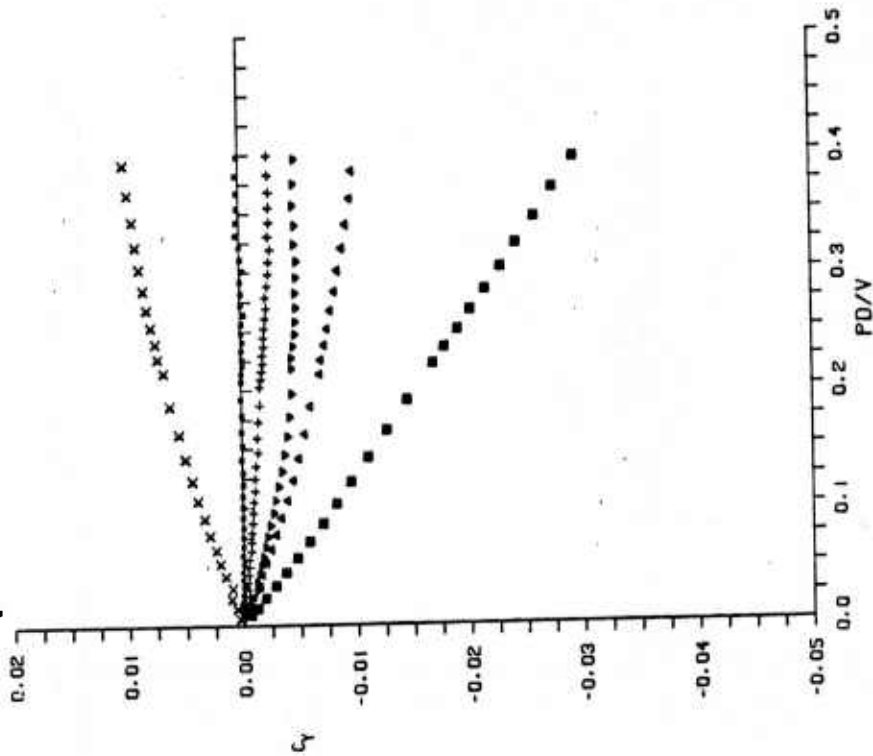
A1-20



A1-19

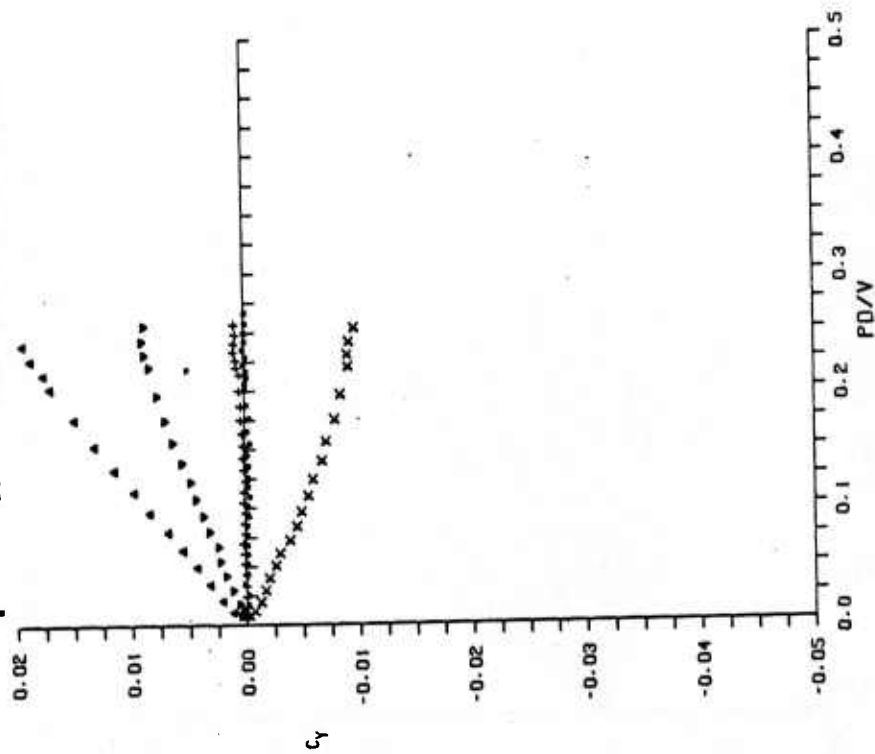
Figure A1. Continued

SYN.	RUN NUMBER	MACH	CONFIG	RE/INCH	ALPHA
■	94	2.00	2.000	594693.	8.71
▲	93	2.00	2.000	596321.	4.35
▼	92	2.00	2.000	593935.	2.16
+	91	2.00	2.000	589031.	1.09
x	89	2.00	2.000	592181.	-4.35
•	90	2.00	2.000	590875.	0.00



A1-22

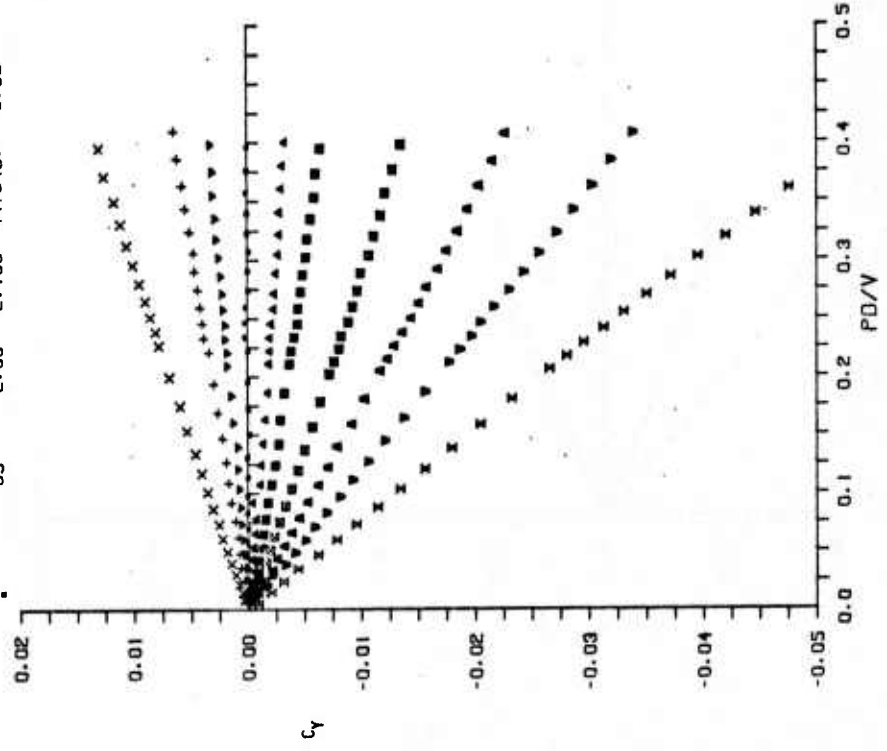
SYN.	RUN NUMBER	MACH	CONFIG	RE/INCH	ALPHA
▲	86	2.00	2.000	445038.	8.59
▼	87	2.00	2.000	445245.	4.28
+	86	2.00	2.000	444608.	1.09
x	85	2.00	2.000	445523.	-4.28
•	84	2.00	2.000	453810.	0.00



A1-21

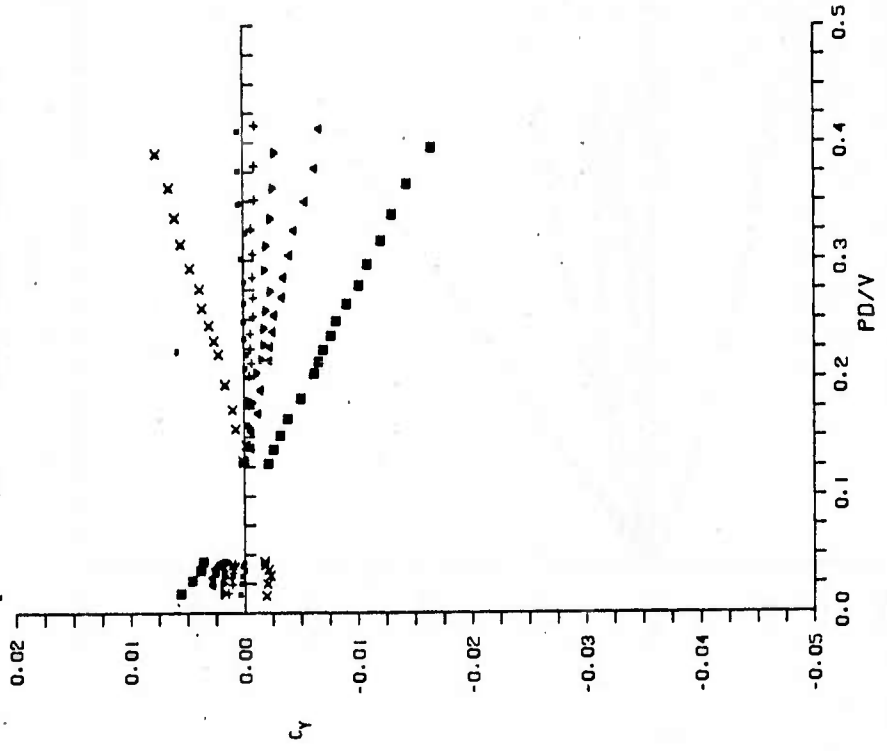
Figure A1. Continued

SYM.	RUN NUMBER	MACH	CONFIG	RE/INCH	ALPHA
x	78	2.00	2.108	448080.	12.74
v	75	2.00	2.108	448159.	8.50
▲	70	2.00	2.108	446283.	8.38
▲	89	2.00	2.106	447197.	4.23
▲	86	2.00	2.108	447103.	2.10
▲	67	2.00	2.108	447628.	1.04
▲	64	2.00	2.108	447665.	-1.07
▲	83	2.00	2.108	448278.	-2.14
▲	82	2.00	2.108	448283.	-4.27
▲	85	2.00	2.108	447649.	-0.02



A1-23

SYM.	RUN NUMBER	MACH	CONFIG	RE/INCH	ALPHA
■	122	2.00	3.000	198584.	8.23
■	121	2.00	3.000	198386.	4.10
▲	120	2.00	3.000	198980.	2.04
▲	119	2.00	3.000	199423.	1.03
x	117	2.00	3.000	198469.	-4.11
•	116	2.00	3.000	199121.	0.00



A1-24

Figure A1. Continued

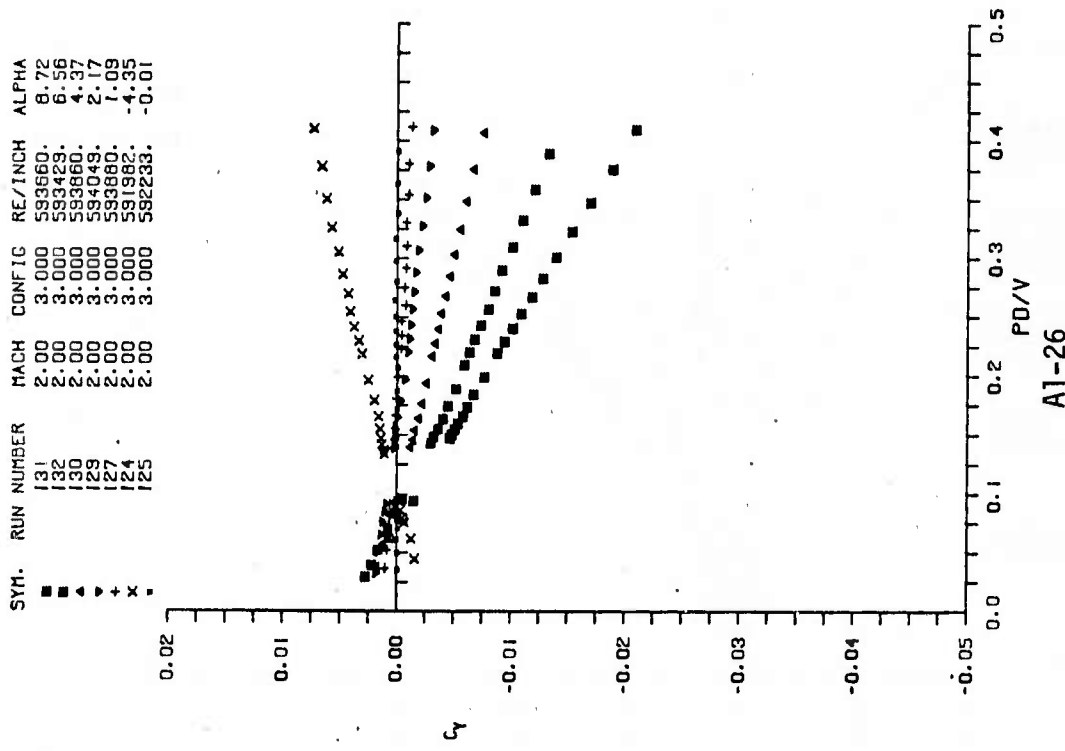
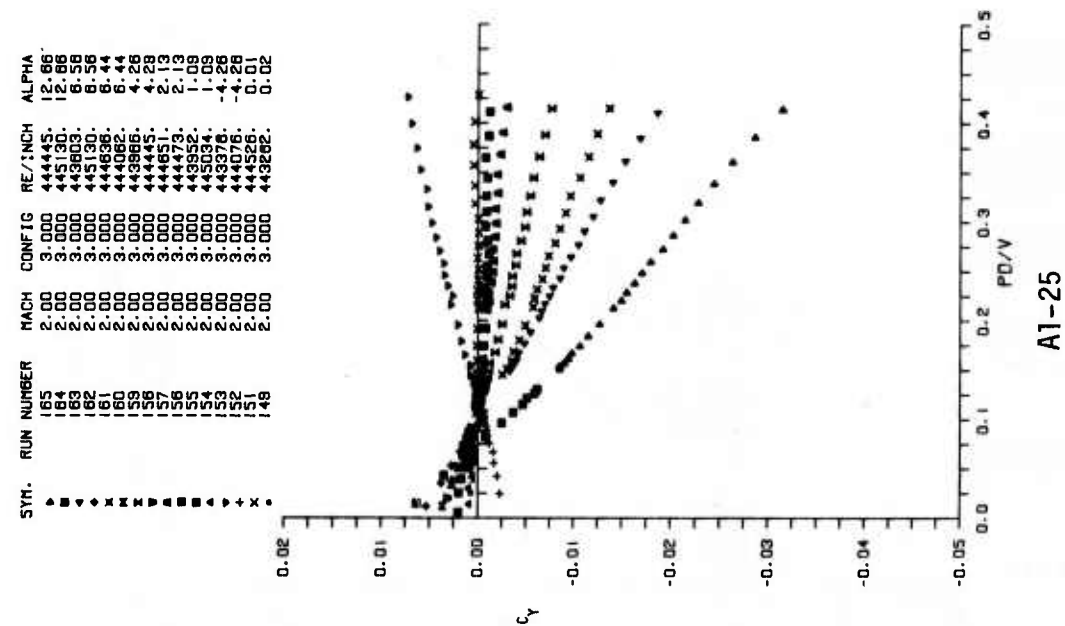
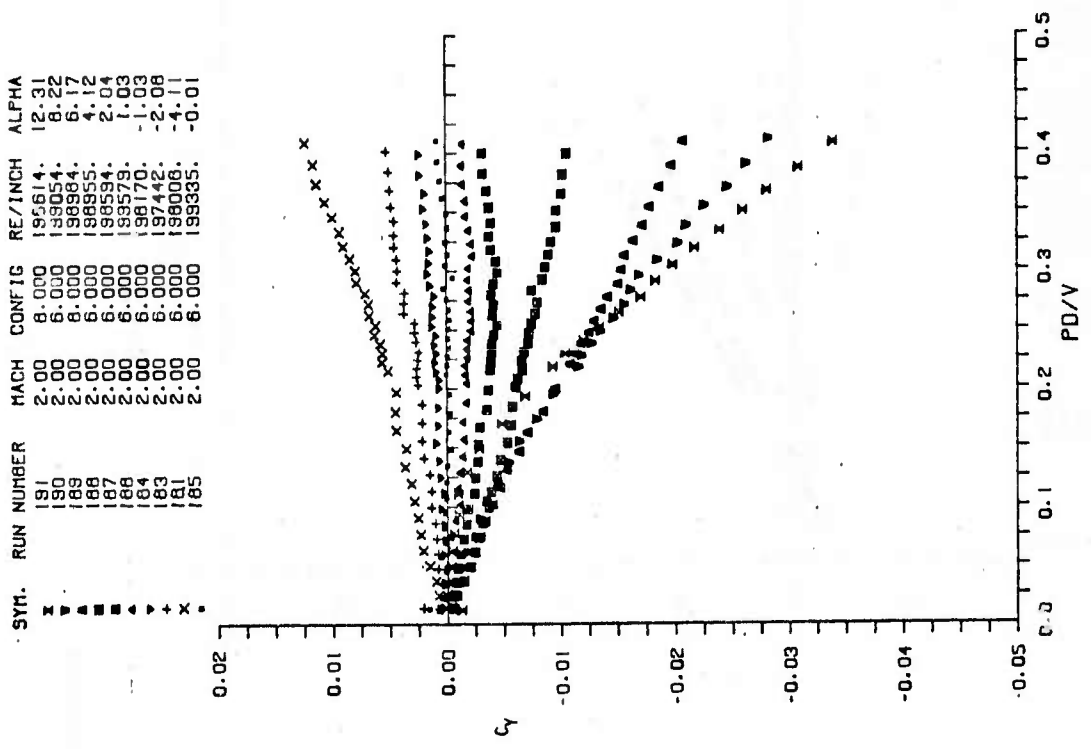
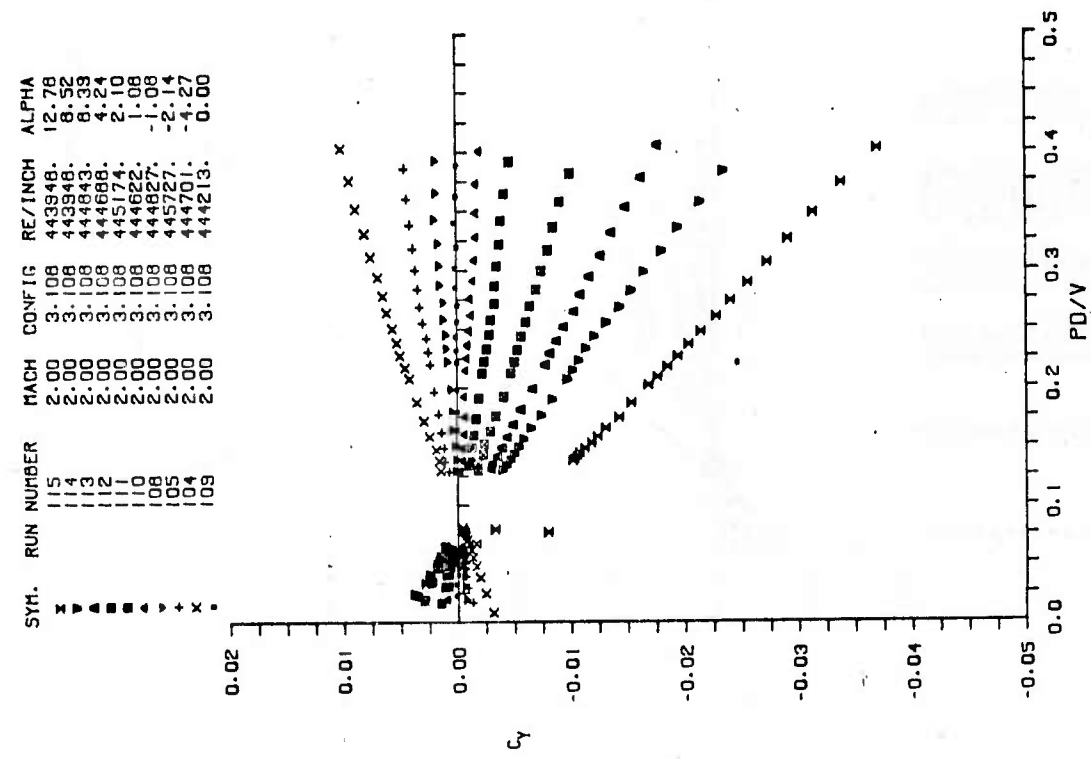


Figure A1. Continued



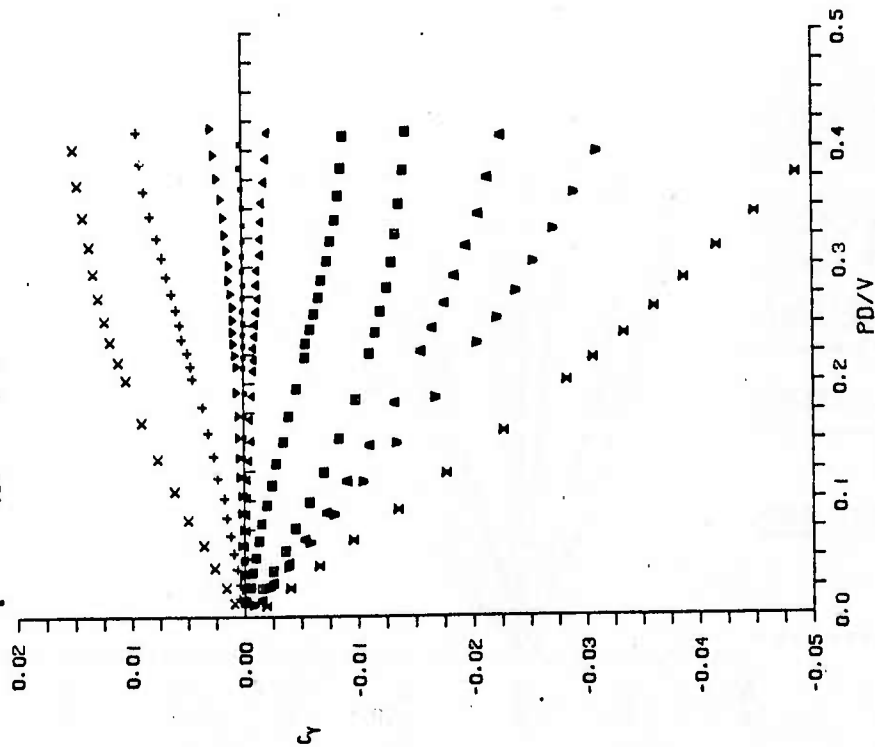
A1-28



A1-27

Figure A1. Continued

SYM.	RUN NUMBER	MACH	CONFIG	RE/INCH	ALPHA
x	201	2.00	6.000	445568.	12.76
▲	200	2.00	6.000	44780.	8.52
▲	199	2.00	6.000	445725.	8.39
▲	198	2.00	6.000	44612.	4.27
■	197	2.00	6.000	445441.	2.10
■	196	2.00	6.000	445378.	1.06
▲	194	2.00	6.000	445757.	-1.07
▲	193	2.00	6.000	445174.	-2.13
+	192	2.00	6.000	445363.	-4.25
x	195	2.00	6.000	445773.	-0.02



SYM.	RUN NUMBER	MACH	CONFIG	RE/INCH	ALPHA
■	209	2.00	6.000	444937.	8.52
▲	207	2.00	6.000	445031.	4.25
▲	206	2.00	6.000	445267.	2.10
+	204	2.00	6.000	444072.	1.06
x	202	2.00	6.000	444825.	-4.28
•	203	2.00	6.000	444717.	-0.02

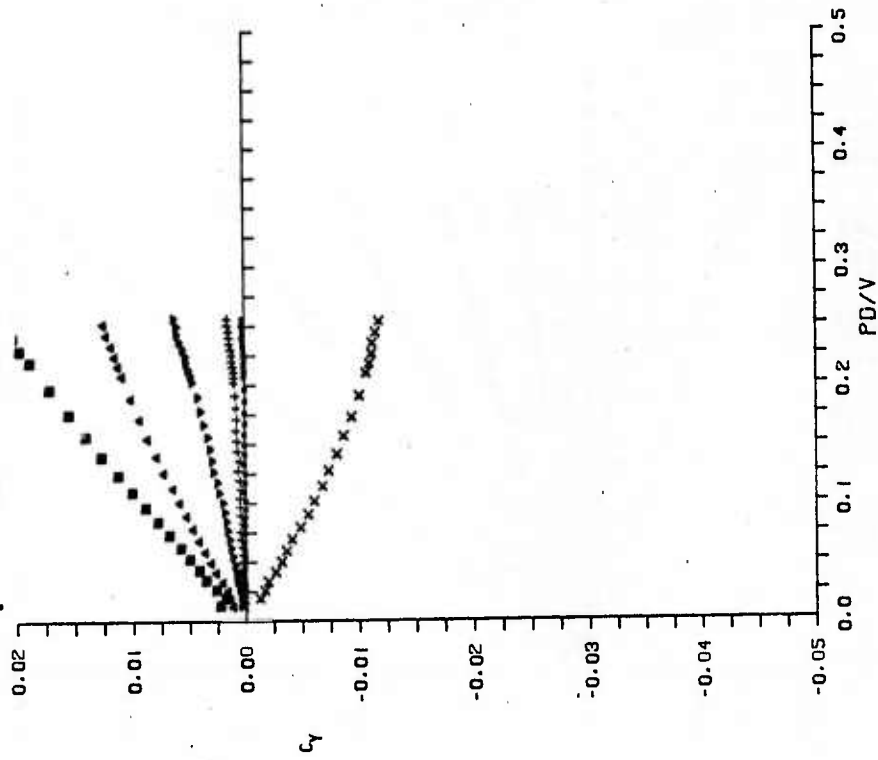
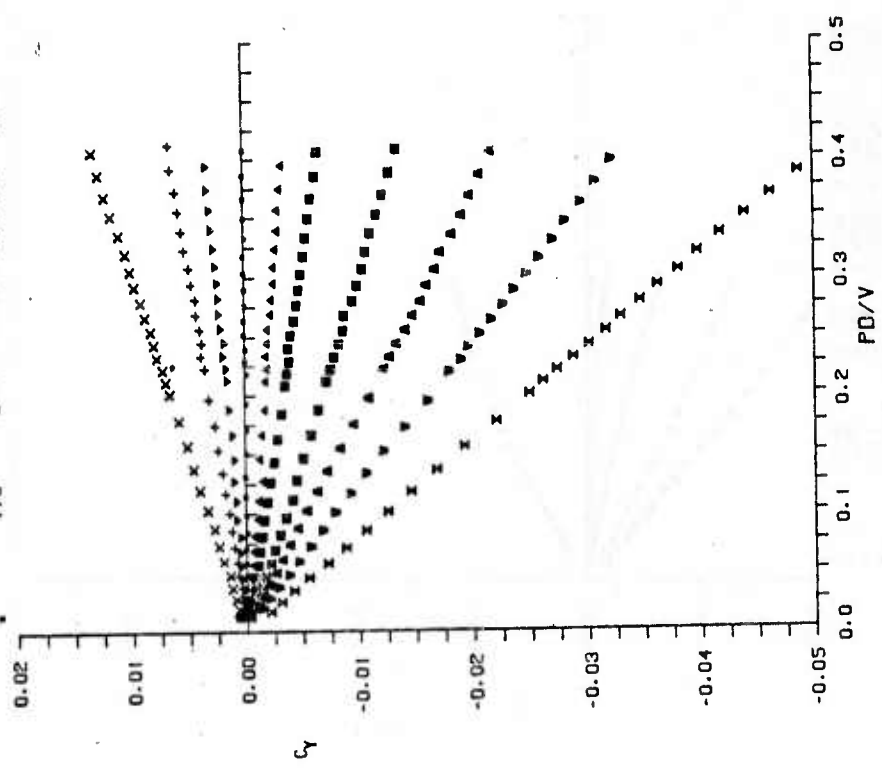


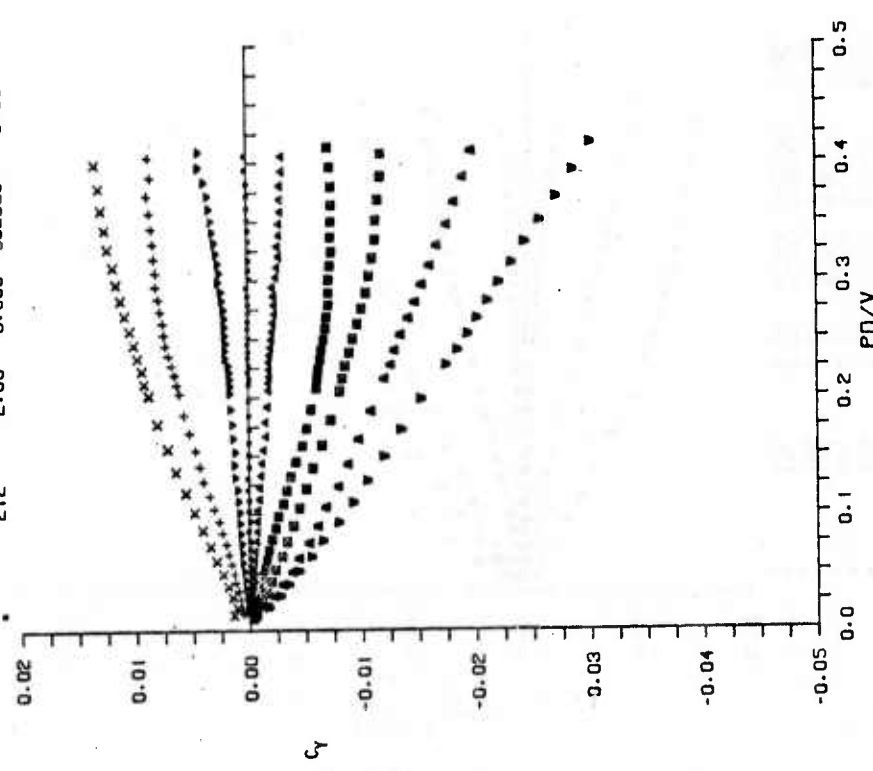
Figure A1. Continued

SYM.	RUN NUMBER	MACH	CONFIG	RE/INCH	ALPHA
x	176	2.00	6.108	443978.	12.78
x	175	2.00	6.108	443999.	8.52
▲	174	2.00	6.108	444544.	8.30
▲	173	2.00	6.108	444418.	4.25
▲	172	2.00	6.108	444607.	2.11
▲	171	2.00	6.108	444838.	1.05
▲	169	2.00	6.108	445032.	-1.08
▲	168	2.00	6.108	445221.	-2.13
+	167	2.00	6.108	445442.	-4.27
x	170	2.00	6.108	444843.	0.00



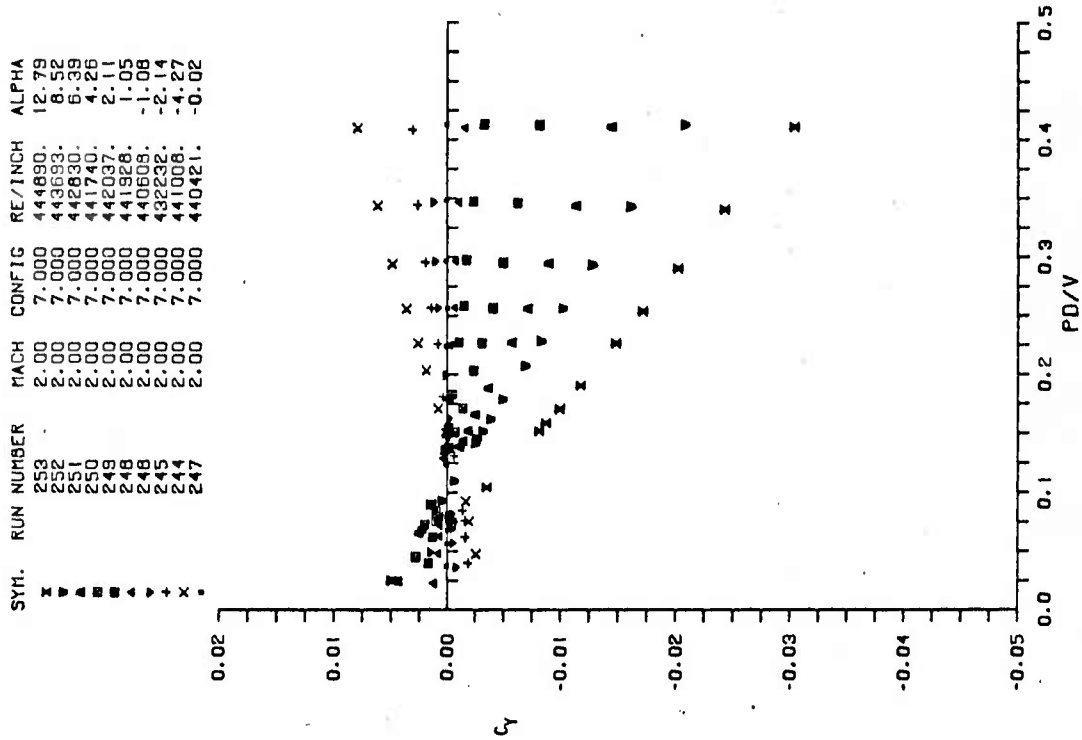
A1-32

SYM.	RUN NUMBER	MACH	CONFIG	RE/INCH	ALPHA
▲	217	2.00	6.000	5841.3.	6.71
▲	218	2.00	6.000	583660.	6.52
▲	215	2.00	6.000	583366.	4.34
▲	214	2.00	6.000	580623.	2.15
▲	213	2.00	6.000	581511.	1.09
▲	211	2.00	6.000	584681.	-1.09
▲	210	2.00	6.000	583902.	-2.19
x	209	2.00	6.000	580095.	-4.36
x	212	2.00	6.000	582925.	0.00

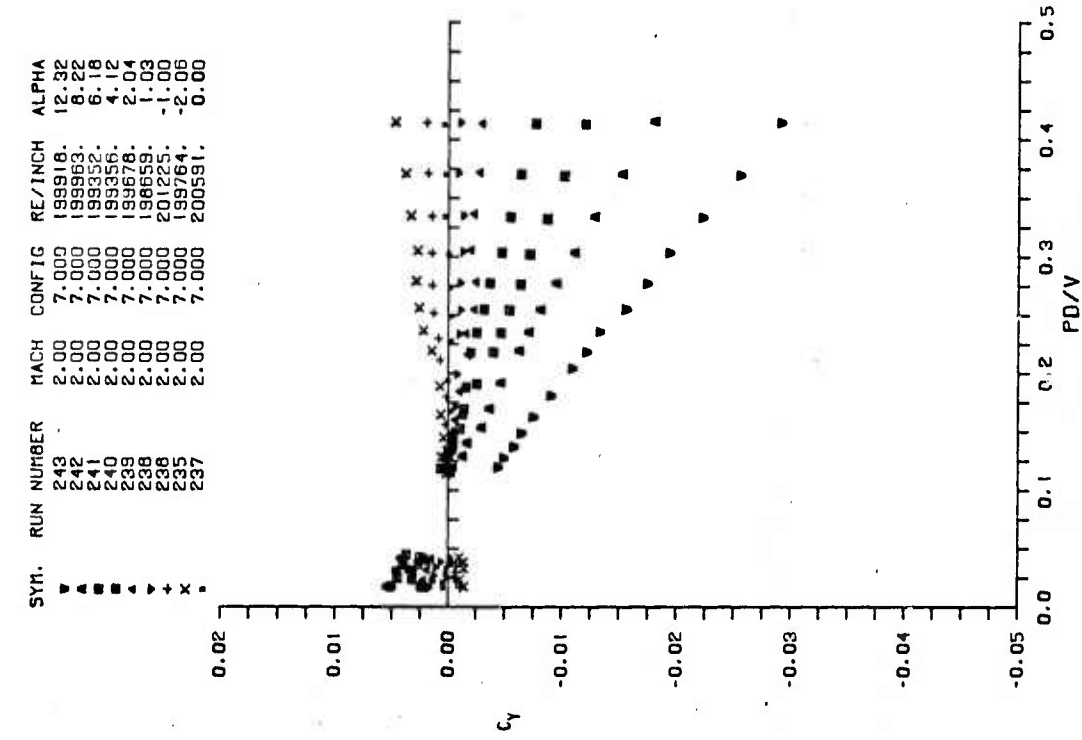


A1-31

Figure A1. Continued

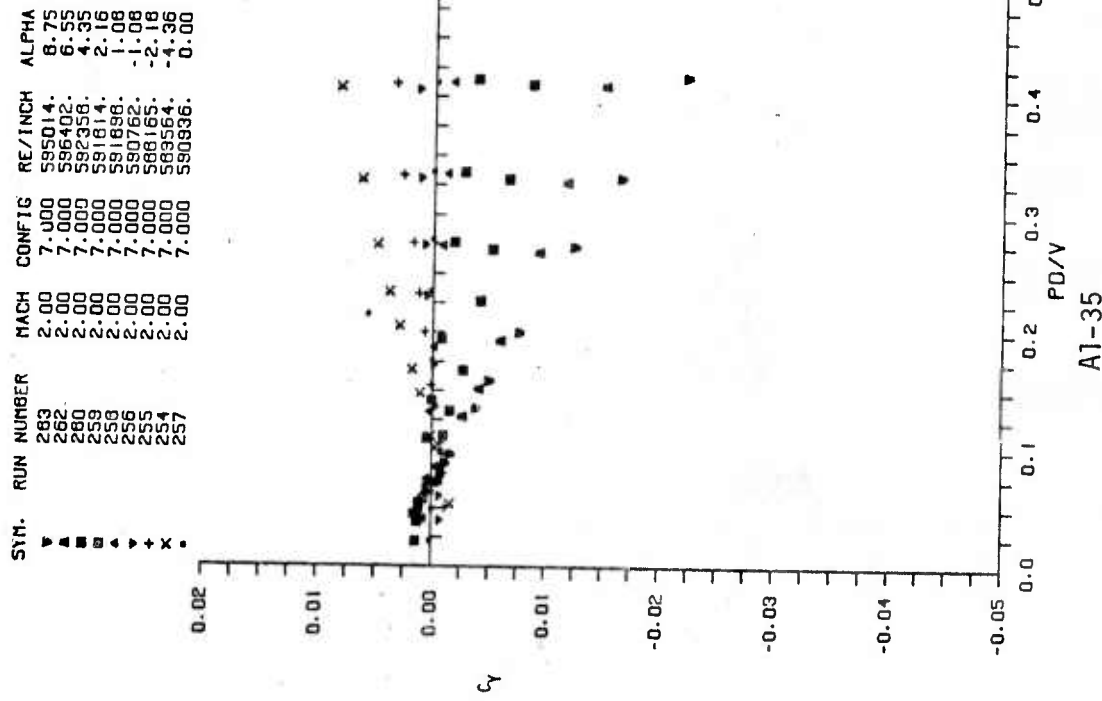


A1-34

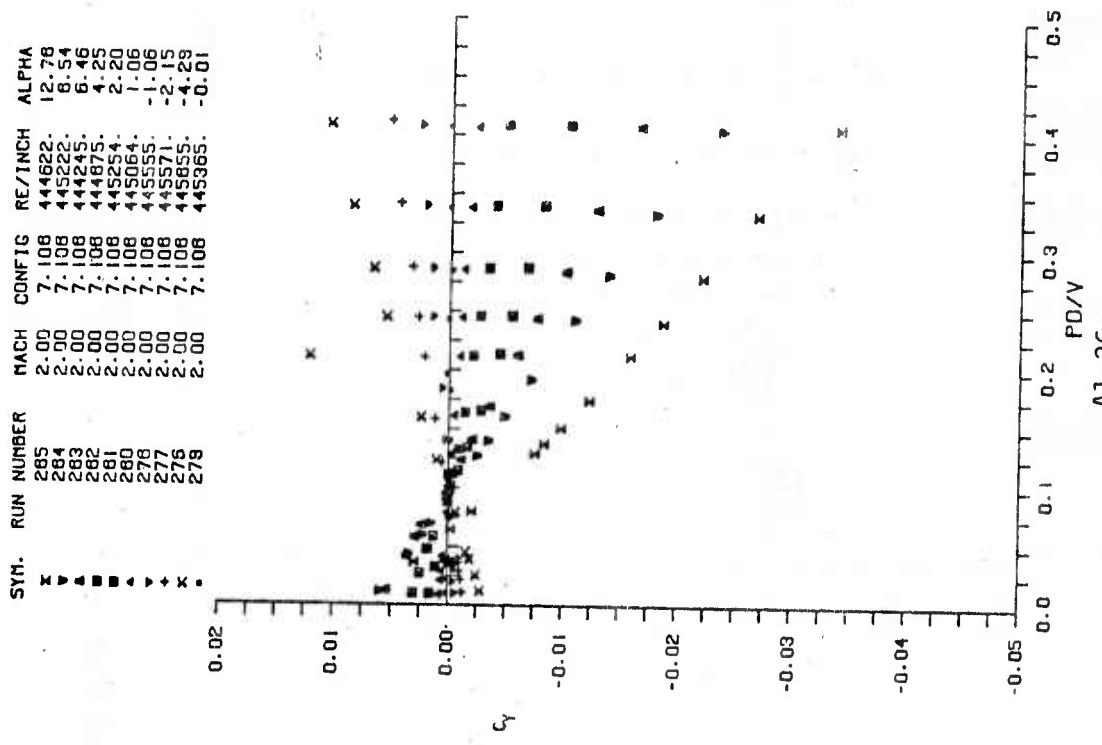


A1-33

Figure A1. Continued



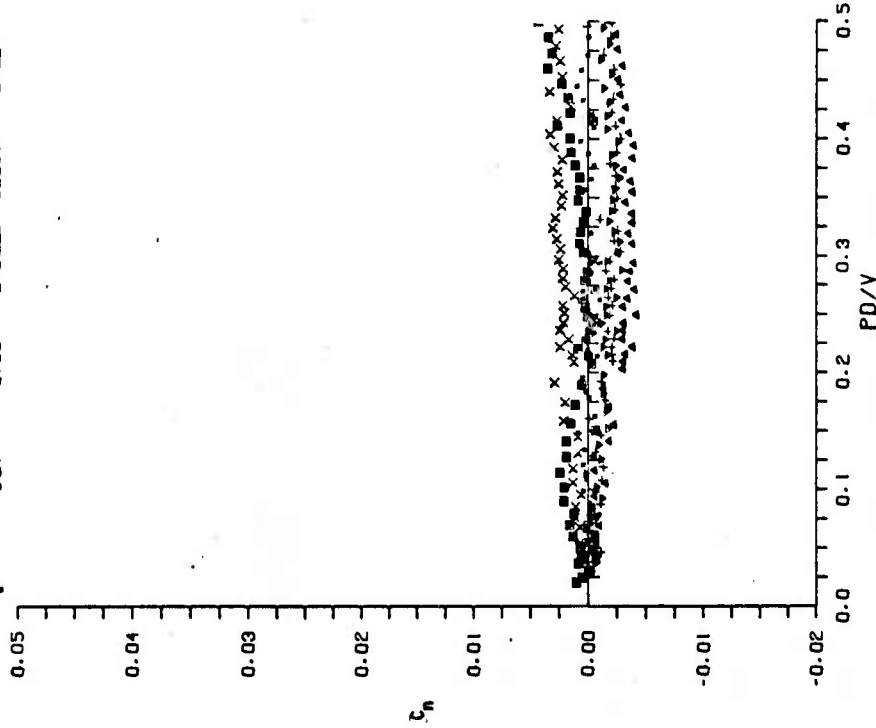
A1-35



A1-36

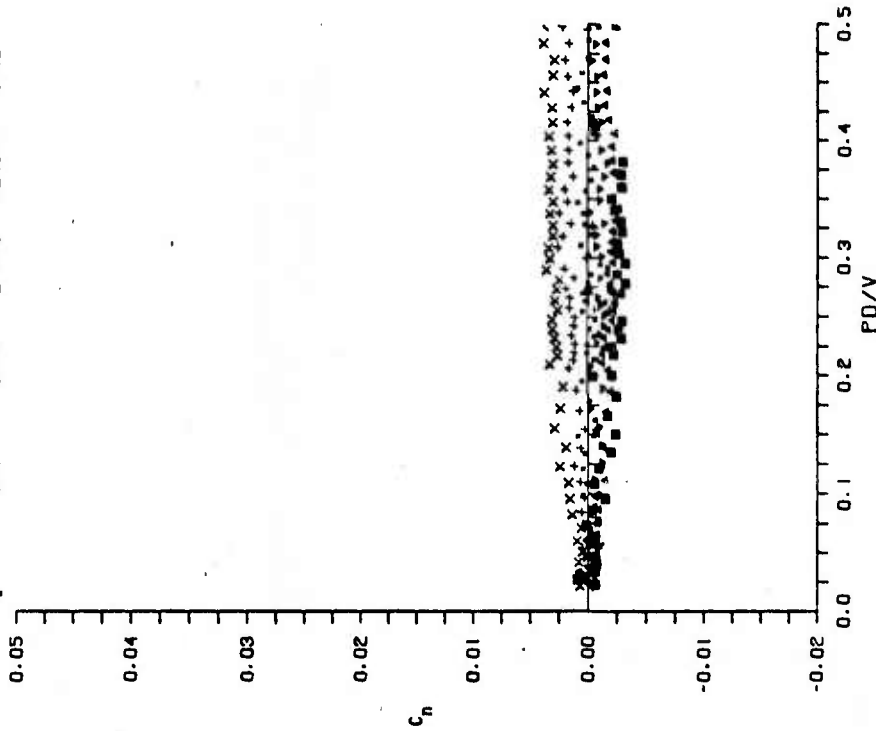
Figure A1. Concluded

SYM.	RUN NUMBER	MACH	CONFIG	RE/INCH	ALPHA
■	614	0.89	2.000	81995.	8.29
▲	608	0.89	2.000	81877.	4.2
▼	606	0.89	2.000	81914.	4.16
+	605	0.90	2.000	81995.	2.16
x	603	0.90	2.000	82199.	-2.02
.	604	0.90	2.000	82067.	0.02



A2-1

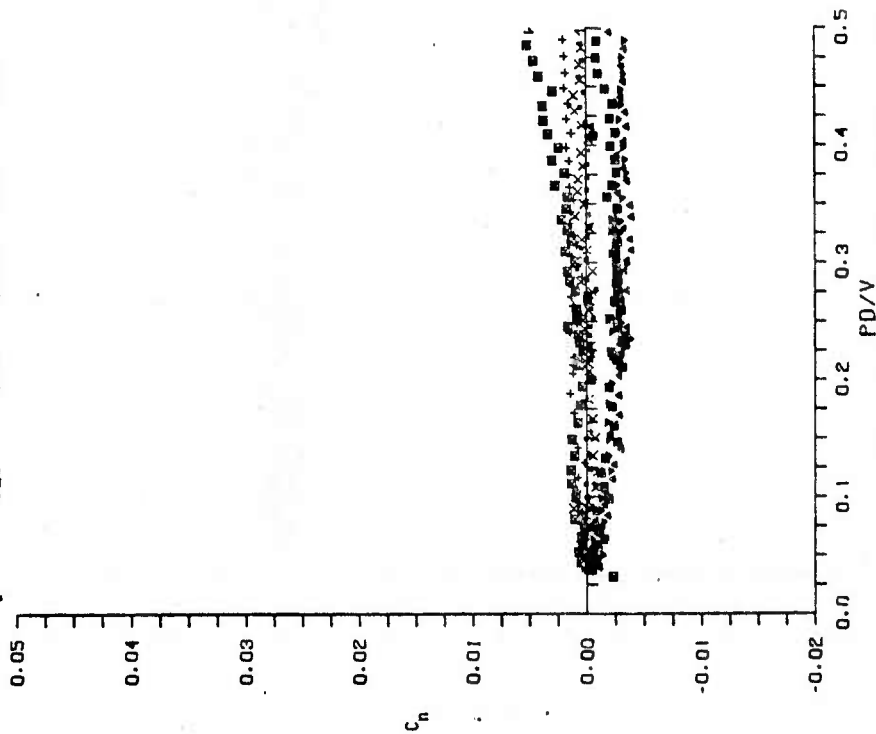
SYM.	RUN NUMBER	MACH	CONFIG	RE/INCH	ALPHA
■	613	0.90	2.000	92095.	5.19
▲	612	0.90	2.000	92173.	3.10
▼	611	0.90	2.000	92419.	1.07
+	610	0.90	2.000	92661.	-0.97
x	609	0.90	2.000	93369.	-3.04
.	604	0.90	2.000	92067.	0.02



A2-2

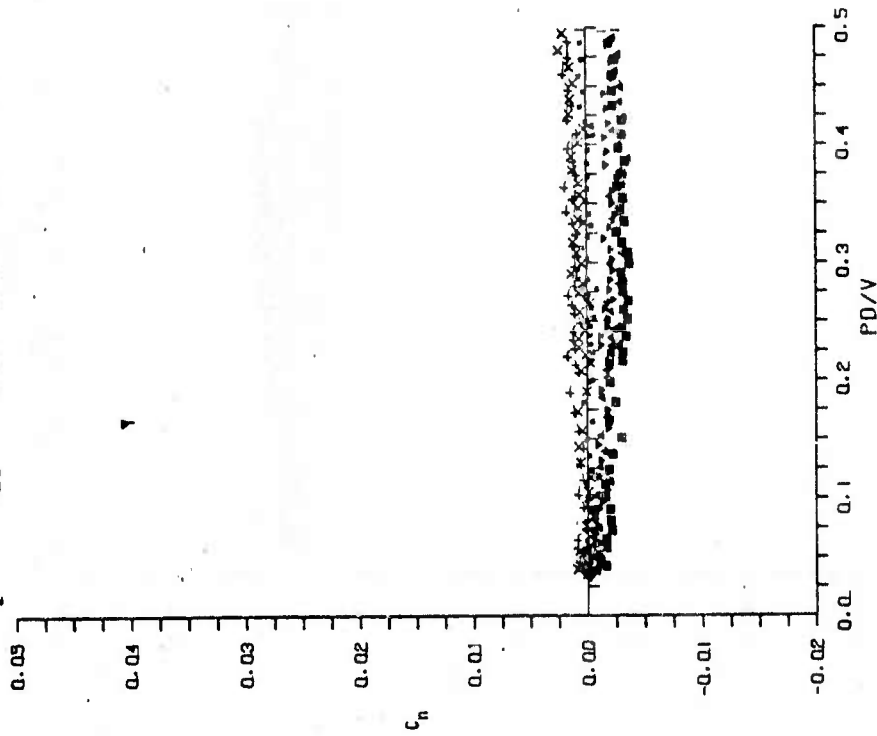
Figure A2. Basic Magnus Moment Data

SYM.	RUN NUMBER	MACH	CONFIG	RE/INCH	ALPHA
■	627	0.87	2.008	90775.	8.27
▲	622	0.88	2.008	90960.	6.23
△	626	0.87	2.008	90817.	4.17
▽	617	0.88	2.008	91425.	2.13
+	623	0.87	2.008	90764.	-2.00
x	615	0.89	2.008	92536.	-4.07
.	620	0.88	2.008	91071.	0.08



A2-3

SYM.	RUN NUMBER	MACH	CONFIG	RE/INCH	ALPHA
■	818	0.88	2.008	91137.	5.21
▲	621	0.88	2.008	91073.	3.19
△	625	0.87	2.008	90782.	1.09
▽	616	0.89	2.008	91733.	-0.98
+	619	0.88	2.008	90968.	-3.03
x	820	0.88	2.008	91071.	0.08



A2-4

Figure A2. Continued

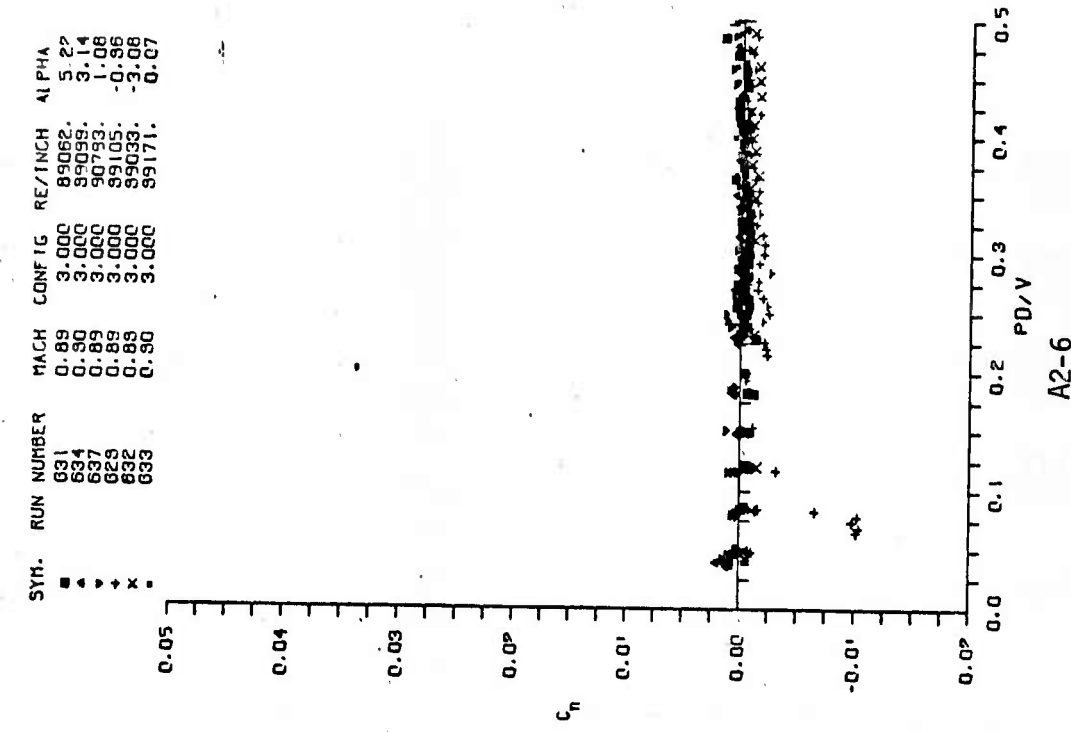
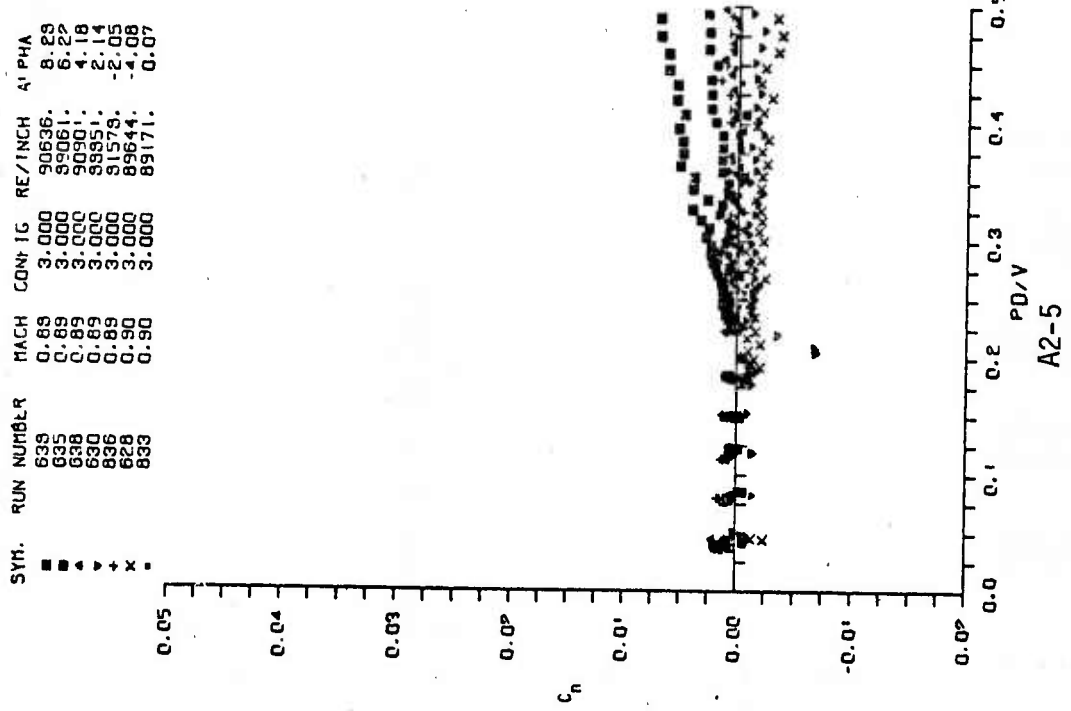
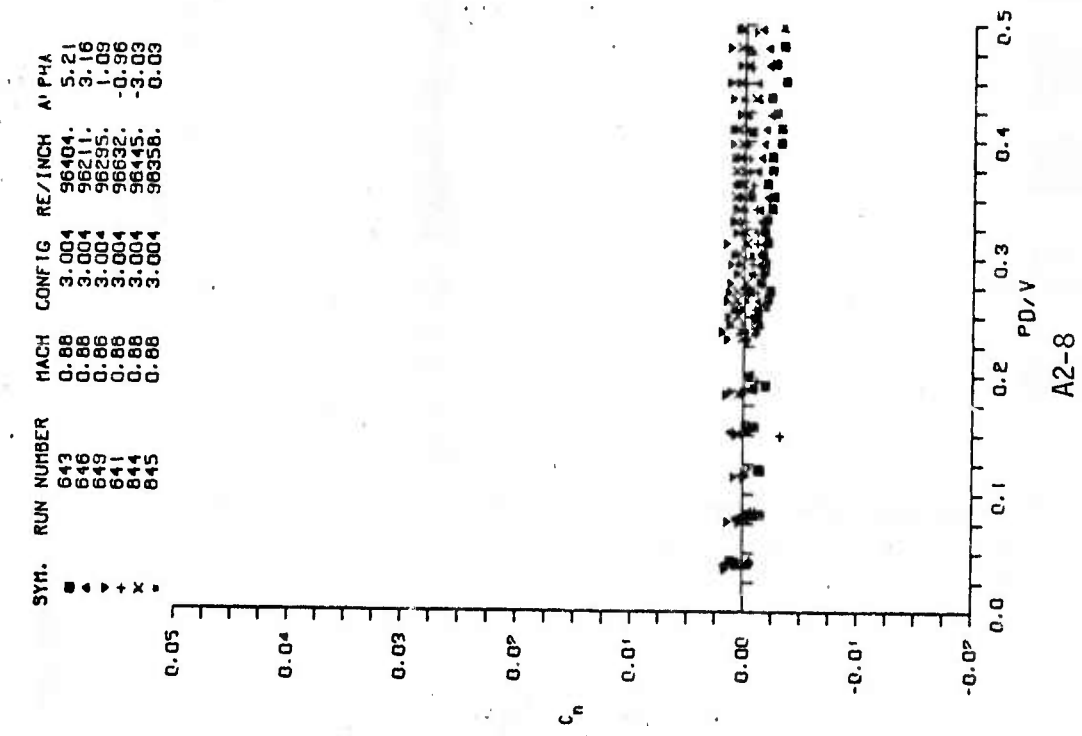
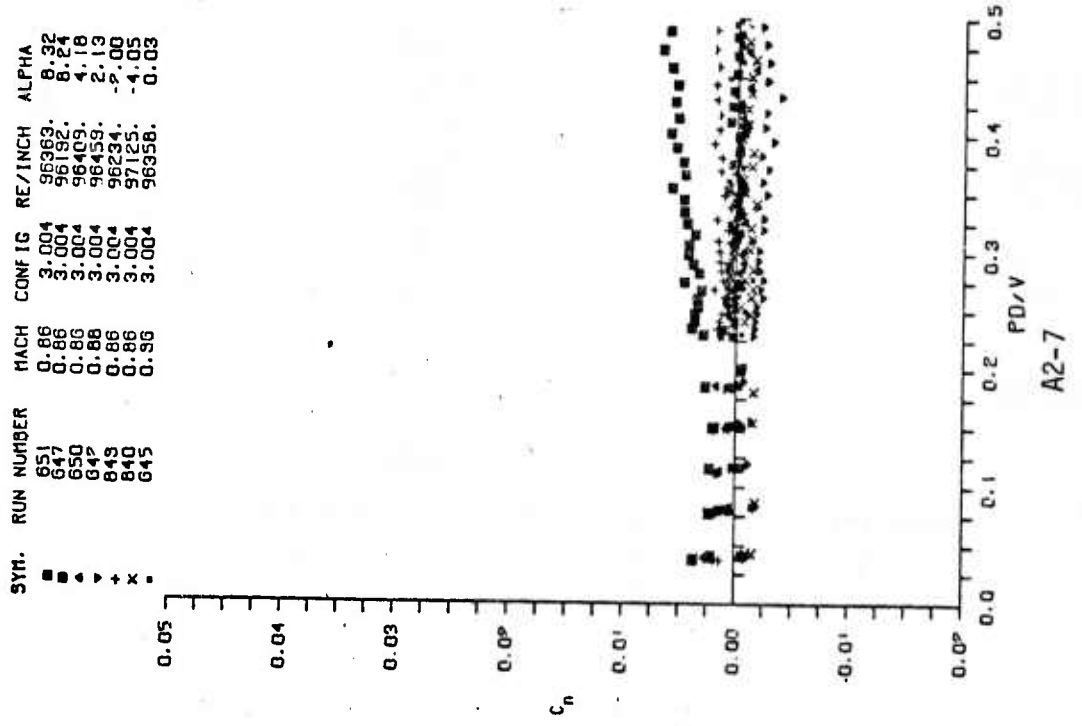


Figure A2. Continued



A2-8



A2-7

Figure A2. Continued

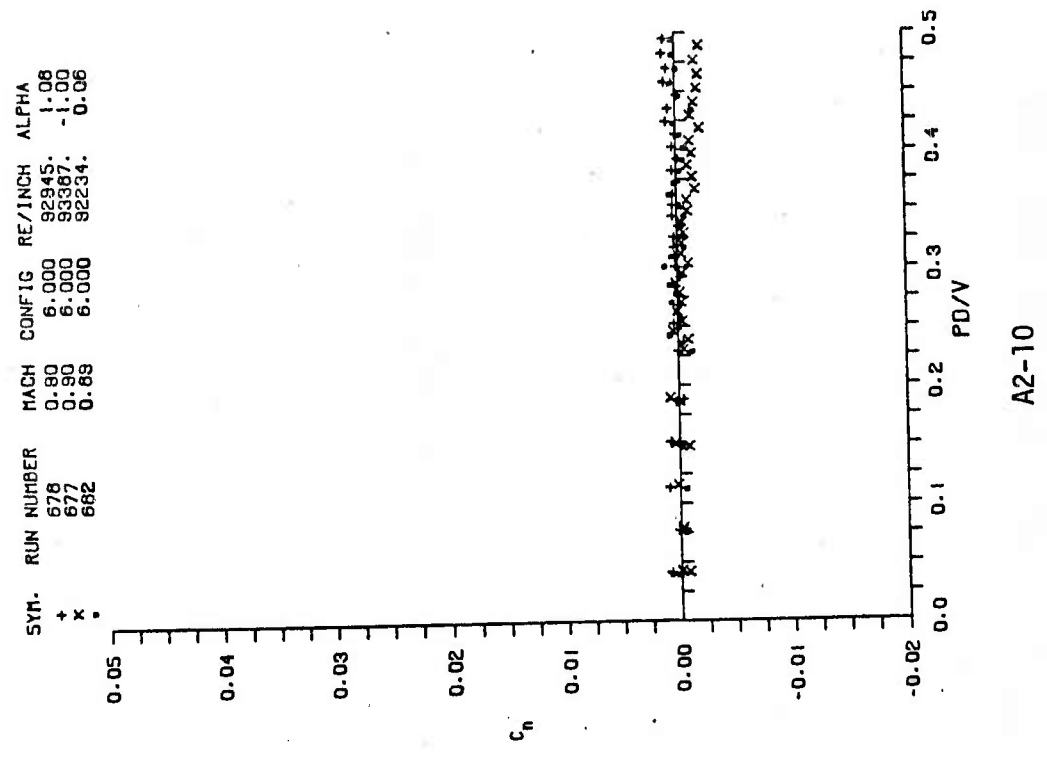
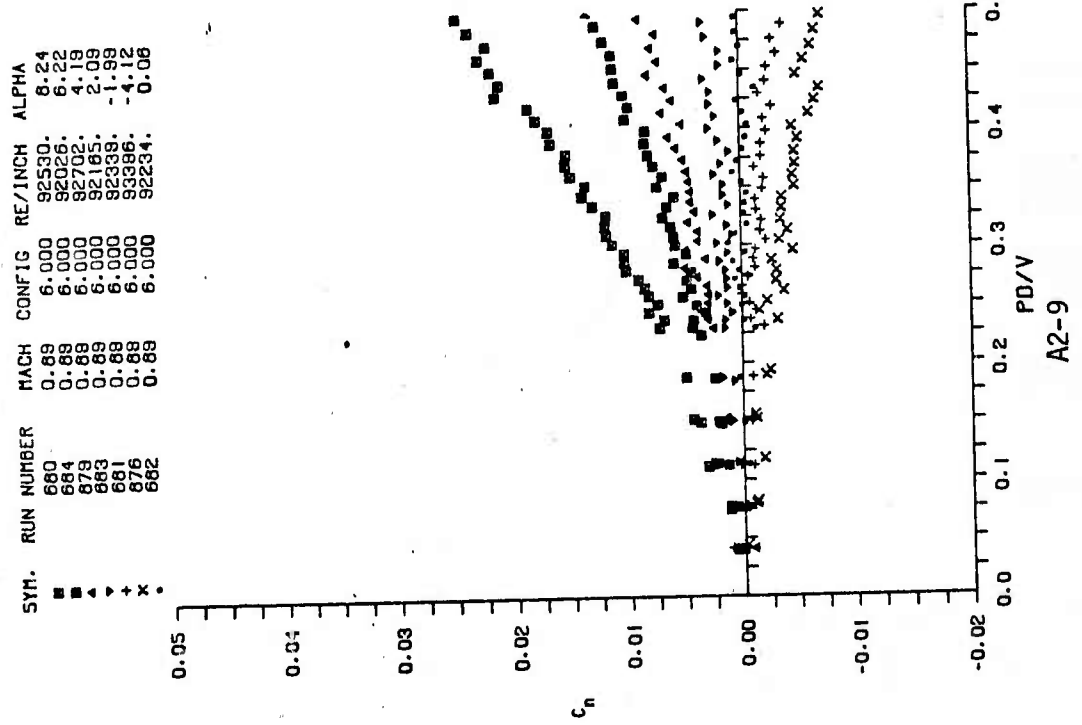
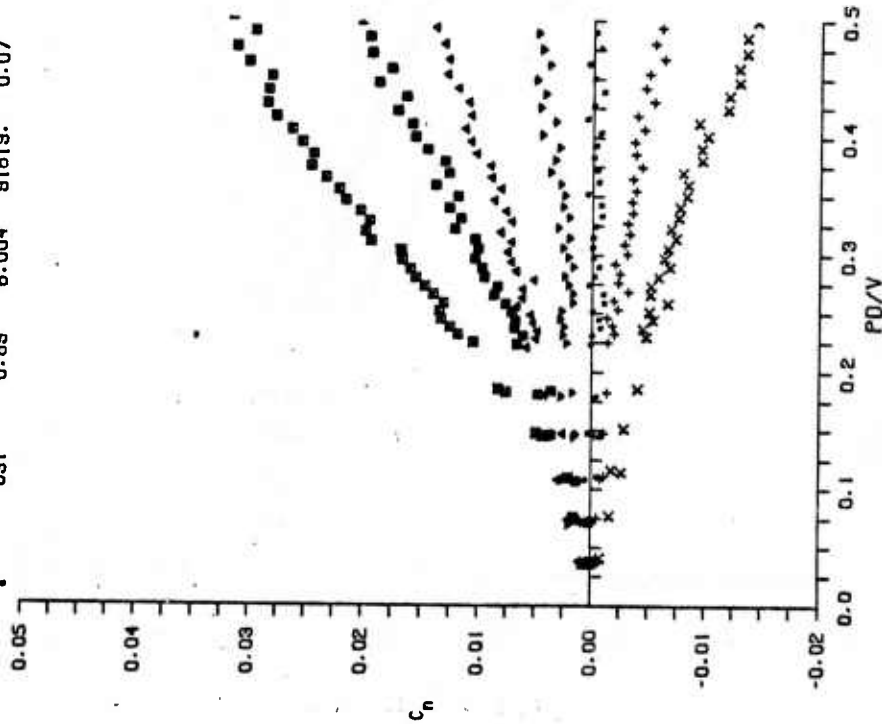


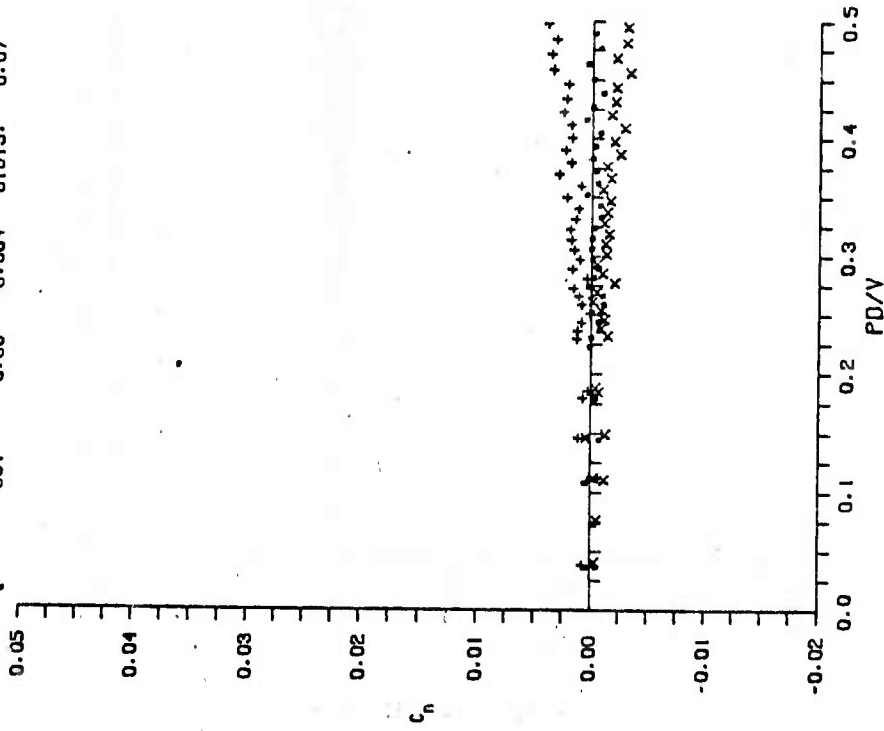
Figure A2. Continued

SYM.	RUN NUMBER	MACH	CONFIG	RE/INCH	ALPHA
■	689	0.89	6.004	81693.	6.25
■	693	0.86	6.004	81712.	6.24
▲	688	0.90	6.004	82009.	4.17
▲	692	0.89	6.004	81678.	2.11
+	690	0.89	6.004	81711.	-2.00
x	685	0.89	6.004	82053.	-4.06
.	691	0.88	6.004	81619.	0.07



A2-11

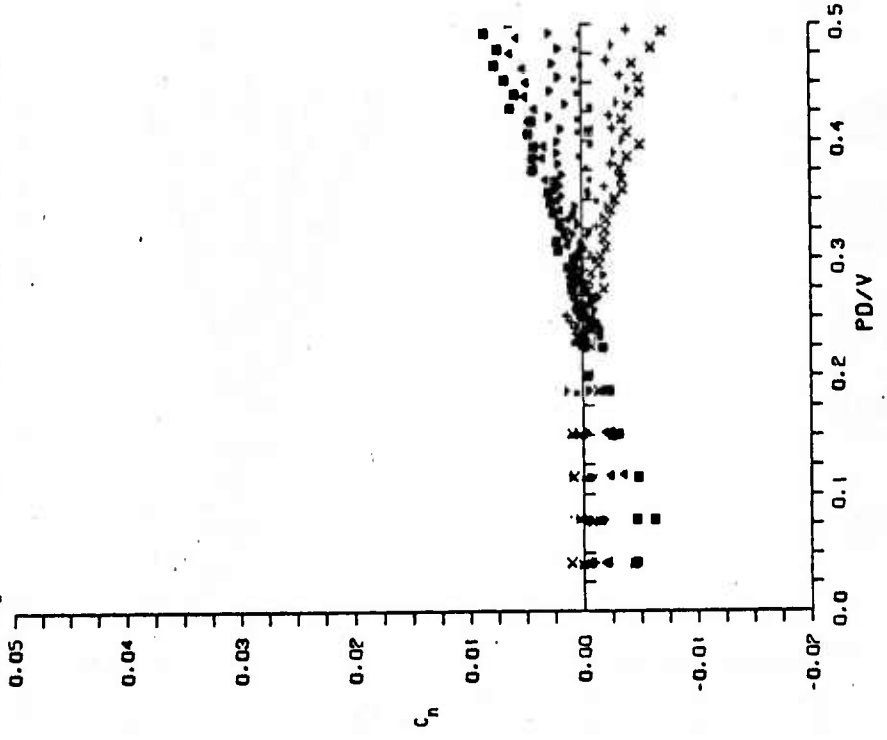
SYM.	RUN NUMBER	MACH	CONFIG	RE/INCH	ALPHA
+	887	0.89	6.004	81988.	1.07
x	886	0.89	6.004	82111.	-0.86
.	891	0.89	6.004	81619.	0.07



A2-12

Figure A2. Continued

SYM.	RUN NUMBER	MACH	CONFIG	RE/INCH	ALPHA
■	667	0.90	7.000	89932.	5.20
▲	670	0.90	7.000	90277.	3.12
▼	673	0.89	7.000	91046.	1.09
+	665	0.90	7.000	90596.	-1.07
x	668	0.89	7.000	89633.	-3.00
.	689	0.89	7.000	89566.	0.06



SYM.	RUN NUMBER	MACH	CONFIG	RE/INCH	ALPHA
■	675	0.89	7.000	90448.	6.25
▲	671	0.89	7.000	89628.	6.21
▼	674	0.89	7.000	90598.	4.14
+	666	0.90	7.000	90169.	2.10
x	672	0.90	7.000	92152.	-1.98
.	664	0.90	7.000	91153.	-4.06
.	689	0.89	7.000	89566.	0.06

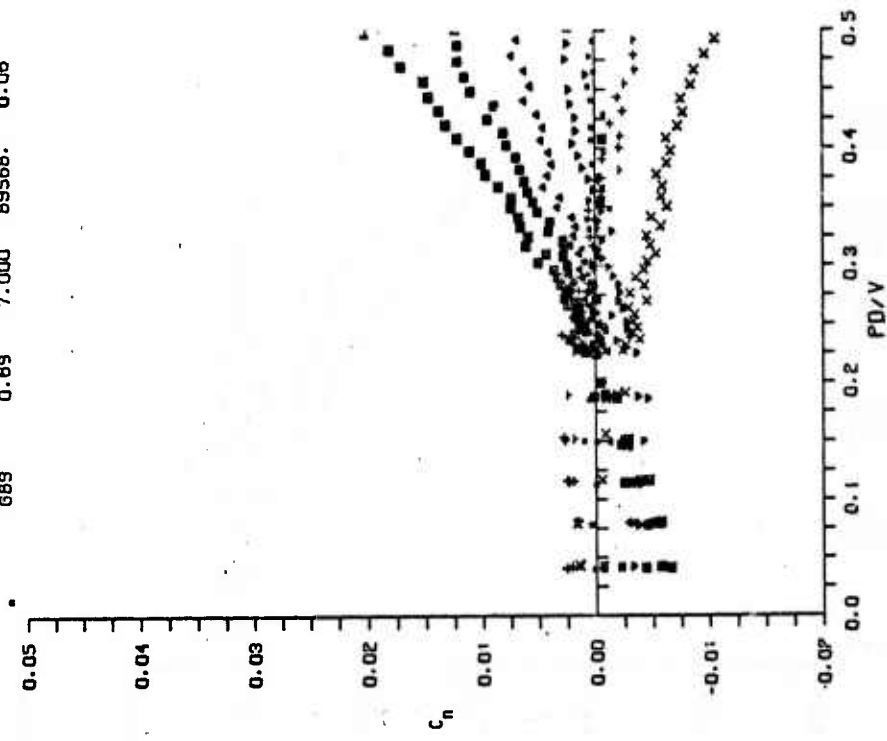
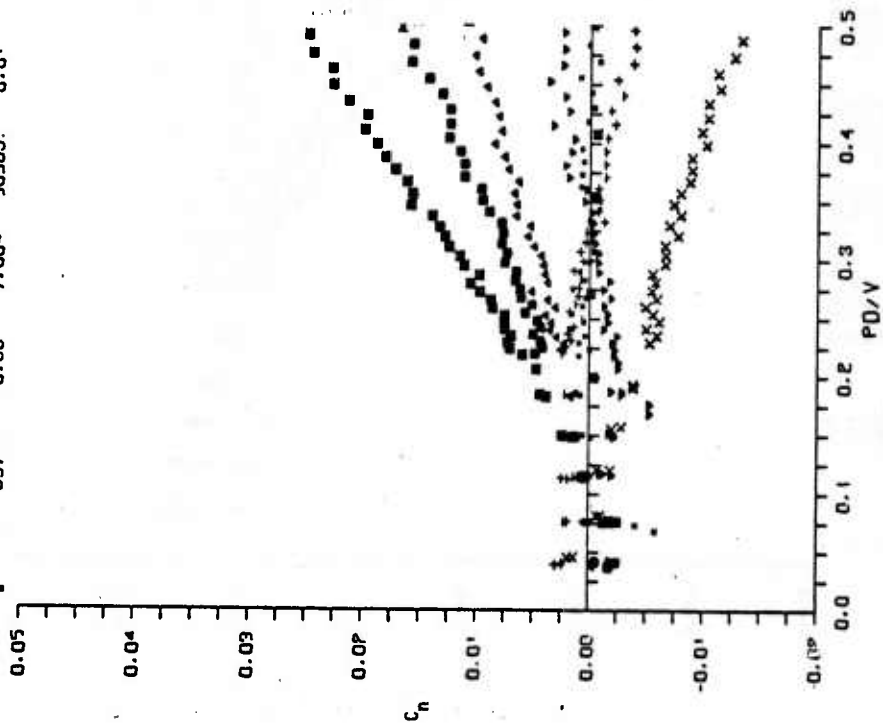


Figure A2. Continued

SYN.	RUN NUMBER	MACH	CONFIG	RE/INCH	ALPHA
■	663	0.89	7.004	88686.	8.25
▲	659	0.89	7.004	90410.	6.24
◆	662	0.89	7.004	89016.	4.15
▼	654	0.90	7.004	90782.	2.10
+	680	0.89	7.004	92555.	-2.07
x	852	0.90	7.004	91183.	-4.09
•	657	0.89	7.004	90389.	0.01



SYN.	RUN NUMBER	MACH	CONFIG	RE/INCH	ALPHA
■	655	0.90	7.004	80605.	5.21
▲	658	0.89	7.004	80409.	3.12
◆	661	0.89	7.004	89252.	1.08
▼	653	0.90	7.004	90872.	-0.97
+	656	0.90	7.004	90478.	-3.07
x	657	0.89	7.004	90389.	0.01

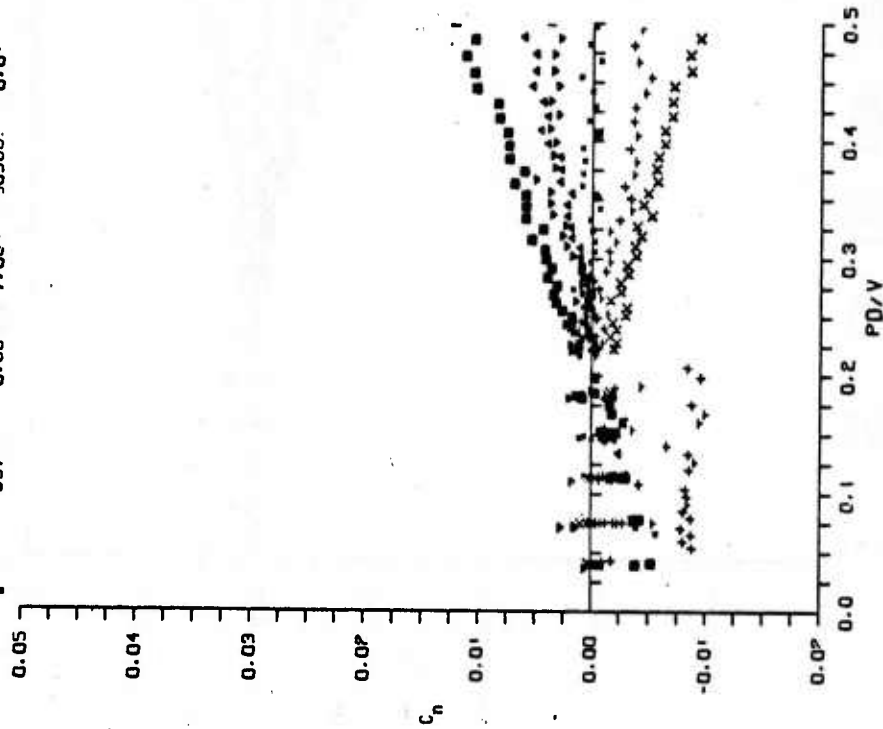
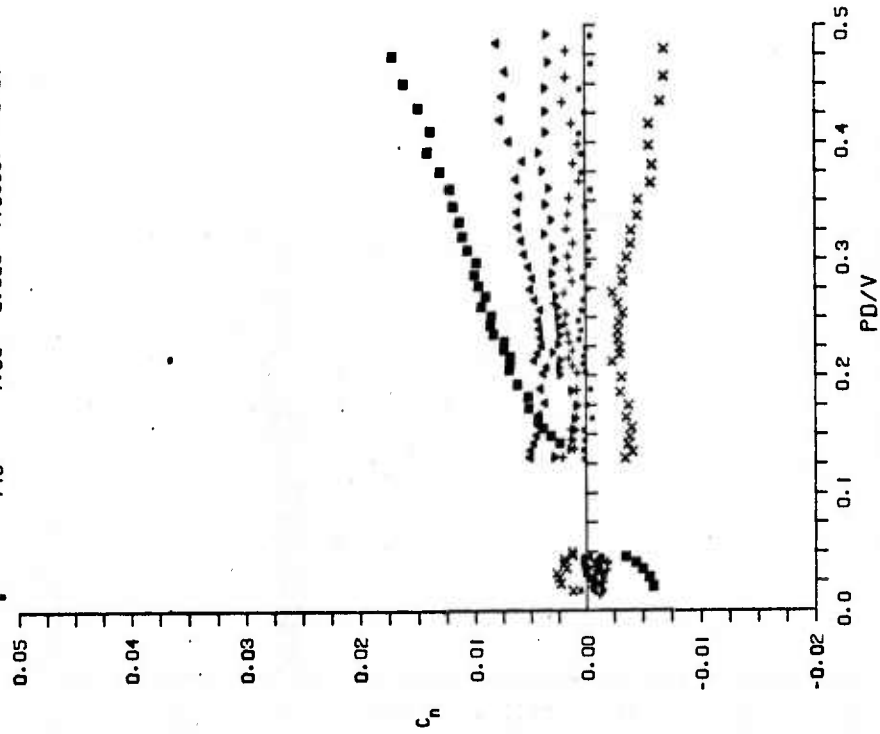


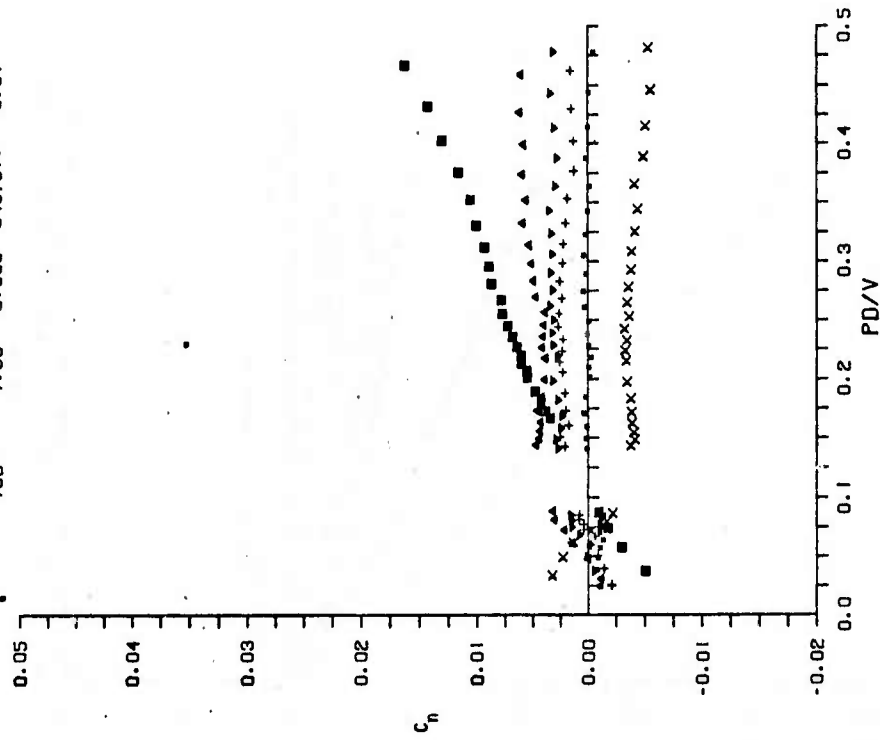
Figure A2. Continued

SYM.	RUN NUMBER	MACH	CONFIG	RE/INCH	ALPHA
■	148	1.50	3.000	175568.	6.19
▲	149	1.50	3.000	175639.	4.09
▼	147	1.50	3.000	175635.	2.03
+	146	1.50	3.000	176233.	1.01
x	144	1.50	3.000	176303.	-4.10
•	145	1.50	3.000	175808.	-0.01



A2-17

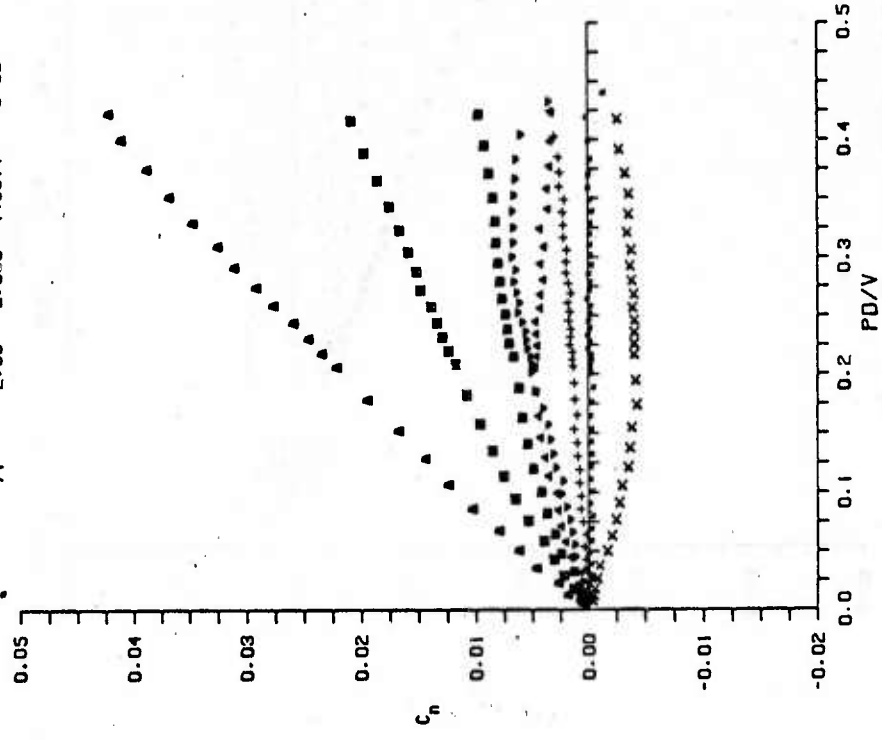
SYM.	RUN NUMBER	MACH	CONFIG	RE/INCH	ALPHA
■	143	1.50	3.000	348695.	6.43
▲	142	1.50	3.000	349171.	4.20
▼	141	1.50	3.000	348920.	2.09
+	140	1.50	3.000	348699.	1.05
x	138	1.50	3.000	348726.	-4.21
•	139	1.50	3.000	348757.	0.01



A2-18

Figure A2. Continued

SYN.	RUN NUMBER	MACH	CONFIC	RE/INCH	ALPHA
▲	76	2.00	2.000	446573.	12.84
■	77	2.00	2.000	446307.	8.57
▲	75	2.00	2.000	447031.	6.43
▲	74	2.00	2.000	445532.	4.27
▲	73	2.00	2.000	445522.	2.11
+	72	2.00	2.000	445413.	1.06
x	71	2.00	2.000	445916.	-4.29
.		2.00	2.000	443571.	-0.02



SYN.	RUN NUMBER	MACH	CONFIC	RE/INCH	ALPHA
■	83	2.00	2.000	199096.	8.21
▲	82	2.00	2.000	199592.	4.09
▲	81	2.00	2.000	199096.	2.02
+	80	2.00	2.000	200527.	1.01
x	78	2.00	2.000	200422.	-4.11
.	79	2.00	2.000	200031.	-0.01

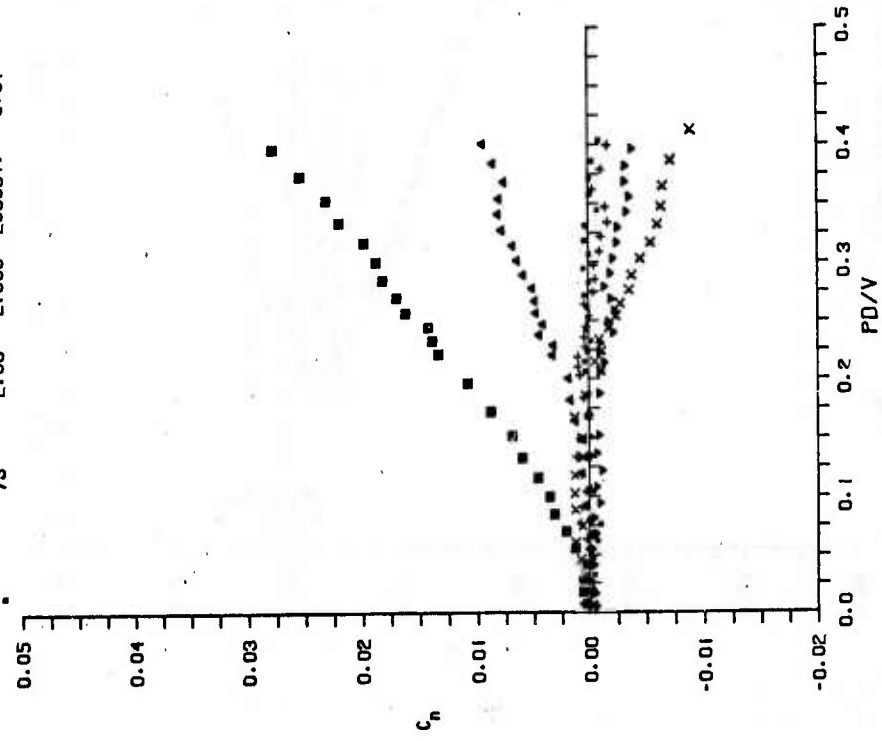
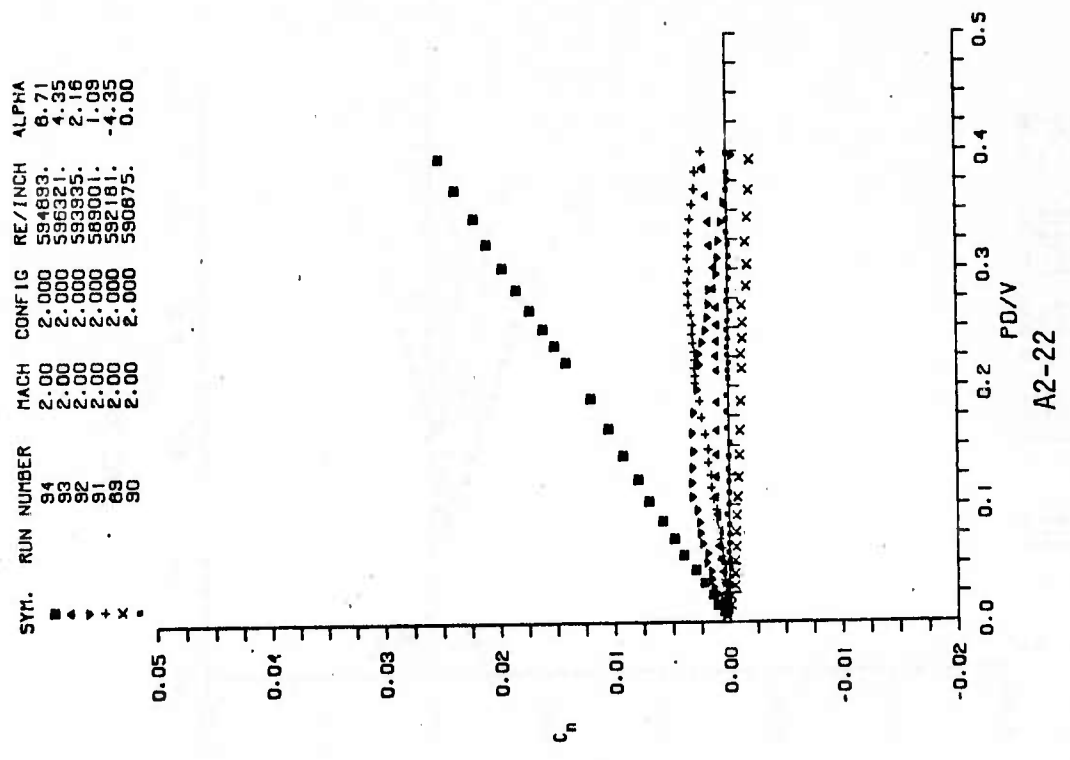
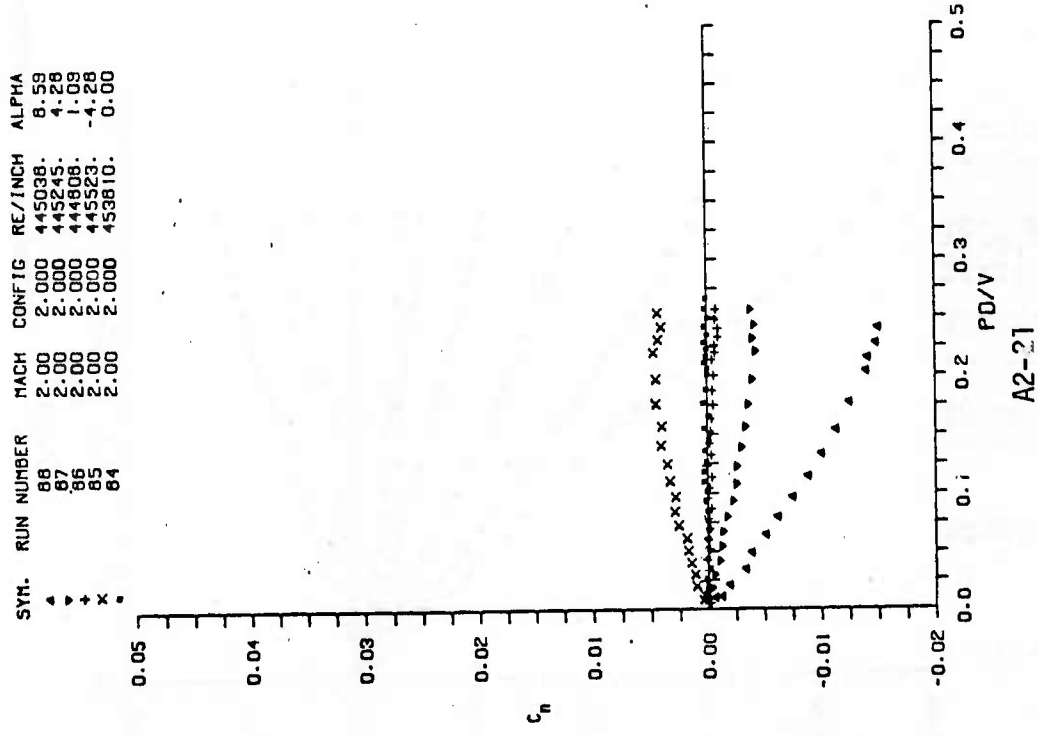


Figure A2. Continued



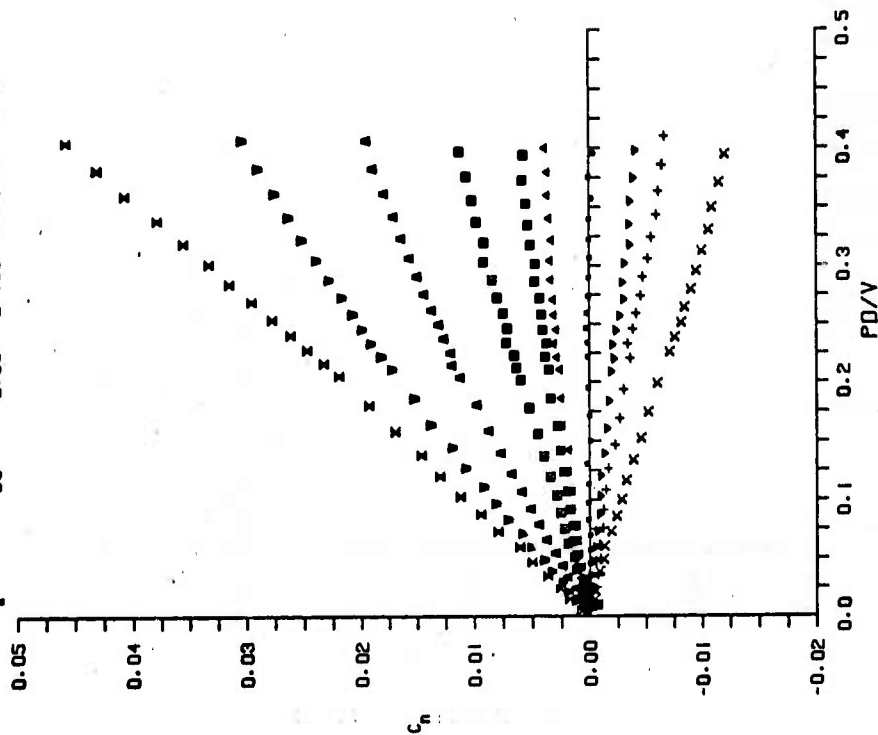
A2-22



A2-21

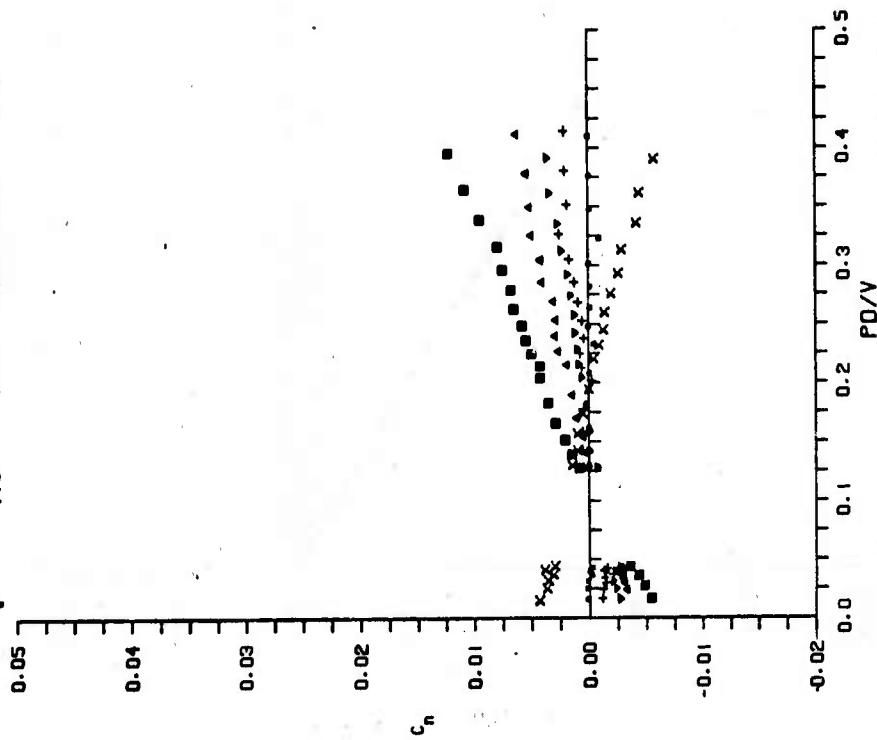
Figure A2. Continued

SYM.	RUN NUMBER	MACH	CONFIG	RE/INCH	ALPHA
x	76	2.00	2.108	448060.	12.74
x	75	2.00	2.108	448158.	6.50
▲	70	2.00	2.108	446263.	6.98
▲	63	2.00	2.108	447197.	4.23
▲	67	2.00	2.108	447103.	2.10
▲	64	2.00	2.108	447626.	1.04
▲	64	2.00	2.108	447865.	-1.07
▲	63	2.00	2.108	446278.	-2.14
x	82	2.00	2.108	448283.	-4.27
x	85	2.00	2.108	447849.	-0.02



A2-23

SYM.	RUN NUMBER	MACH	CONFIG	RE/INCH	ALPHA
■	122	2.00	3.000	198584.	8.23
▲	121	2.00	3.000	198386.	4.10
▲	120	2.00	3.000	198980.	2.04
▲	119	2.00	3.000	198423.	1.03
x	117	2.00	3.000	198469.	-4.11
●	118	2.00	3.000	198121.	0.00



A2-24

Figure A2. Continued

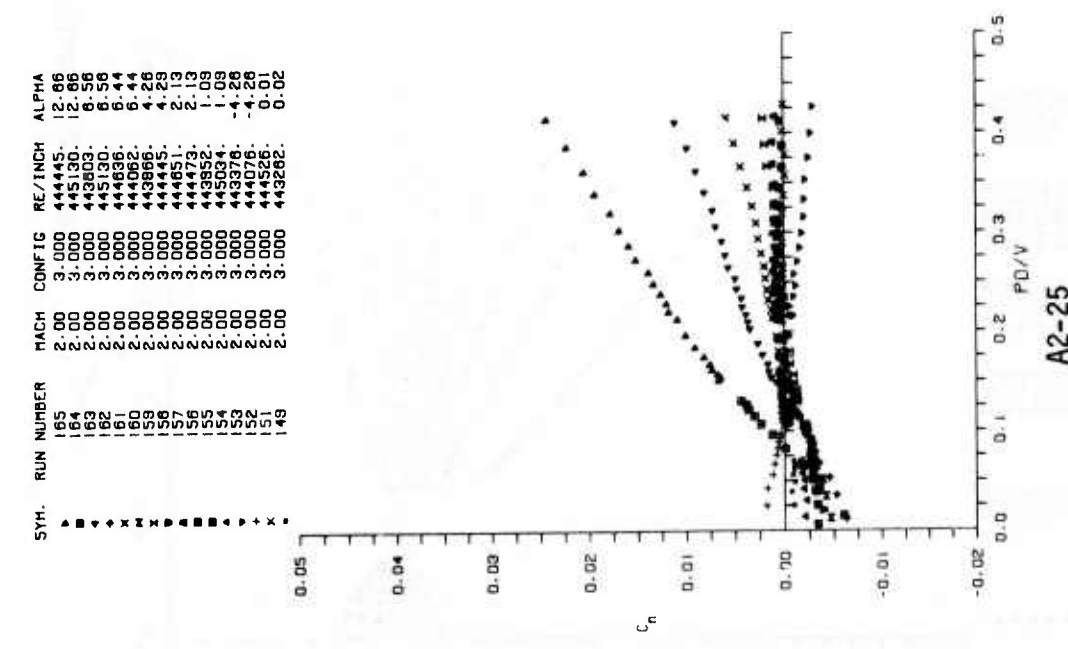
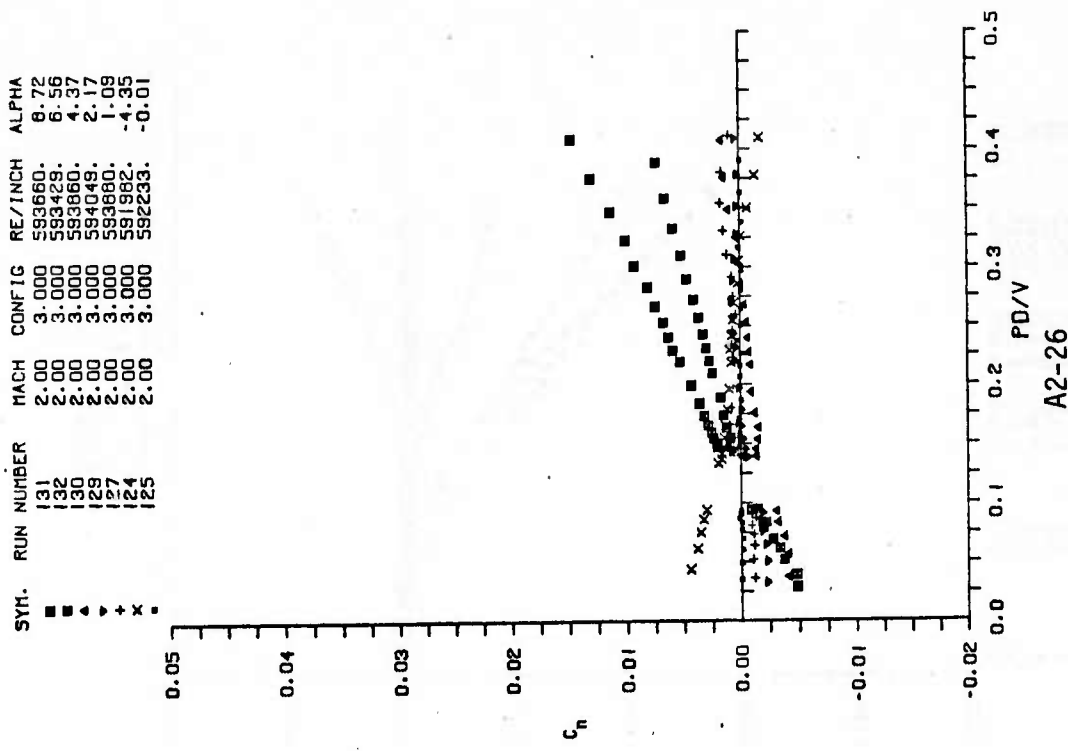
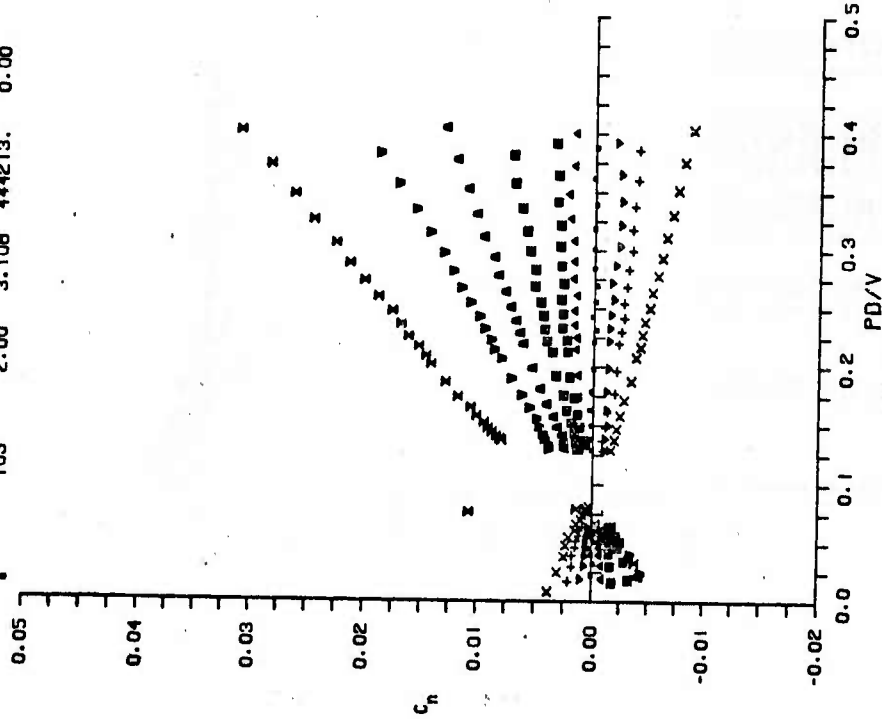


Figure A2. Continued

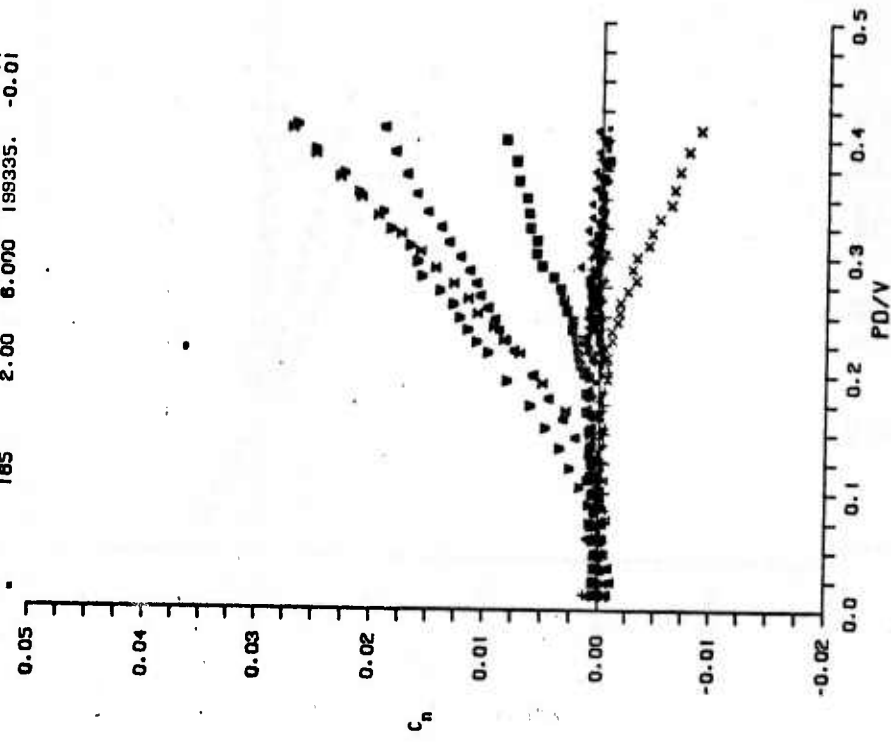
SYM.	RUN NUMBER	MACH	CONFIG	RE/INCH	ALPHA
x	115	2.00	3.108	443946.	12.78
x	114	2.00	3.108	443946.	6.52
▲	113	2.00	3.108	444843.	6.39
▲	112	2.00	3.108	444686.	4.24
■	111	2.00	3.108	445774.	2.10
▲	110	2.00	3.108	444822.	1.08
▼	109	2.00	3.108	445727.	-1.08
▼	104	2.00	3.108	444701.	-4.27
x	103	2.00	3.108	444213.	0.00



A2-27

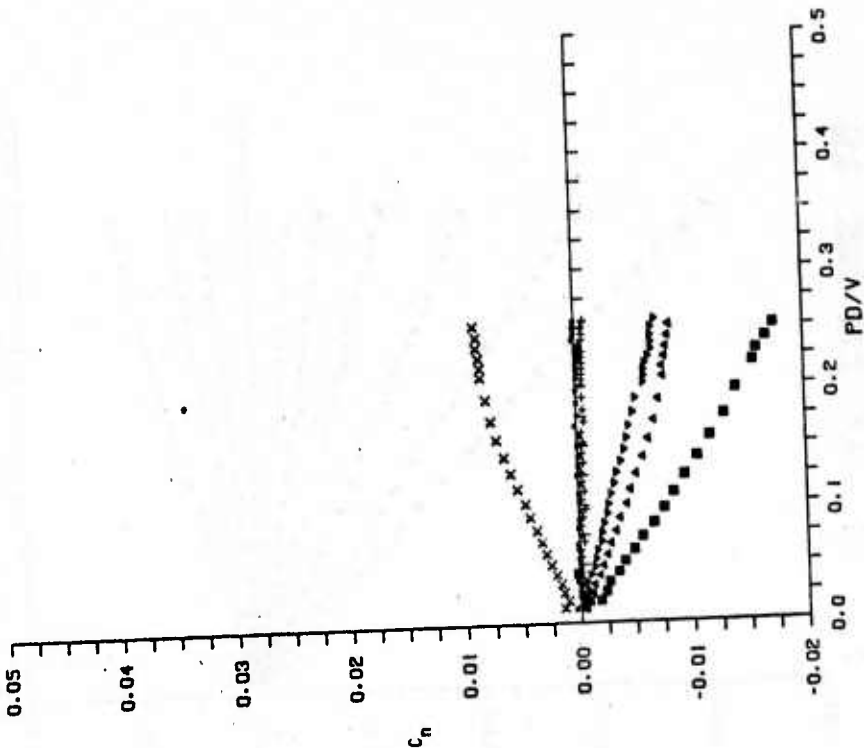
Figure A2. Continued

SYM.	RUN NUMBER	MACH	CONFIG	RE/INCH	ALPHA
x	181	2.00	6.000	198614.	12.31
▼	180	2.00	6.000	198054.	6.22
▲	189	2.00	6.000	198984.	6.17
■	188	2.00	6.000	198955.	4.12
▲	187	2.00	6.000	198584.	2.04
▲	186	2.00	6.000	199579.	1.03
▼	184	2.00	6.000	198170.	-1.03
▼	183	2.00	6.000	197442.	-2.08
x	181	2.00	6.000	198008.	-4.11
x	185	2.00	6.000	199335.	-0.01



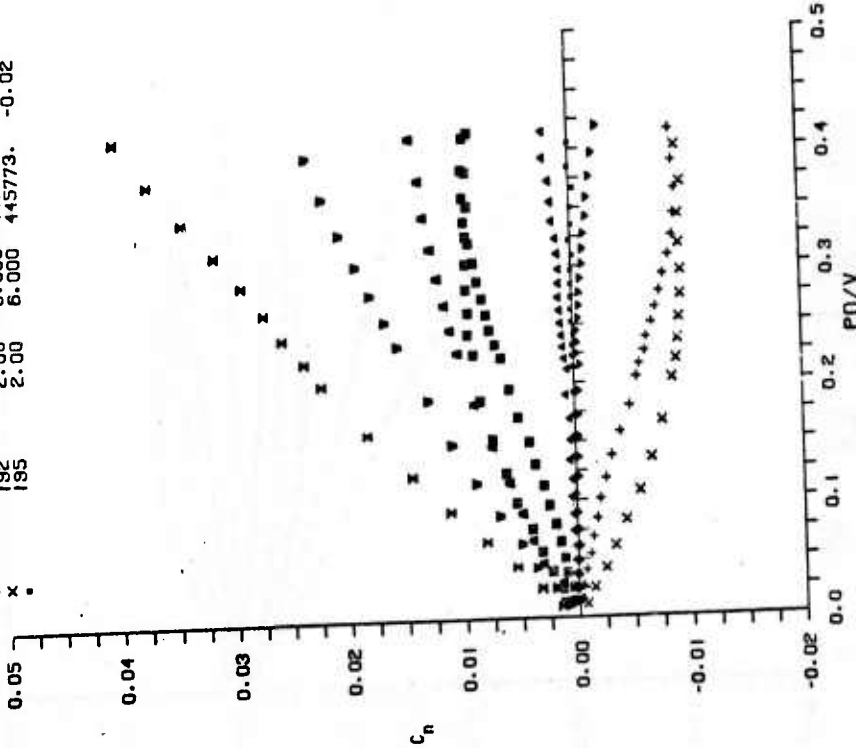
A2-28

SYM.	RUN NUMBER	MACH	CONFIG	RE/INCH	ALPHA
■	208	2.00	6.000	444937.	8.52
▲	207	2.00	6.000	445031.	4.25
△	206	2.00	6.000	445267.	2.10
+	204	2.00	6.000	444072.	1.06
x	202	2.00	6.000	444827.	-4.68
•	203	2.00	6.000	444717.	-0.02



A2-30

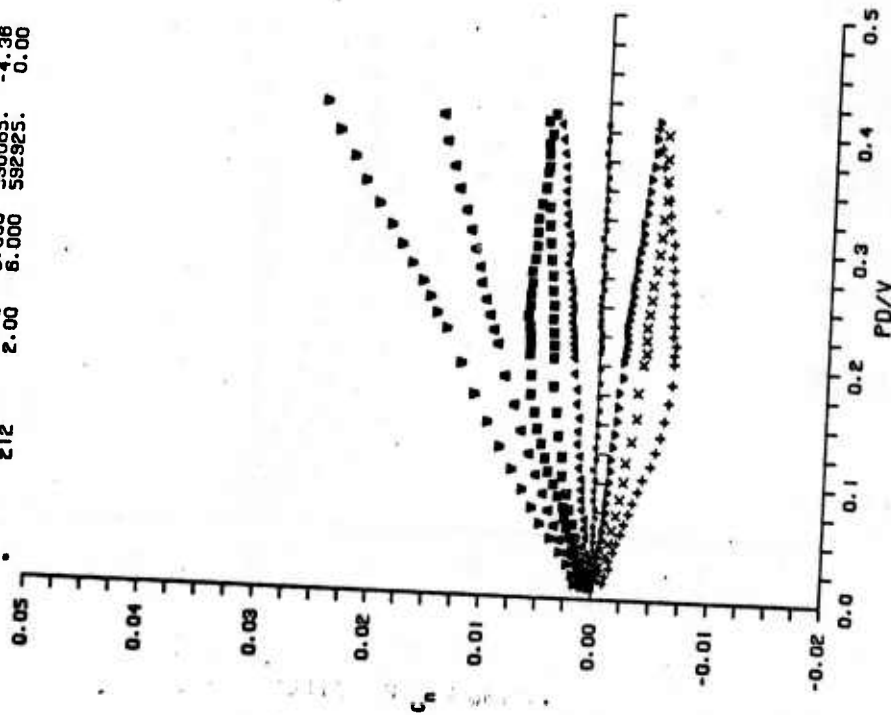
SYM.	RUN NUMBER	MACH	CONFIG	RE/INCH	ALPHA
x	201	2.00	6.000	445568.	12.76
▲	200	2.00	6.000	444780.	8.52
△	199	2.00	6.000	445725.	6.39
■	198	2.00	6.000	44612.	4.27
•	197	2.00	6.000	443441.	2.10
+	196	2.00	6.000	445379.	1.06
•	194	2.00	6.000	445757.	-1.07
•	193	2.00	6.000	445174.	-2.13
•	192	2.00	6.000	445363.	-4.25
•	195	2.00	6.000	445773.	-0.02



A2-29

Figure A2. Continued

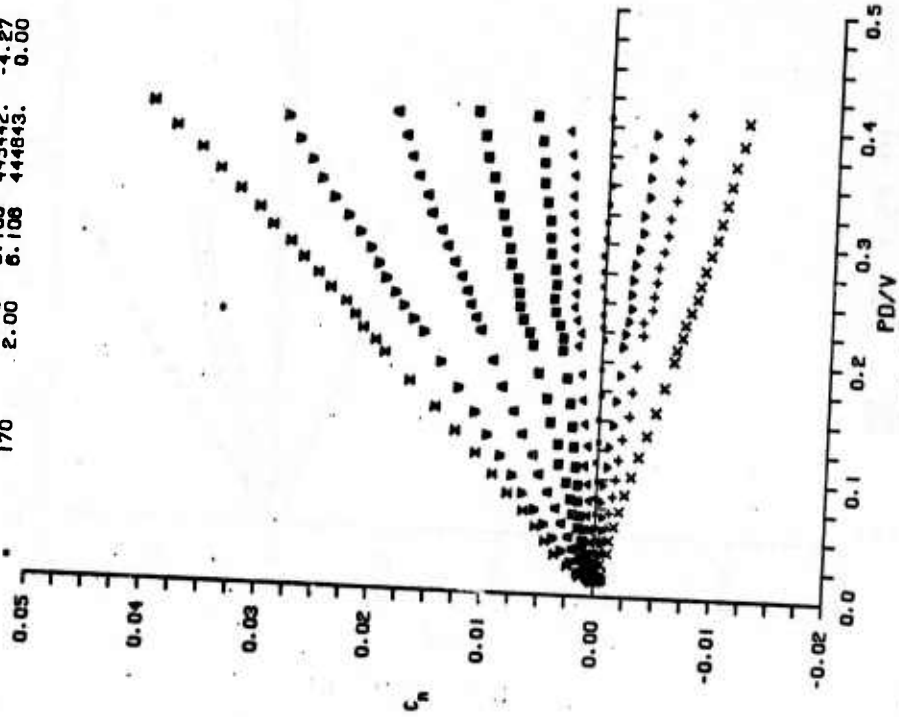
SYN.	RUN NUMBER	MACH	CONFIG	RE/INCH	ALPHA
▲	217	2.00	6.000	594113.	6.71
▲	218	2.00	6.000	592869.	6.52
▲	219	2.00	6.000	592369.	4.34
▲	214	2.00	6.000	590623.	2.15
▲	213	2.00	6.000	591511.	1.03
▲	211	2.00	6.000	584661.	-1.09
▲	210	2.00	6.000	583902.	-2.19
▲	209	2.00	6.000	590085.	-4.36
▲	212	2.00	6.000	592925.	0.00



A2-31

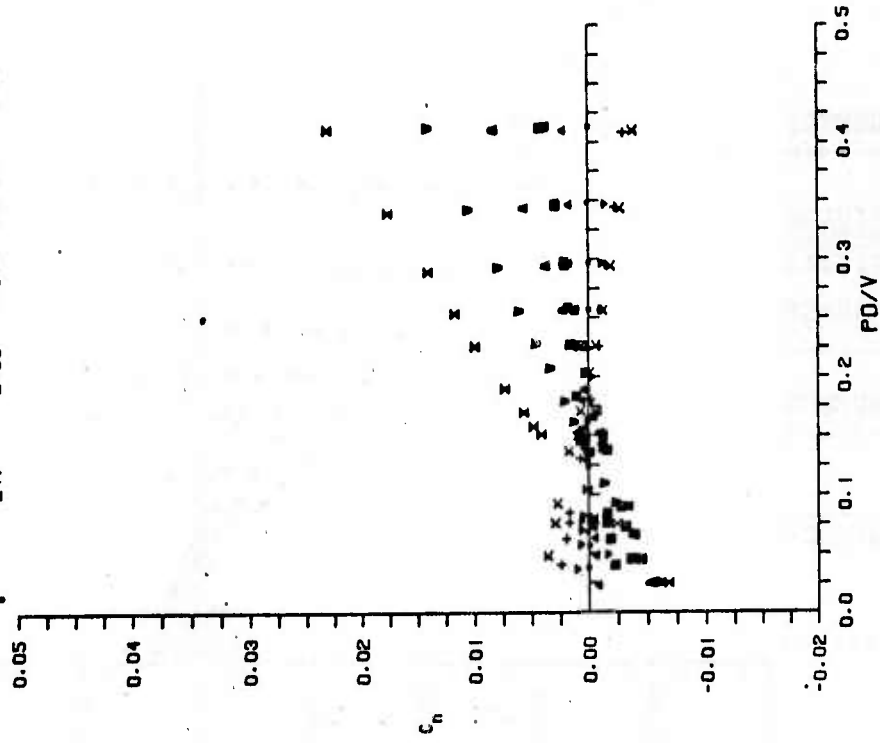
Figure A2. Continued

SYN.	RUN NUMBER	MACH	CONFIG	RE/INCH	ALPHA
▲	176	2.00	6.108	443976.	12.76
▲	175	2.00	6.108	443899.	6.52
▲	174	2.00	6.108	443549.	6.38
▲	173	2.00	6.108	44416.	4.25
▲	172	2.00	6.108	44416.	2.11
▲	171	2.00	6.108	444607.	1.05
▲	169	2.00	6.108	444638.	-1.09
▲	168	2.00	6.108	445032.	-2.13
▲	167	2.00	6.108	445442.	-4.27
▲	170	2.00	6.108	444843.	0.00



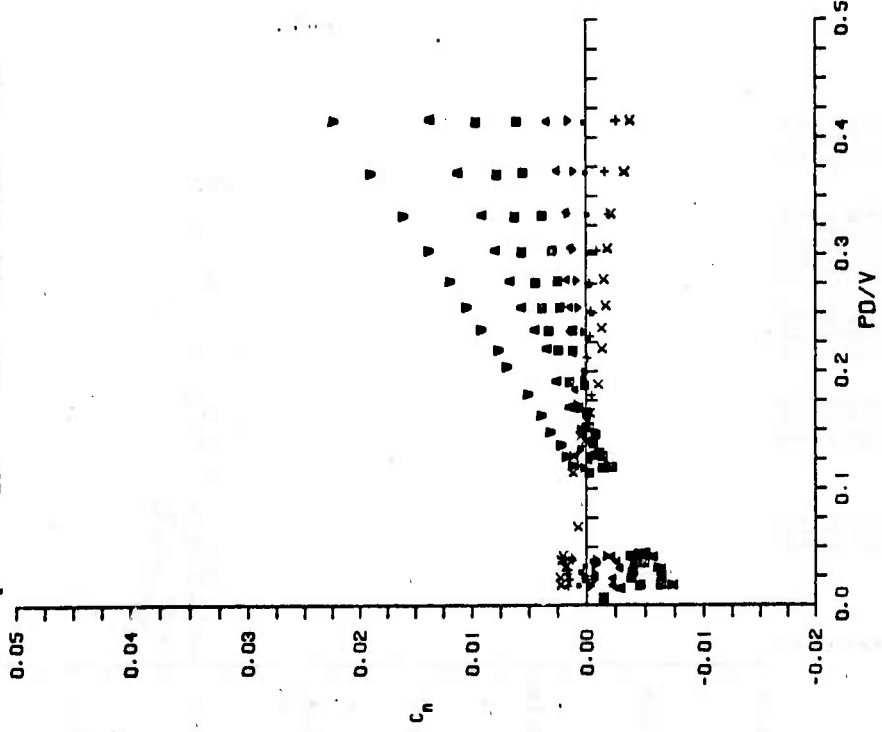
A2-32

SYN.	RUN NUMBER	MACH	CONFIG	RE/INCH	ALPHA
x	253	2.00	7.000	444890.	12.79
v	252	2.00	7.000	443699.	6.52
▲	251	2.00	7.000	442699.	6.35
■	250	2.00	7.000	441740.	4.56
●	249	2.00	7.000	442037.	2.11
▲	248	2.00	7.000	441828.	1.05
▼	246	2.00	7.000	440606.	-1.08
+	245	2.00	7.000	432292.	-2.14
x	244	2.00	7.000	441006.	-4.27
•	247	2.00	7.000	440421.	-0.02



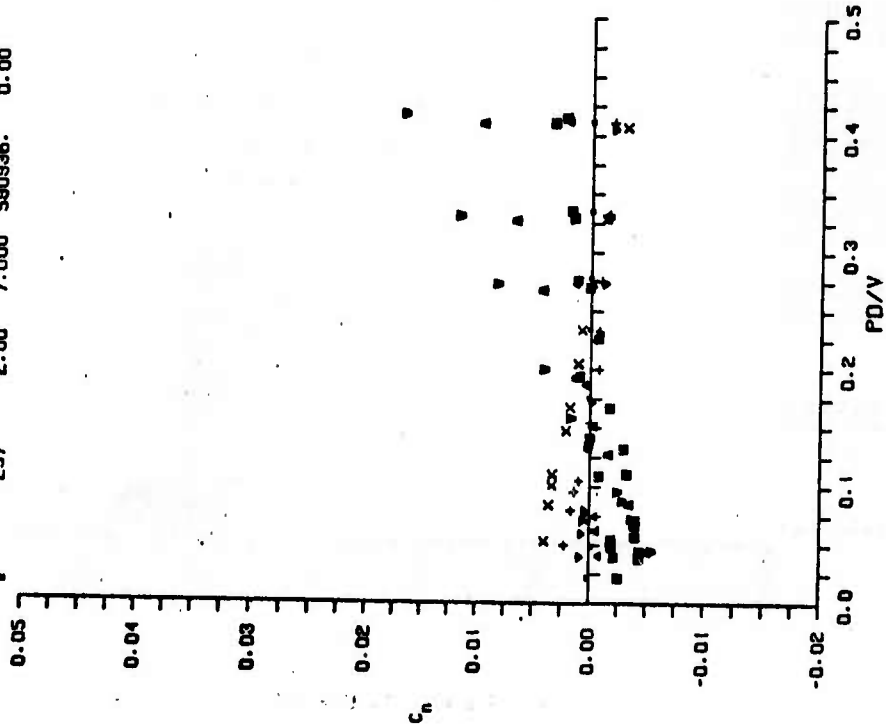
A2-33

SYN.	RUN NUMBER	MACH	CONFIG	RE/INCH	ALPHA
▲	243	2.00	7.000	199916.	12.32
▲	242	2.00	7.000	199963.	6.22
▲	241	2.00	7.000	199352.	6.16
▲	240	2.00	7.000	199356.	4.12
▲	239	2.00	7.000	199678.	2.03
▲	238	2.00	7.000	199659.	1.03
▲	236	2.00	7.000	201225.	-1.06
▲	235	2.00	7.000	199764.	-2.06
x	237	2.00	7.000	200591.	0.00



A2-34 Figure A2. Continued

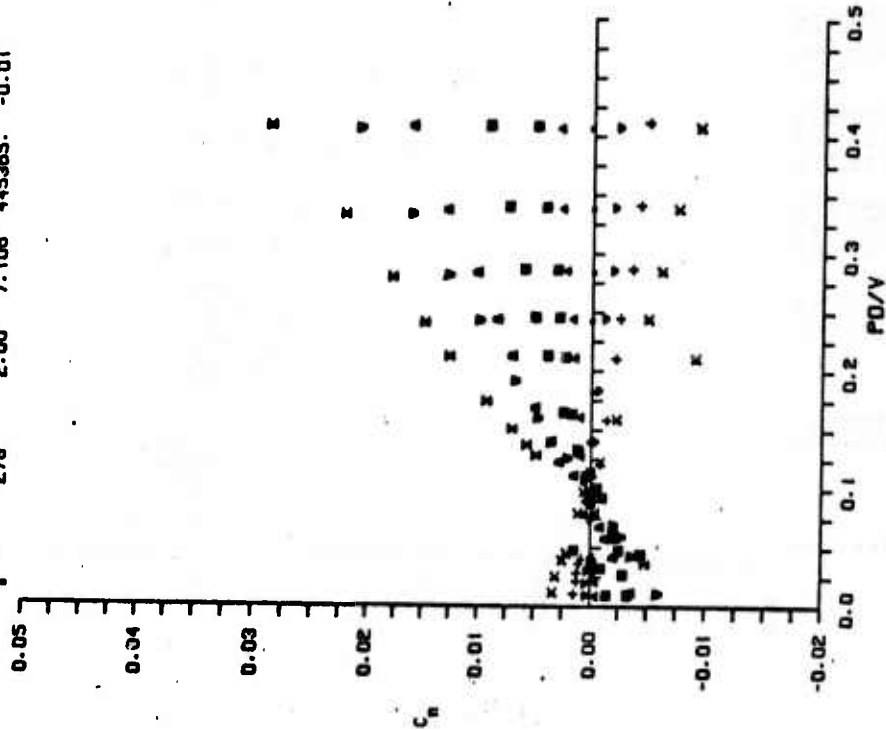
SYN.	RUN NUMBER	MACH	CONFIG	RE/INCH	ALPHA
▽	263	2.00	7.000	595014.	8.75
△	262	2.00	7.000	596402.	6.55
■	259	2.00	7.000	592356.	4.35
▲	258	2.00	7.000	591814.	2.16
▼	256	2.00	7.000	591896.	1.08
◆	255	2.00	7.000	590762.	-1.08
×	254	2.00	7.000	588165.	-2.16
·	257	2.00	7.000	589366.	-4.36
·					0.00



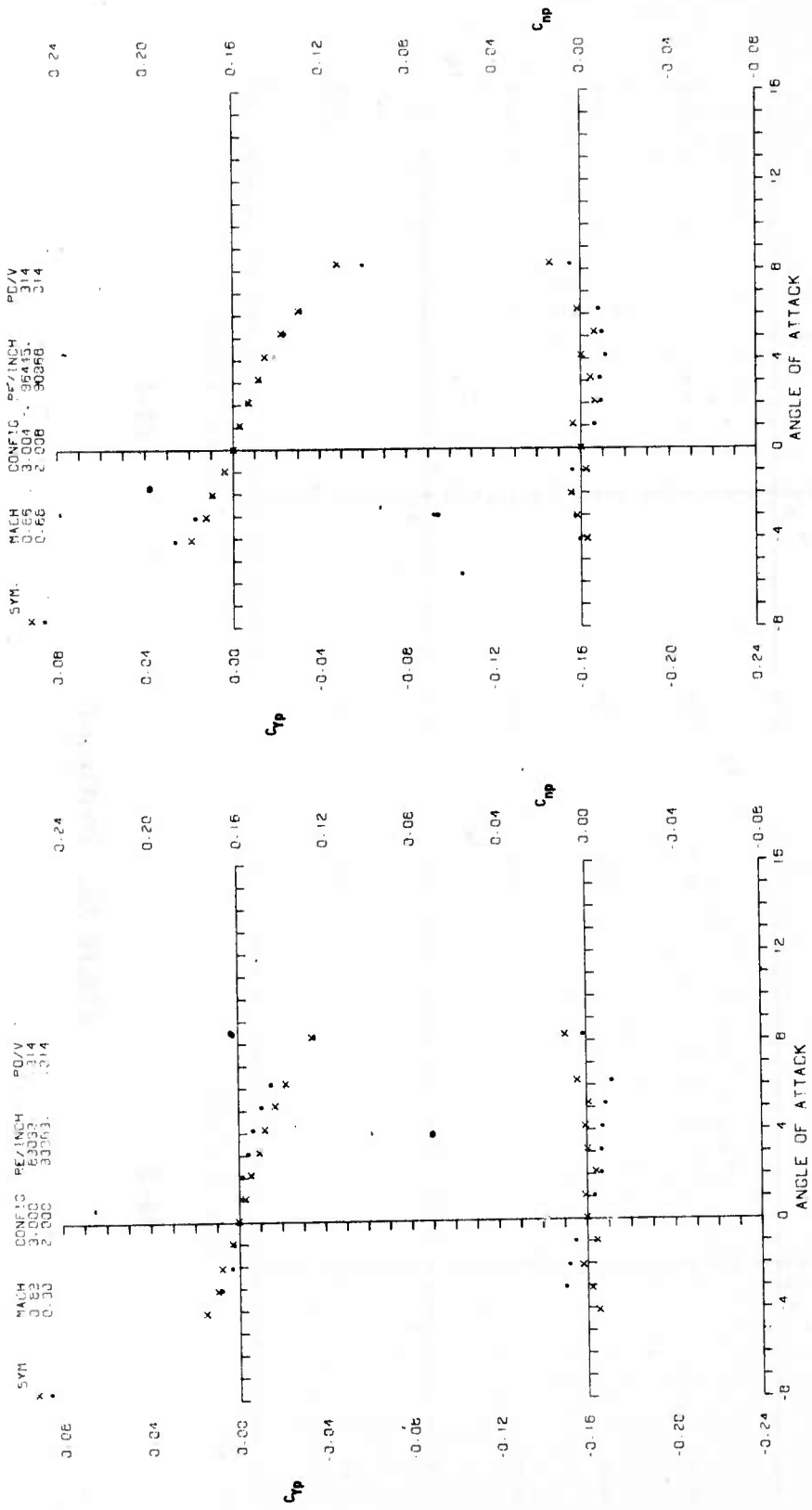
A2-35

Figure A2. Concluded

SYN.	RUN NUMBER	MACH	CONFIG	RE/INCH	ALPHA
×	265	2.00	7.108	44622.	12.78
△	264	2.00	7.108	44522.	8.54
▽	263	2.00	7.108	44425.	6.46
■	262	2.00	7.108	44325.	4.25
▲	261	2.00	7.108	44234.	2.20
▼	260	2.00	7.108	44104.	1.06
◆	259	2.00	7.108	44055.	-1.06
×	257	2.00	7.108	44571.	-2.15
·	256	2.00	7.108	44585.	-4.28
·	278	2.00	7.108	44585.	-0.01



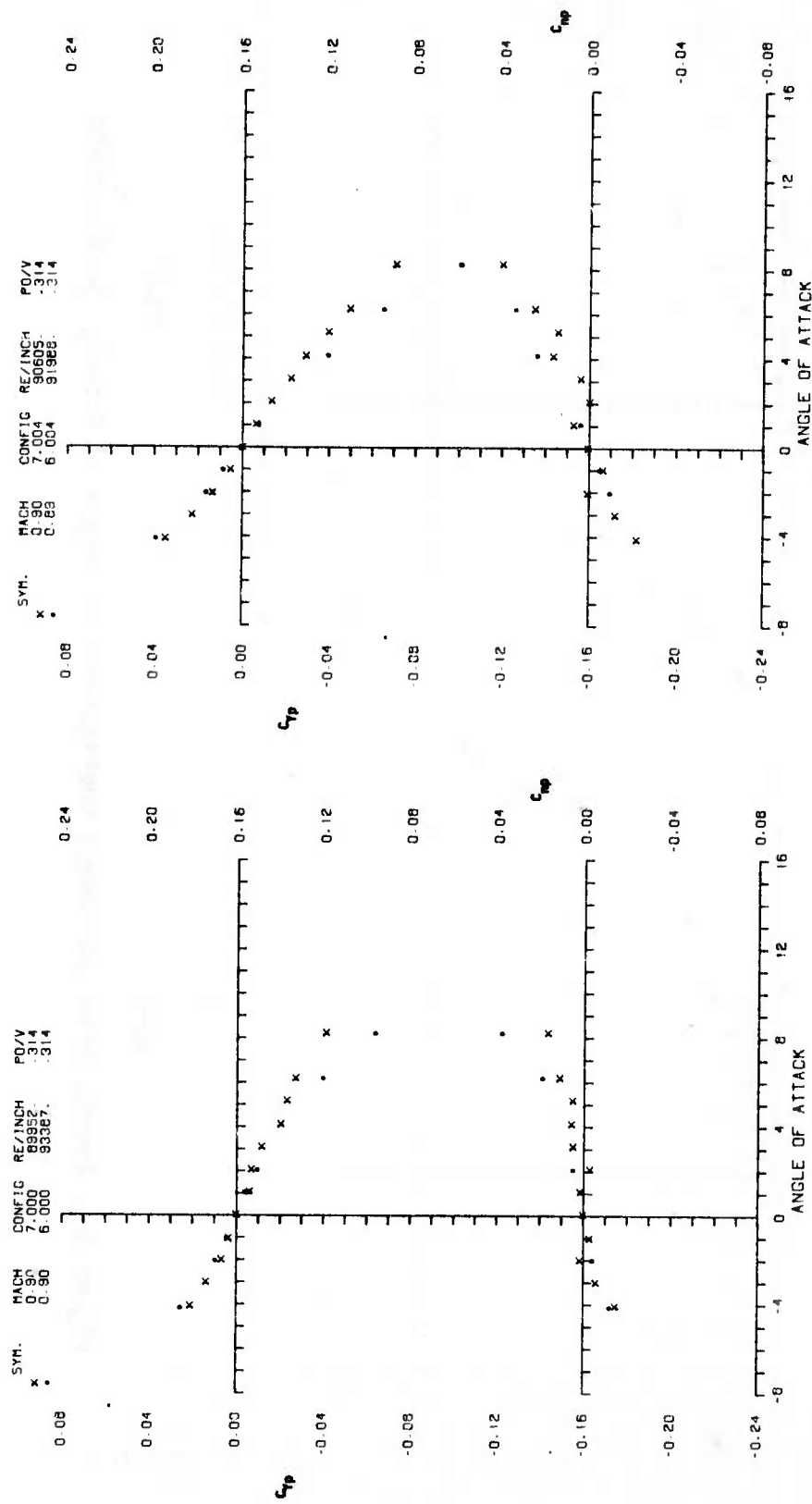
A2-36



A3-2

A3-1

Figure A3. Magnus Force and Moment Coefficients vs. Angle of Attack; $pd/V = 0.314$

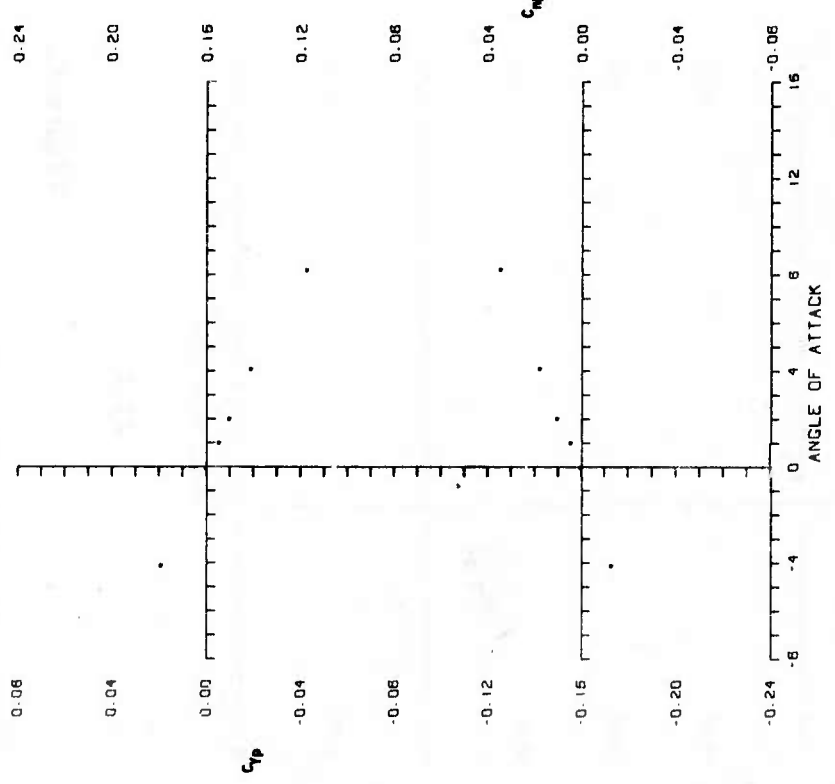


A3-3

A3-4

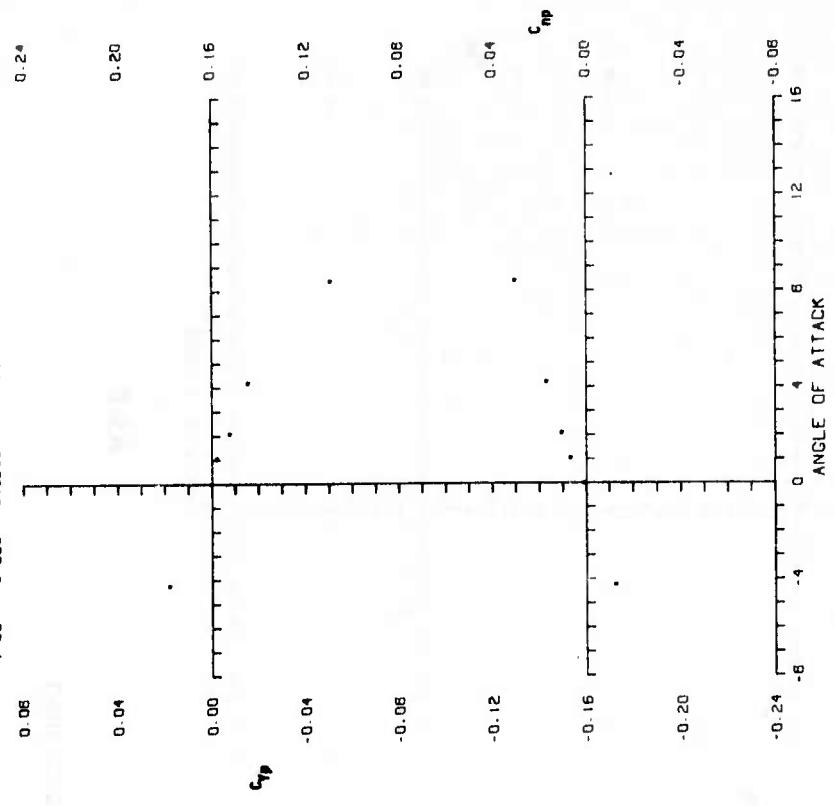
Figure A3. Continued

MACH 1.50 CONFIG RE/INCH 175566 PD/V .314



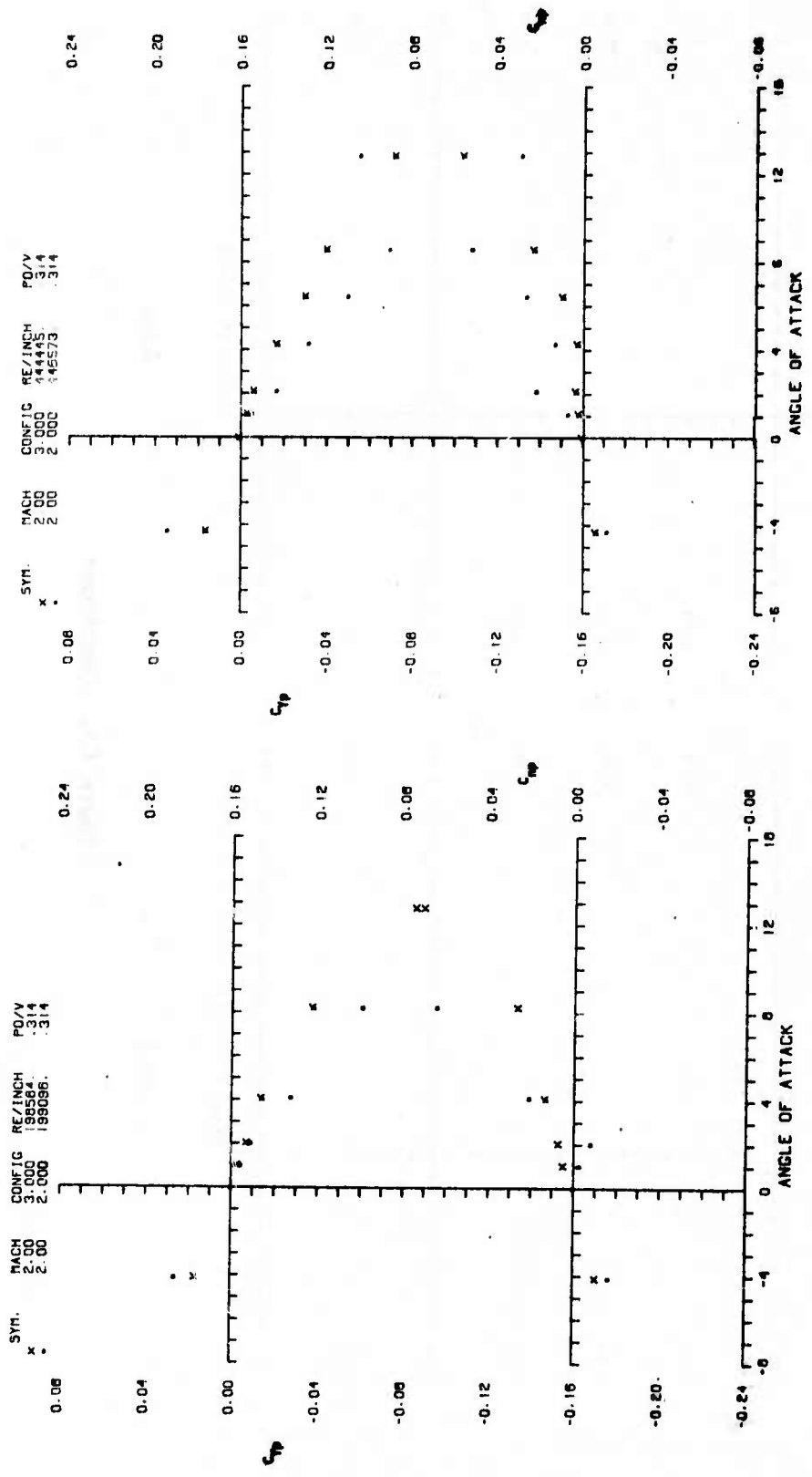
A3-5

MACH 1.50 CONFIG RE/INCH 346695 PD/V .314



A3-6

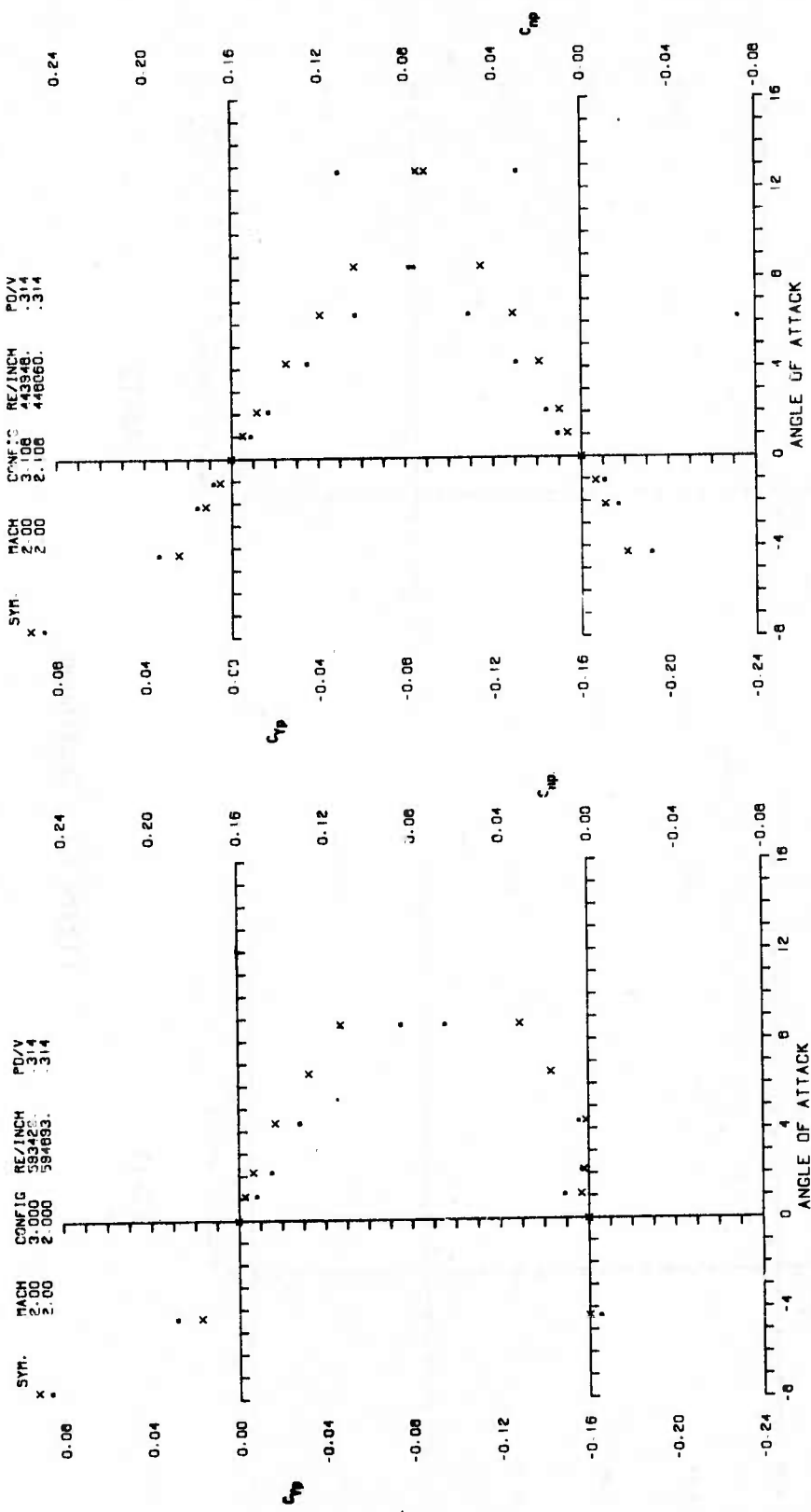
Figure A3. Continued



A3-7

A3-8

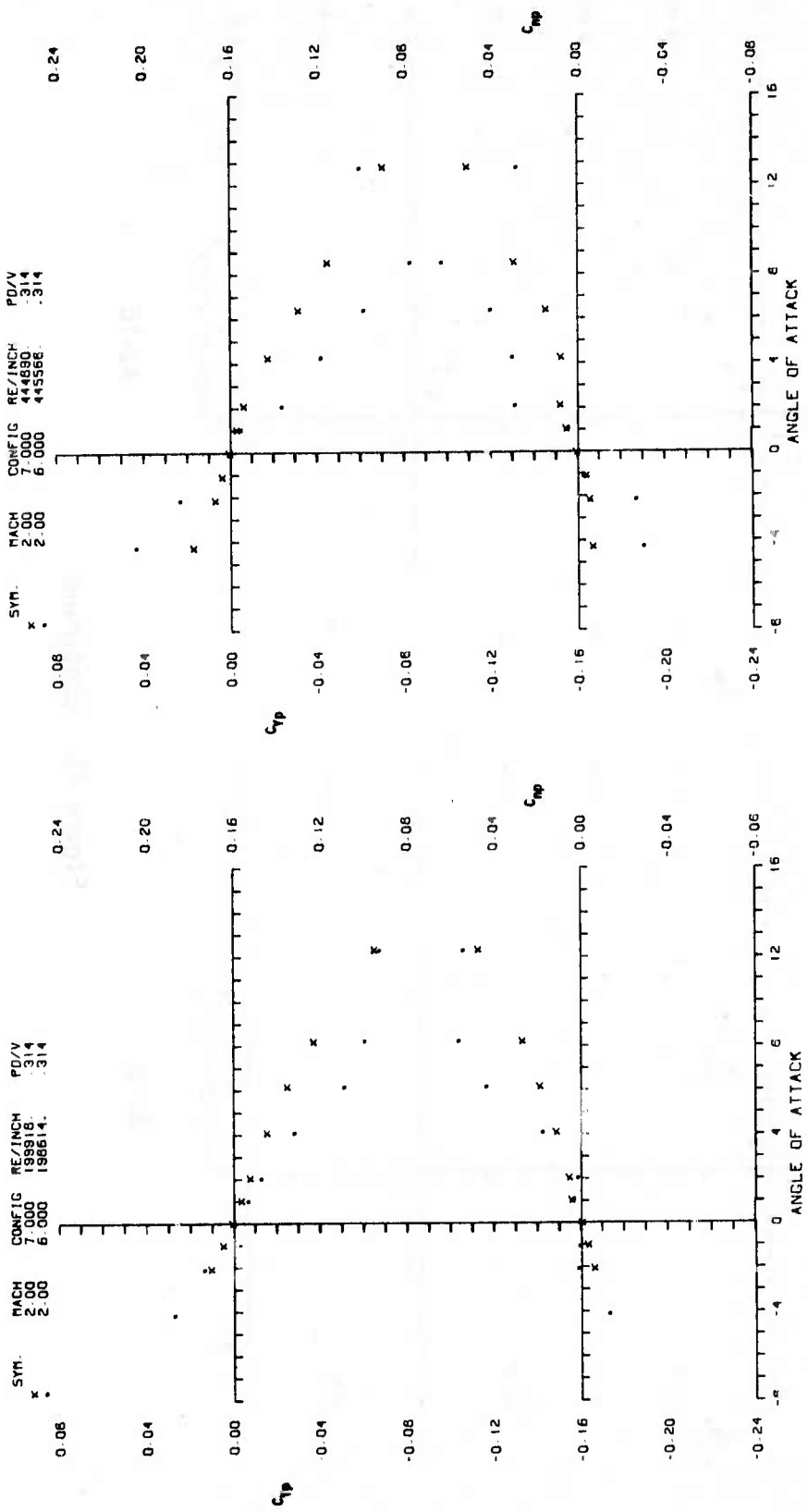
Figure A3. Continued



A3-10

Figure A3. Continued

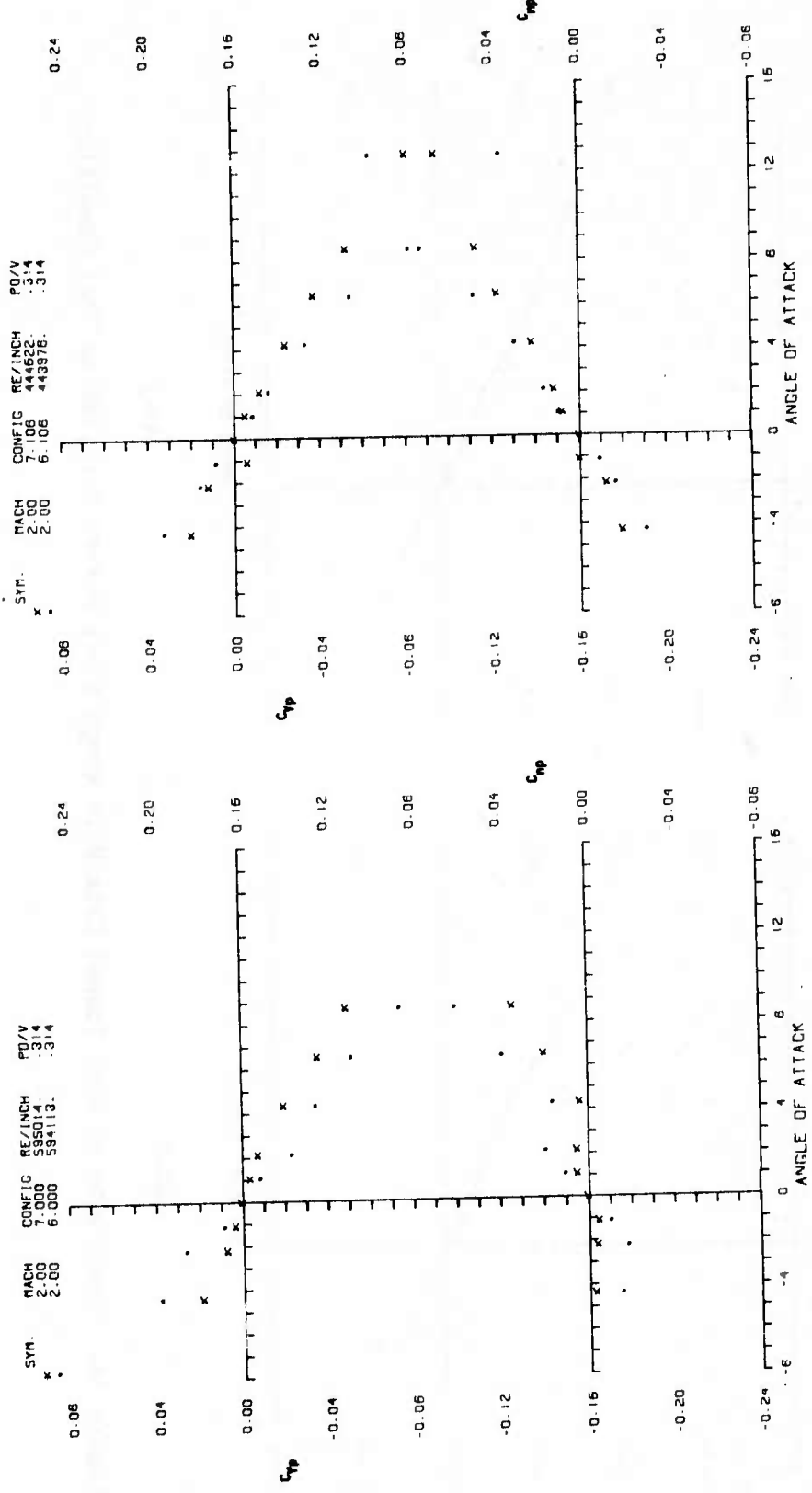
A3-9



A3-12

A3-11

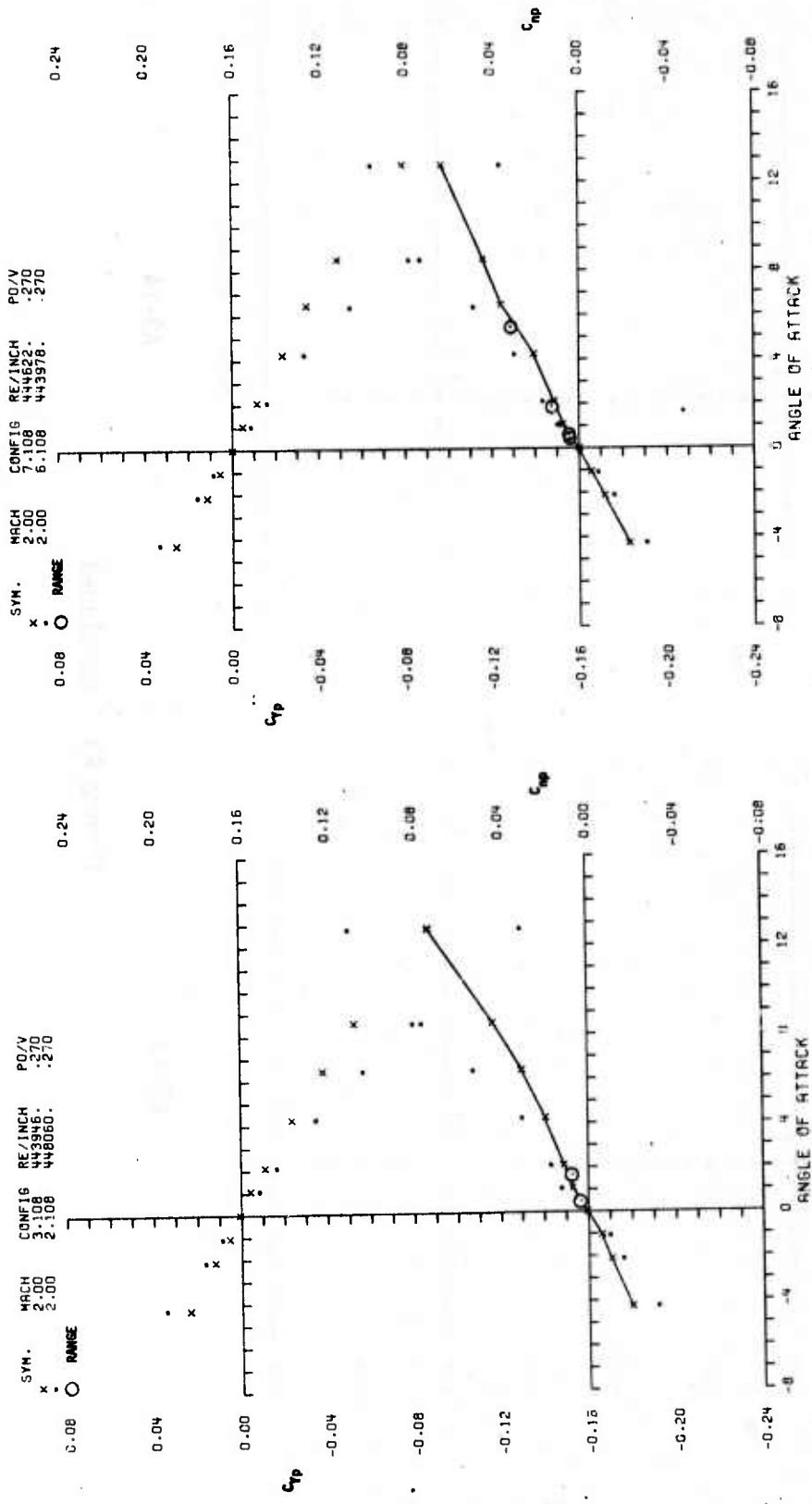
Figure A3. Continued



A3-14

A3-13

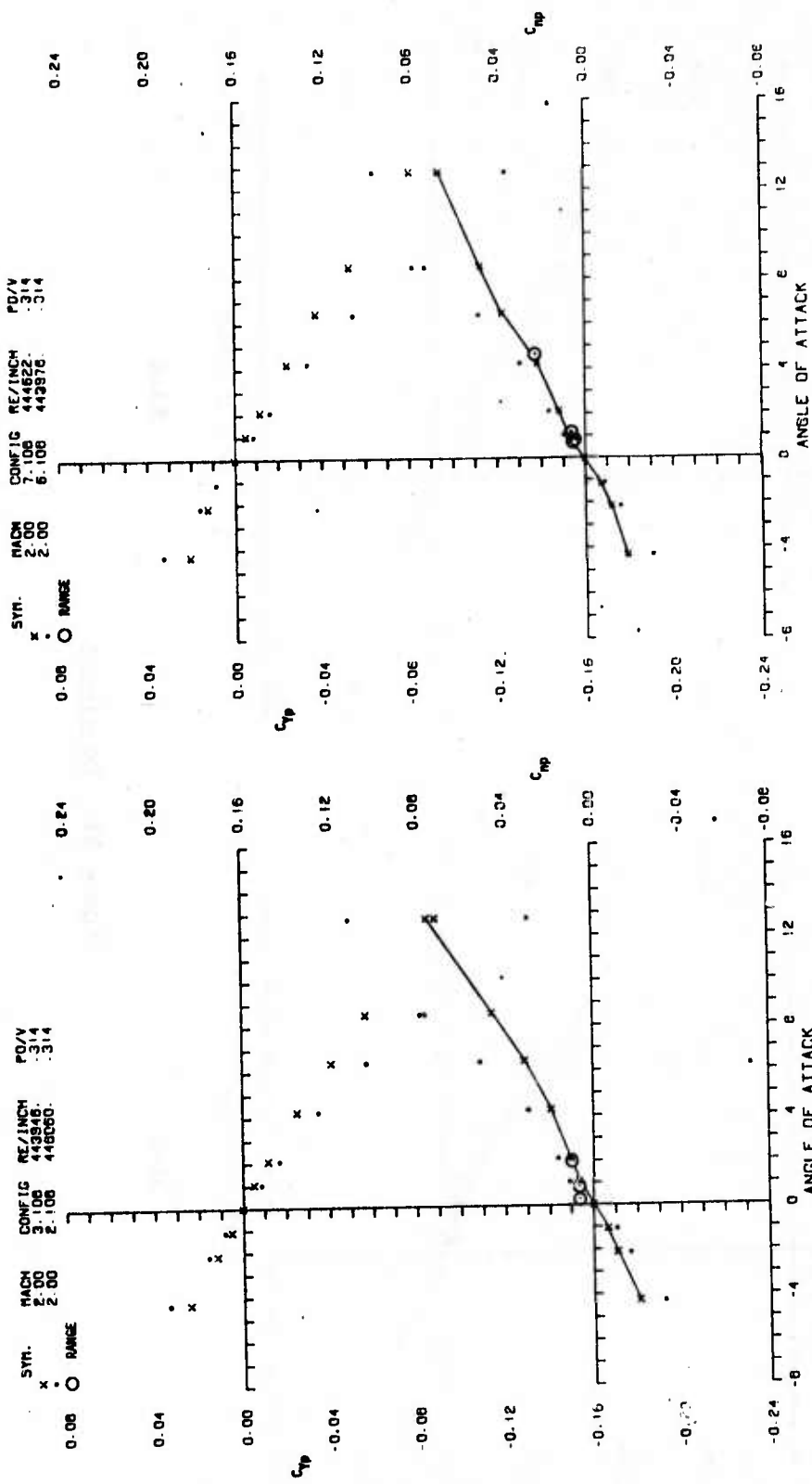
Figure A3. Concluded



A4-2

A4-1

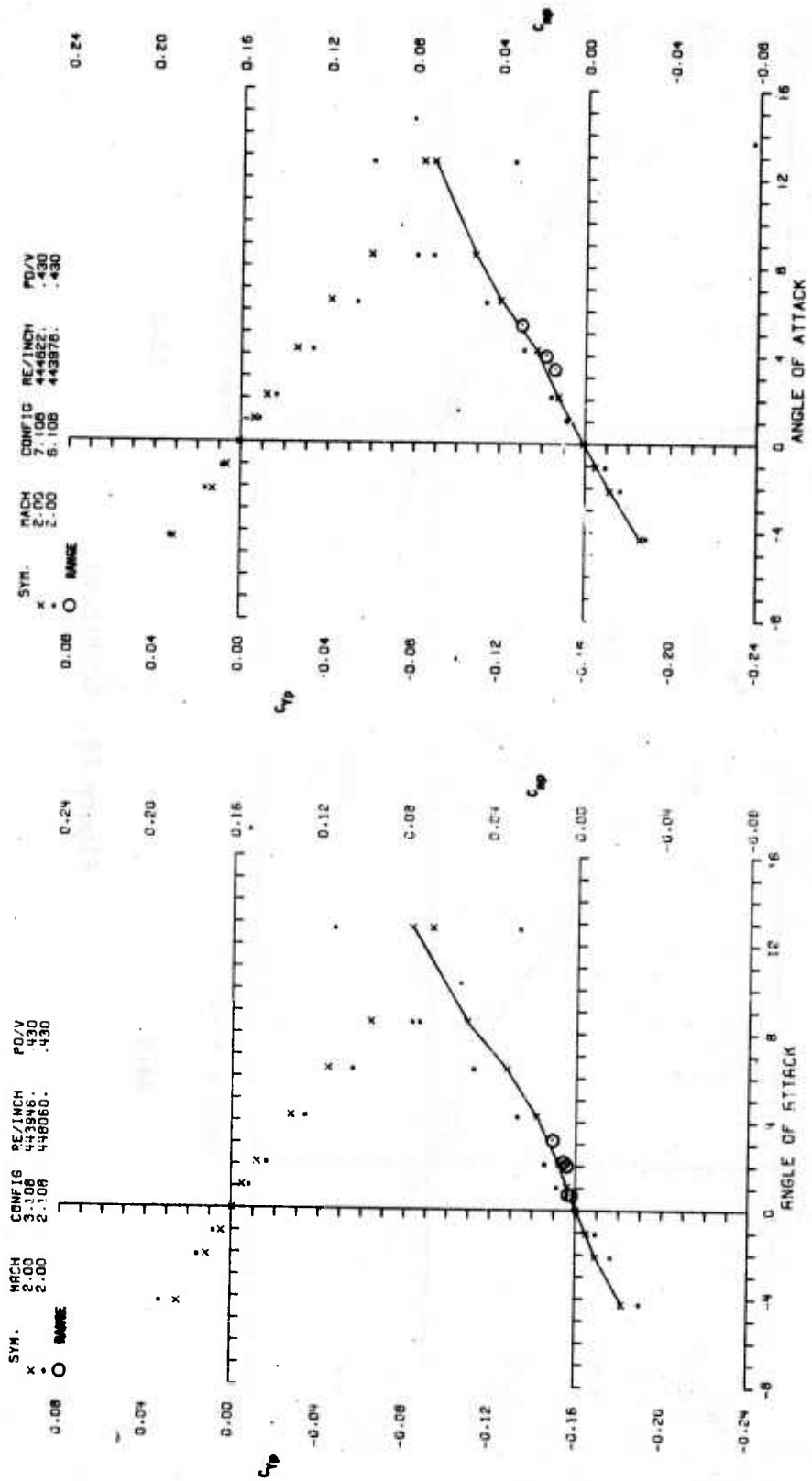
Figure A4. Comparison of Wind Tunnel Data With Range Check Points for Similar Test Conditions



A4-3

A4-4

Figure A4. Continued



A4-5

A4-6

Figure A4. Concluded

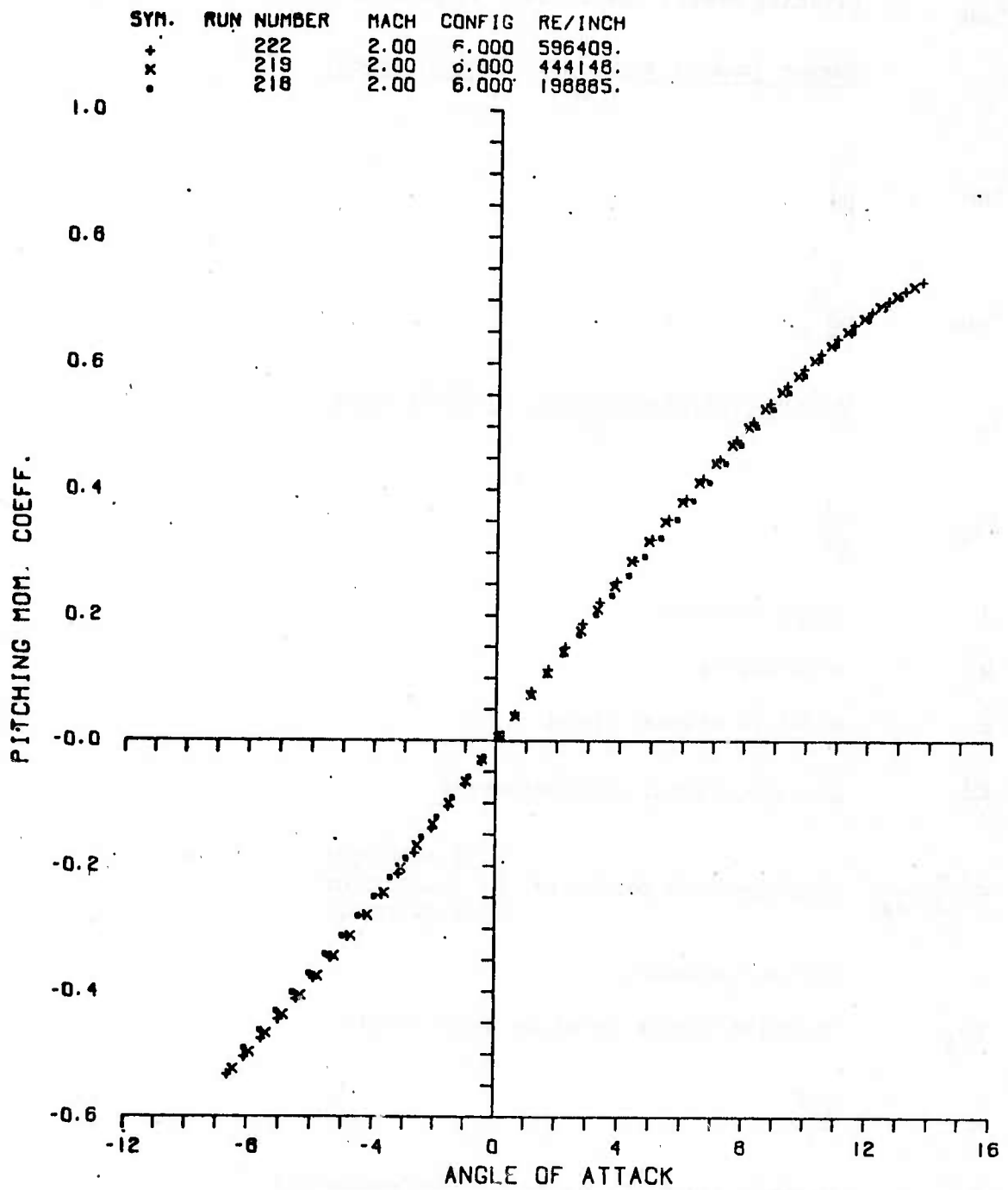


Figure A5. Typical Pitching Moment Data

LIST OF SYMBOLS

$C_{m\alpha 0}$	pitching moment coefficient slope at $\alpha = 0$
C_n	<u>Magnus (and/or asymmetry-induced) moment</u> qSd
C_{np}	$\frac{C_n}{\frac{pd}{V}}$
$C_{np\alpha}$	$\frac{C_n}{\frac{pd}{V}} \alpha$
C_Y	<u>Magnus (and/or asymmetry-induced) force</u> qS
C_{Yp}	$\frac{C_Y}{\frac{pd}{V}}$
d	model diameter
M	Mach number
p	model rotational speed
$\frac{pd}{V}$	non-dimensional spin parameter
$\frac{pd/V}{2 \tan \delta g}$	spin mismatch parameter $\begin{cases} 1 & \text{matchspin} \\ < 1 & \text{underspin} \\ > 1 & \text{overspin} \end{cases}$
q	dynamic pressure
Re_λ	Reynolds number based on model length
S	$\frac{\pi d^2}{4}$
S_d	dynamic stability parameter (reference 21)
S_g	gyroscopic stability parameter (reference 21)

LIST OF SYMBOLS (Continued)

V	free stream or bullet velocity
α	total angle of attack
δ_g	groove angle
$\lambda_{1,2}$	exponential damping coefficients for fast and slow modes (reference 21)
ϕ	viewing position for oil flow measurements (measured clockwise around model, looking forward, with $\phi = 0$ at top)

Subscript

N	nominal value
---	---------------